Recovery of cold energy from LNG regasification: applications beyond Power Cycles

J.O. Khor[a], F. Dal Magro[b], T. Gundersen[c], A. Romagnoli[d1]
[a]Energy Research Institute @ Nanyang Technological University, Singapore.
[b]Department of Mechanical Engineering, Universita' di Udine, Italy.
[c]Department of Energy and Process Engineering, NTNU, Norway.
[d]School of Mechanical and Aerospace Engineering, Nanyang Technological University, 50 Nanyang Avenue, Singapore 639798.

Abstract

Liquefied Natural Gas (LNG) releases large amounts of cold energy during the conventional regasification process. It is estimated that when the LNG is regasified to an ambient temperature of 20°C, approximately 860kJ/kg of LNG of cold energy can be recovered. Currently, most of this cold energy is wasted and several studies have investigated the opportunity to recover and re-use this wasted cold energy for power cycles; fewer studies focus on the direct reuse of this wasted cold for applications requiring cold energy as main input. In this paper, different LNG cold recovery approaches are considered and compared depending on the *energy vectors* (i.e. electricity, liquid CO_2, cold water, liquid air/nitrogen and latent heat storage) used to support a few cold applications (air separation units, dry ice production, freezing and district cooling). Using different transportation methods, these energy vectors produced using LNG cold as part or all of their energy input is coupled to these cold applications with different temperature requirements and located 5 km away from the LNG regasification facilities. This paper aims to investigate the change in overall exergy efficiency and carbon emission throughout the whole process from energy vector generation to the cold applications when the cold applications are coupled to different alternative energy vectors, compared to the baseline case which is the conventional setups and designs. With the availability of these alternative energy vectors, conventional cold applications can be modified to reduce their dependency on electricity and try to improve on the performance. The baseline setup has an overall exergy efficiency of ≈ 13% while using electricity generated by LNG assisted power cycles as energy vector yields overall exergy efficiency of ≈ 13.2%. Using energy vectors charged with LNG cold such as liquid CO_2/water, latent heat thermal storage and liquid nitrogen yields lower overall exergy efficiencies of ≈ 9.7%, 11.5% and 10.2% respectively, largely due to the poor temperature match and thus large amount of exergy destructions during the heat exchange process. For the carbon emission analysis, the baseline setup yields carbon emission of ≈ 22.3 kTPA. Using electricity generated with LNG assisted power cycle yields improvement on carbon emission of ≈ 18.3% while those using liquid CO_2/water, latent heat thermal storage and liquid nitrogen yield improvements on carbon emission of ≈ 38.0%, ≈ 37.0% and ≈ 6.0% respectively.

Keywords: *Liquefied Natural Gas; Cold to cold applications; Exergy analysis; Liquid Air Energy Storage; LNG cold energy; District Cooling*

[1] Corresponding author, email: a.romagnoli@ntu.edu.sg Phone: +65 6790 5940

Nomenclature			
Acronyms		E_L	Exergy loss as waste stream
ASU	Air separation unit	E_M	Exergy contained in material stream
BC	Brayton cycle	E_P	Physical exergy
CC	Combustion chamber	E_R	Exergy recovered
CO_2	Carbon dioxide	f	Friction factor
CP	Compressor	h	Specific enthalpy
DEC	Direct expansion cycle	H	Convective heat transfer coefficient
EP	Expander	k	Thermal conductivity
HPC	High pressure column	L	Length of pipe
HRSG	Heat recovery steam generator	$\dot{m}$	Mass flow rate
HTF	Heat transfer fluid	R	Thermal resistance
HX	Heat exchanger	V	Velocity of working fluid
IE	Isothermal expander	$\dot{W}$	Power
JV	Joule-Thompson valve		
LNG	Liquefied natural gas	Subscripts	
LN_2	Liquid nitrogen	ASU	Air separation unit
LO_2	Liquid oxygen	BCC	Baseline combined cycle
LPC	Low pressure column	CC	Combustion chamber
MSHE	Multi stream heat exchanger	CP	Compressor
PCM	Phase change material	cond	Conduction
PP	Pump	conv	Convection
RC	Rankine cycle	CW	Chilled water
SC	Separation column	DF	Deep freezing
		DI	Dry ice production
Greek symbols		EP	Expander
η_{ex}	Exergy efficiency	HX	Heat exchanger
η_{th}	Thermal efficiency	in	Inlet
η_{net}	Net efficiency	ins	Insulation
ΔT	Temperature difference	JV	Joule-Thompson valve
ρ	Density	LAPC	LNG assisted power cycle
		LCO_2	Liquid carbon dioxide
Roman symbols		misc	Miscellaneous
A	Heat transfer area	NG	Natural gas
D	Pipe diameter	out	Outlet
e	Specific exergy	PP	Pump
E_C	Chemical exergy	TN	Thermal network
E_D	Exergy destruction	TS	Thermal storage
E_{IN}	Inlet exergy	0	Reference condition

1. Introduction

Use of natural gas is expected to grow significantly over the next decades due to its abundance and relatively lower environmental impact compared to oil and coal. Pipelines are usually employed to distribute natural gas from the production site to the consumers. However, to transport natural gas from reserves which are situated in remote areas or to supply natural gas to locations unreachable by pipelines, Liquefied Natural Gas (LNG) has been proven to be a better option [1]. During the liquefaction process, the volume of natural gas is reduced to $1/600^{th}$ the original volume, with its temperature reduced to below -160°C. LNG must be regasified before it can be distributed to end users, with about 860 kJ/kg of cold energy [2] or 370 kJ/kg of cold exergy [3] released in the process. Conventional LNG regasification involves direct heat exchange between the LNG and sea water or other heat sources, meaning that the cold energy is wasted

alongside with large mechanical power required to drive the seawater pumps. With the projection of world LNG trade from about $1.53 \cdot 10^{11}$ tonnes in 2012 to about $3.70 \cdot 10^{11}$ tonnes in 2040[2] [4], the wasted cold energy released during the regasification process could be meaningfully reused and monetized by LNG plants operators.

Various processes to recover the LNG cold have been discussed and implemented in different countries as reported in Table 1. As the world's largest importer of LNG, Japan demonstrates a large variety of LNG cold recovery technologies in use. Between 20 and 30% of LNG cold energy is utilized in Japan [5], with Osaka Gas Co. becoming the first plant in Japan to achieve 100% utilization of LNG cold energy by cascading different cold applications with different temperature requirement for cold exchange with the LNG to be regasified [6]. South Korea as the world's second largest importer of LNG has also utilized LNG cold for air separation and cryogenic comminution [7].

Table 1
Processes and countries where LNG cold energy recovery has been implemented [5, 8, 9]

Process	Temperature range (°C)	Country
Air separation	-191 to -130	China, France, Japan, South Korea
Electricity generation	-160 to 0	Japan
Hydrocarbon liquefaction	-120 to -60	Japan
Cryogenic comminution	-110 to -60	Japan, South Korea
Liquid CO_2/ dry ice	-60	Japan
Refrigeration/cold storage	-30 to 0	Japan, South Korea
Seawater desalination	-10 to 10	United States
Gas turbine inlet air cooling	0 to 10	India, Japan

Several research studies discuss utilizing the LNG cold energy to reduce the compressor inlet temperature in Brayton Cycles (BC) or to reduce the working fluid condensation temperature in Rankine Cycles (RC)/Kalina Cycles (KC) [3]. Besides, Direct Expansion Cycle (DEC) of regasified LNG through a turbine is also used to harvest the mechanical exergy contained in LNG.

Table ***2*** reports some of the power cycles reported in the literature which utilize LNG cold energy to improve thermal and exergy efficiency, with thermal and exergy efficiency tabulated as η_{th} and η_{ex} respectively.

Table 2
Summary of power cycles reported in the literature which utilize cold from LNG regasification[3]

T_{min} (°C)	T_{max} (°C)	Type of cycle	Heat source	Working fluid	Efficiency	Ref.
-160	80	2 Series RC+DEC with CO_2 capture	Flue gas	CF_4/propane	η_{th} not reported $\eta_{ex} = 52.00\%$	[10]
-150	30	RC+DEC	Exhaust heat	CH_4+R1150+ propane mixed	η_{th} not reported $\eta_{ex} = 38.90\%$	[11]
-145.7	800	BC	Fuel	Nitrogen	$\eta_{th} = 69.00\%$ η_{ex} not reported	[12]
-144	1000	Series BC+RC	Fuel	Helium/steam	$\eta_{th} = 65.61\%$ $\eta_{ex} = 55.09\%$	[13]
-144	1000	BC+RC (combined cycle) with CO_2 capture	Fuel	Helium/carbon dioxide	$\eta_{th} = 65.07\%$ $\eta_{ex} = 53.70\%$	[14]
-141.9	10	KC	Seawater	CF_4+propane mixed	$\eta_{th} = 23.50\%$ η_{ex} not reported	[15]

[2] LNG density is assumed as 450kg/m^3 or 12.74kg/ft^3
[3] The reported efficiencies for the case studies of Table 2 are not solely affected by the LNG cold energy recovery but also by some other energy recovery method, such as DEC, which is a method to recover the kinetic energy of the gas instead of the waste cold inside the LNG.

-139.3	800	BC	Fuel	Air	$\eta_{th} = 67.50\%$ η_{ex} not reported	[12]
-129	1290	BC+BC+DEC	Fuel	Flue gas/Nitrogen	$\eta_{th} = 75.50\%$ $\eta_{ex} = 52.60\%$	[16]
-128	10	3 Series RC+DEC	Seawater	Argon/CH_4/CF_4	η_{th} not reported $\eta_{ex} = 85.60\%$	[17]
-122.6	10	RC+RC+DEC	Seawater	CH_4/argon	$\eta_{th} = 24.10\%$ $\eta_{ex} = 42.70\%$	[18]
-120.8	600	BC	Fuel	Argon	$\eta_{th} = 58.00\%$ η_{ex} not reported	[12]
-120	1000	BC	Fuel	Nitrogen	$\eta_{th} = 78.86\%$ η_{ex} not reported	[19]
-120	1000	Series BC+RC	Fuel	Nitrogen/carbon dioxide	$\eta_{th} = 67.90\%$ η_{ex} not reported	[19]
-115.6	10	RC	Waste steam	Pentane + CHF_3 + CF_4 mixed	$\eta_{th} = 23.70\%$ $\eta_{ex} = 27.00\%$	[20]
-103.4	108	RC	Flue gas	Pentane + CF_4 + CHF_3 mixed	$\eta_{th} = 30.30\%$ $\eta_{ex} = 46.20\%$	[21]
-76.2	90	RC+RC+DEC	Solar	Ammonia/ethane	$\eta_{th} = 33.49\%$ η_{ex} not reported	[22]
-71	10	RC+DEC	Seawater	Ammonia	$\eta_{th} = 8.10\%$ η_{ex} not reported	[23]
-65	134	KC+DEC	Waste heat	Ammonia + water mixed	$\eta_{th} = 39.33\%$ $\eta_{ex} = 50.15\%$	[24]
-60	75	RC+DEC	Solar	CH_3F	$\eta_{th} = 25.25\%$ $\eta_{ex} = 12.20\%$	[25]
-55.8	900	RC	Solar + Fuel	Carbon dioxide	$\eta_{th} = 61.00\%$ $\eta_{ex} = 61.30\%$	[26]
-54.4	150	KC+DEC	Waste heat	Ammonia + water mixed	$\eta_{th} = 33.28\%$ $\eta_{ex} = 48.87\%$	[27]
-53	1200	RC with CO_2 capture	Oxy-fuel	Carbon dioxide	$\eta_{th} = 71.04\%$ $\eta_{ex} = 50.53\%$	[28]
-50.4	400	RC+RC+DEC	Waste heat	Steam/ammonia	$\eta_{th} = 34.20\%$ η_{ex} not reported	[29]
-50	700	RC	Fuel	Carbon dioxide	$\eta_{th} = 59.00\%$ η_{ex} not reported	[30]
-50	900	RC with CO_2 capture	Oxy-fuel	Carbon dioxide	$\eta_{th} = 59.06\%$ $\eta_{ex} = 39.79\%$	[31]
-46.9	190	RC	Waste heat	Ammonia + water mixed	η_{th} not reported $\eta_{ex} = 25.88\%$	[32]
-42	10	RC	Seawater	Propane	$\eta_{th} = 12.50\%$ $\eta_{ex} = 65.20\%$	[33]
-20	190	RC+DEC	Waste heat	Isobutane	$\eta_{th} = 21.00\%$ η_{ex} not reported	[34]
-10	65	RC	Solar	Carbon dioxide	$\eta_{th} = 8.48\%$ η_{ex} not reported	[35]
9	1300	BC+RC (combined cycle)	Fuel	Flue gas/steam	$\eta_{th} = 59.30\%$ $\eta_{ex} = 54.98\%$	[36]

With the correct choice of working fluid for the power cycles, LNG cold can be utilized at different temperature ranges well below ambient temperature. By decreasing the condensation temperature of the working fluid between ≈ -50°C and ≈ -120°C (as reported in [20-22, 25, 33] in Table 2), efficiencies between ≈ 12% and ≈ 34% can be achieved even with low to medium temperature heat sources such as seawater, solar power or industrial waste heat. Rankine cycles with carbon dioxide as working fluid [26, 28, 30, 31] can undergo larger temperature change compared to organic working

fluids, which allows high temperature heat source such as combustion heat to be used and can achieve higher thermal efficiency between ≈ 59% and ≈ 71%.

Real gases such as nitrogen, argon, air and helium have very low triple point temperature and thus they can be used to recover LNG cold at lower temperatures than those considered for Rankine cycle (temperature range between ≈ -120°C and ≈ -145°C). Closed Brayton cycles utilizing nitrogen or argon as working fluid can achieve thermal efficiencies between ≈ 58% and ≈ 69% [12, 19]. The efficiency is further increased by coupling the closed Brayton cycle with an open air Brayton cycle which is heated up to 1290°C, which achieves a thermal efficiency of ≈ 75.5% [16].

Combined cycles normally consist of a Brayton cycle coupled with a Rankine cycle. With LNG cold input, the Brayton cycle can benefit when the compressor inlet temperature is reduced, reducing the compressor work required [3] while for the Rankine cycle, the working fluid condensation temperature is reduced, thus increasing the pressure ratio across the expander [13, 19, 36].

Table 3
Cold applications utilizing LNG cold and the energy vectors used

Energy vector temperature (°C)	Usage	Energy vector used	Ref.
-160	Air liquefaction/separation	Nitrogen	[37]
-150	Olefin (alkene) Separation	Olefin	[6]
-115	Cryogenic comminution	R22	[38]
-60	Solid/liquid CO_2 production	CO_2	[37-39]
-43	Freezing and refrigeration	CO_2	[40, 41]
-5	Butane liquefaction	Butane	[37]
5	Gas turbine inlet air cooling	Water	[37]

Direct utilization of the LNG cold for *cold-to-cold* applications (CTC) is generally less discussed. Table 3 reports some case studies of cold applications utilizing LNG cold. For such applications, the LNG cold energy is recovered by using different heat transfer fluids and delivered to various cold applications. One of the well-known existing facilities for CTC applications is in Osaka Gas Co. where the cold is cascaded to serve different cold applications [6], aiming to utilize the whole range of available LNG cold from cryogenic to ambient temperature. In this particular case, the cold applications are located next to the LNG regasification terminal. This allows for the usage of hydrocarbons and hydrofluorocarbon refrigerants as cold energy vectors. However due the high global warming potential of hydrofluorocarbon refrigerants, alternative working fluids such as water, CO_2 or hydrofluoroolefins should be considered, especially if the cold had to be delivered over longer distances [42].

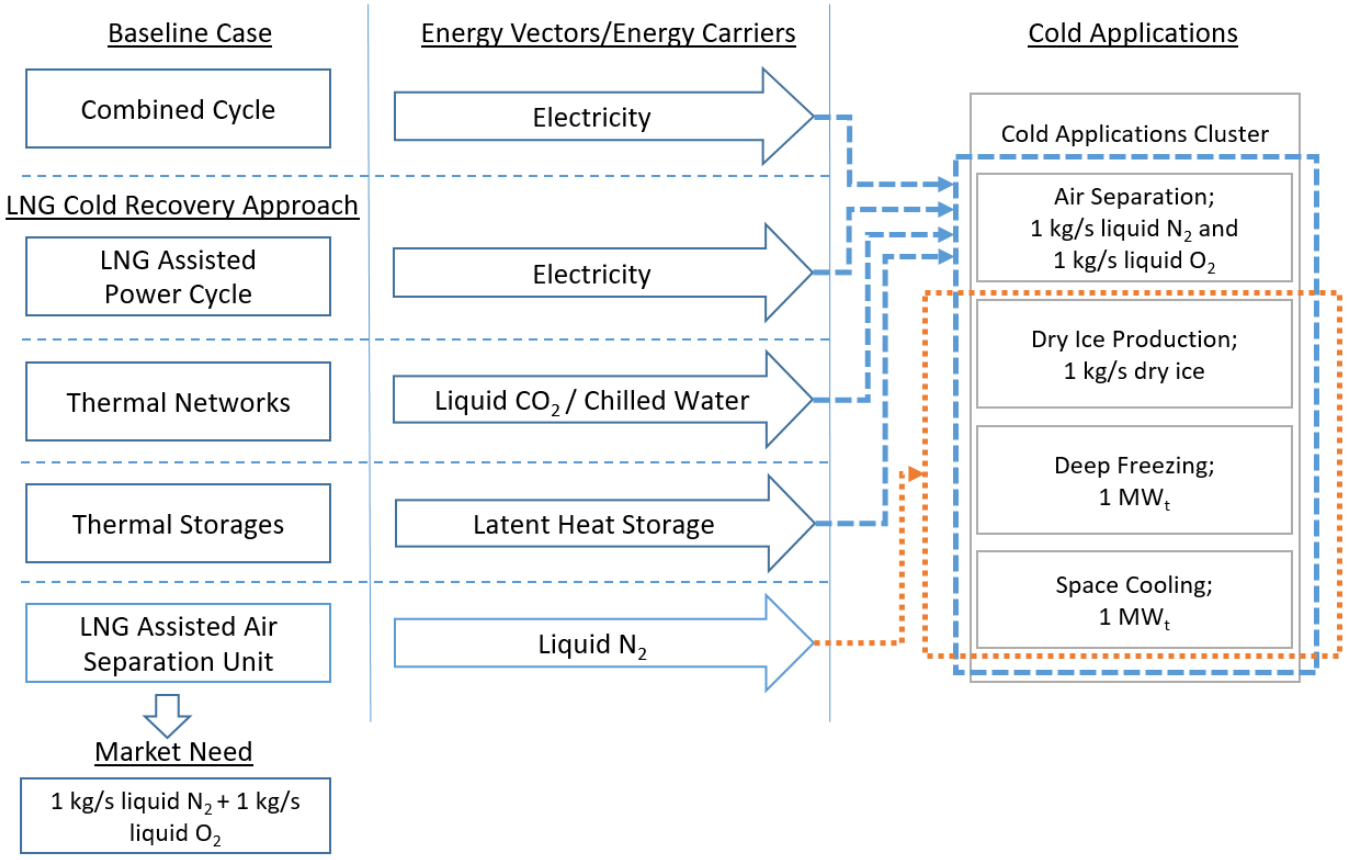

Fig. 1. Coupling of LNG cold energy recovery approaches with different cold applications

In this paper, we intend to assess the potential of recovering the LNG cold energy for CTC applications only. Four different cold applications – air separation, dry ice production, deep freezing and district cooling – have been considered within this study. Each of these applications require a different grade of cold and two Key Performance Indices, *exergy efficiency* and *carbon emissions*, have been considered throughout the study.

In this paper, the energy demand of various cold applications is assumed to fulfil the following output quantities: production of 1 kg/s of liquid nitrogen and 1 kg/s liquid oxygen from the air separation unit, 1 kg/s production of dry ice, 1 MW_t for deep freezing and 1 MW_t for district cooling (refer to Fig. 1). It is also assumed that the amount of LNG regasified is scaled according to the demand of the cold applications, meaning that the amount of the energy which needs to be transferred by the energy vector will be scaled accordingly. The LNG regasification terminal is assumed to be located at 5 km away from the cold applications. Each of the LNG cold energy recovery approaches will be used to generate (or charge) different energy vectors:

- Electricity is generated from a combined cycle power plant or an LNG assisted power cycle (combination of two Brayton cycles to utilize LNG cold) in which the LNG cold is used to cool the working fluids (i.e. air and nitrogen) entering the two compressors
- Liquid CO_2 and chilled water used to recover and distribute the LNG cold to the downstream cold applications in a dual-temperature thermal network
- Latent heat storage (solid-to-liquid phase change materials - PCMs) is used to recover the LNG cold which is then trucked to the downstream cold applications
- Liquid nitrogen and oxygen is produced by the LNG assisted air separation unit, where part of the liquid nitrogen will be used as energy vector to provide cold to the downstream cold applications.

By means of different energy vectors, alternative layouts and configurations for the cold applications are proposed, assessed and compared to the conventional ones. For high-grade cold applications (i.e. air separation process) which cannot

be solely supported by specific energy vectors (i.e. liquid CO_2 or PCMs) and thus requiring electricity input in the process, it is assumed that the electricity is obtained from the power cycle mentioned in the baseline combined cycle power plant, with the same transmission distance.

In this paper, the *baseline case* is a combined cycle power plant using natural gas as fuel. Under this scenario, the cold applications in Fig. 1 operate based on their conventional process configuration, which utilize electricity as power input and cooling water as their heat sink [43, 44]. In the baseline case, electricity is produced as an energy vector and distributed over the electricity grid. Likewise the baseline case, the *LNG assisted power cycle* output energy vector is electricity which is distributed using the same electricity grid; the cold applications operate according to their conventional process configuration.

For the *thermal networks*, the cold released during the LNG regasification process is recovered by two different working fluids: CO_2 and water. CO_2 vapor is liquefied by the LNG cold energy and distributed to the cold applications side, exploiting its latent heat to provide cooling. Water is returned at a warmer temperature and cooled to a lower temperature before being supplied to the cold applications; in this case, water uses its sensible heat to supply cooling to the cold applications; both CO_2 and water are transported to the cold applications using insulated pipelines.

In the *thermal storage*, the LNG cold energy is recovered by means of different types of thermal storage materials. In particular, in this paper various types of PCMs having different phase change temperatures are evaluated. These PCMs are chosen by matching their melting temperature with the temperature requirement of the cold applications, and transported to their respective cold applications by means of trucks.

For the *LNG assisted air separation unit*, alongside producing the market requirement of 1 kg/s liquid nitrogen and liquid oxygen each, the air separation unit will produce extra liquid nitrogen as cold energy vector to be supplied to the cold applications by trucks. The existence of these liquid CO_2, chilled water, PCMs and liquid nitrogen provides possibilities that the cold applications can be modified to reduce their dependence on electricity and thus reducing the overall CO_2 emission.

This paper is structured as follows: in Section 2, the modelling approach and key performance indices are introduced. Various methods for energy vector generation with or without LNG cold input are discussed in Section 3, while transportation of these energy vectors is discussed in Section 4. In Section 5, various cold applications, assumed as a stand-alone cold application for each, are introduced and analyzed based on the exergy analysis and CO_2 emission of the application after each of them is coupled to different possible source of energy vectors. In the same section, the overall performance when the cold applications are assumed to be clustered together are shown. Finally the conclusions are drawn in Section 6.

2. Methodology and Modelling

2.1 Assumptions

In this paper, the following assumptions have been made to facilitate the study:

- The composition of LNG is assumed to be 100% methane;
- The composition of air is assumed to be 79% nitrogen and 21% oxygen by volume;
- Heat losses and friction losses in all system connections are neglected;
- All components operate under steady state condition.

2.2 Energy analysis

Thermal efficiency is used as the main design criteria for most thermal cycles and is defined as the ratio of total net work production to heat addition to the system. The thermal efficiency is calculated in accordance with:

Energy balance for compressors and pumps:

$$\dot{W} = \dot{m}_{in}(h_{out} - h_{in}) \quad (1)$$

Energy balance for turbines or expanders:

$$\dot{W} = \dot{m}_{in}(h_{in} - h_{out}) \quad (2)$$

Net power output:

$$\dot{W}_{net} = \sum \dot{W}_{EP} - \sum \dot{W}_{CP} - \sum \dot{W}_{PP} \quad (3)$$

Heat input to thermal cycles is calculated based on the enthalpy difference across the combustion chamber:

$$\dot{Q}_{in} = \dot{m}_{out} h_{out} - \sum \dot{m}_{in} h_{in} \quad (4)$$

Thermal and net efficiency of power cycles can then be calculated with:

$$\eta_{th} = \frac{\dot{W}_{net}}{\dot{Q}_{in}} \quad (5)$$

$$\eta_{net} = \frac{\dot{W}_{net}}{\dot{Q}_{fuel}} \quad (6)$$

2.3 Exergy analysis

Physical exergy of a stream can be determined using the following formula:

$$e = h - h_0 - T_0(s - s_0) \quad (7)$$

where h_0 and s_0 are the fluid properties under reference conditions of $T_0 = 15°C$ and $p_0 = 1atm$. The rate of physical exergy of a stream can be calculated as follow:

$$\dot{E} = \dot{m}e \quad (8)$$

The exergy efficiency can then be calculated using the following formula:

$$\eta_{ex} = 1 - \frac{\sum \dot{E}_L + \sum \dot{E}_D}{\sum \dot{E}_{in}} \quad (9)$$

3. Generation of Energy Vectors

According to Fig. 1, there are four different types of energy vectors that have been considered by using five different generation methods.

3.1 Baseline Case

A combined cycle power plant composed of an open air Brayton cycle as topping cycle and a closed steam Rankine cycle as bottoming cycle is modelled. The energy vector produced by this baseline case is electricity. The flow diagram of the combined cycle power plant is shown in Fig. 2. In the topping cycle, which is represented by state points (1)-(6), the inlet air is compressed (CP-1) before mixed with fuel and heated to 1400°C in a combustion chamber (CC-1). The flue gas leaving the combustion chamber is then passed through an expander (EP-1) before passed through the heat recovery steam generator (HRSG) where heat of the flue gas is utilized to evaporate the water of the bottoming cycle.

In the steam Rankine cycle, which is represented by state points (11)-(14), water from the condenser (HX-1) is pumped (PP-1) into the HRSG; the superheated steam is then passed through an expander (EP-2).

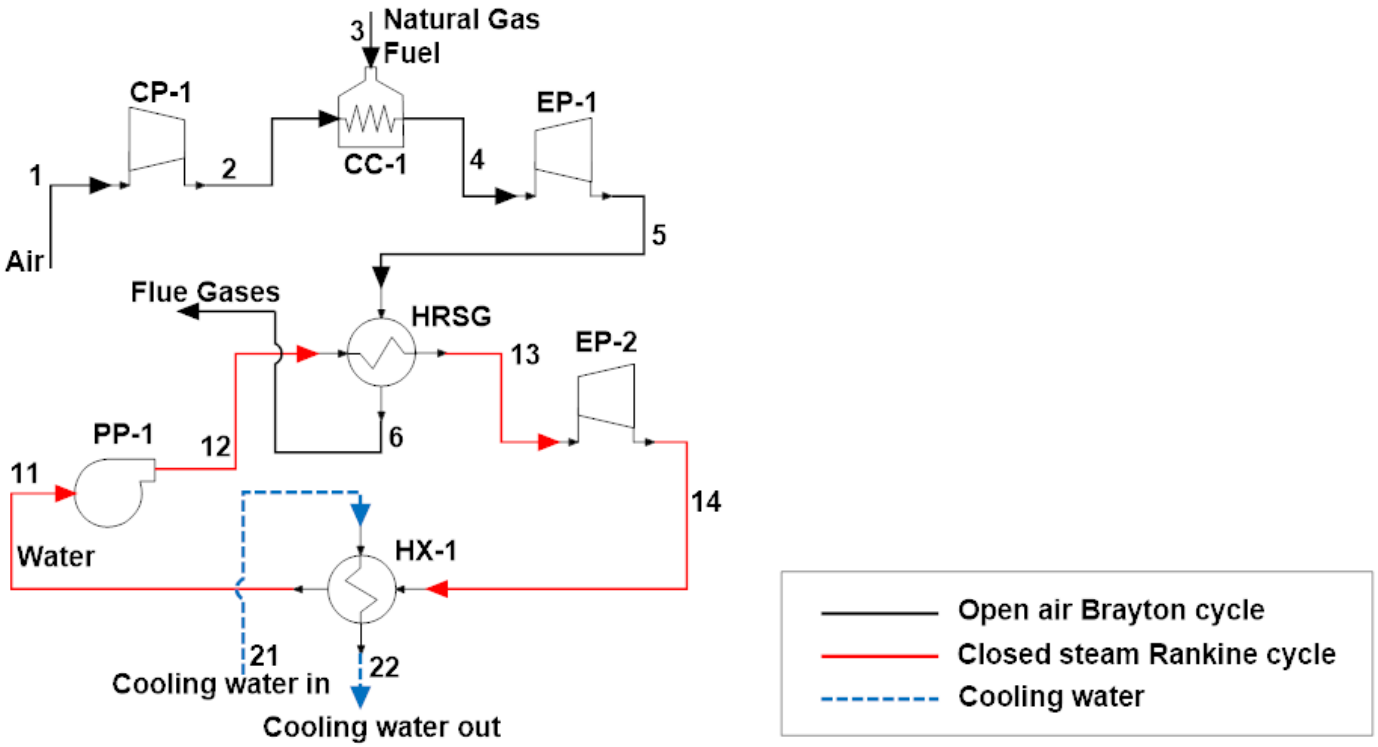

Fig. 2. Schematic diagram of the baseline combined cycle

The parameters used for the simulation and the results obtained are reported in Table 4. Fig. 3 shows the exergy flows and the respective exergy destruction in each of the components.

Table 4
Main parameters and performance for the baseline combined cycle power plant

OPERATING PARAMETERS	VALUES
Air BC pressure ratio - (CP-1)	15
Turbine inlet temperature (°C) - (EP-1)	1400
Pressure drop across heat exchangers (%) - (HRSG & HX-1)	1-3
Compressor isentropic efficiency (%) - (CP-1)	85.0
Turbine isentropic efficiency (%) - (EP-1 & EP-2)	90.0
Steam RC pressure ratio - (PP-1)	550
Pump isentropic efficiency (%) - (PP-1)	85.0
Steam condensation temperature (°C) - (HX-1)	40
CYCLE EFFICIENCY	
Thermal efficiency (%)	53.5
Exergy efficiency (%)	50.5

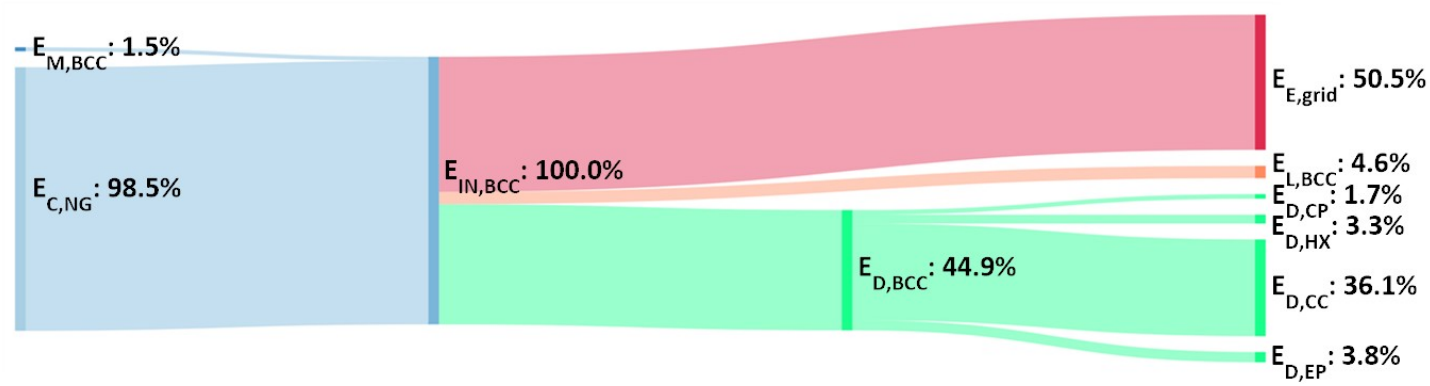

Fig. 3. Exergy flows for the baseline combined cycle

Although a dual-pressure and a triple-pressure steam generator in the steam Rankine cycle is shown to yield a thermal efficiency increase of 0.8% and 1.0% respectively [45]. In this paper, for simplicity, combined cycle with single pressure steam generator is modelled.

From Fig. 3 it can be seen that the main source of exergy comes from the chemical exergy of the natural gas fuel ($E_{C,NG}$). The exergy efficiency for this baseline combined cycle is 50.5%, which is the amount of electricity delivered to the grid. Waste stream exergy ($E_{L,BCC}$) is 4.6%, which accounts for exergy stream leaving the cycle (i.e. stack gas and cooling water). Exergy destruction ($E_{D,BCC}$) accounts for 44.9% of the total exergy input, in which the main source of exergy loss comes from the combustion chamber ($E_{D,CC}$) due to chemical reaction and large temperature mismatch between the burner gases and the other components of air present. Thermal losses to the surroundings also contributed to the exergy destruction in the combustion chamber. Other source of irreversibilities includes exergy destruction in the turbomachineries (i.e. compressor, pump, heat exchangers and the expanders), which accounts for 8.8% of the total exergy input.

3.2 LNG Assisted Power Cycle

In this section, the combination of an open air Brayton cycle with a closed nitrogen Brayton cycle and an LNG direct expansion cycle is modelled, with electricity as the energy vector generated. As reported in Table 2, several LNG assisted power cycles have been assessed with different ranges of maximum temperature (i.e. turbine inlet temperature) and minimum temperature (i.e. compressor or pump inlet temperature), leading to different ranges of efficiencies. From Table 2 it can be observed that real gas Brayton cycles, carbon dioxide Rankine cycles and combined cycles can achieve thermal efficiencies above 60%. Despite the high thermal efficiencies reported, single closed real gas Brayton cycles have a relatively lower net efficiency than open air Brayton cycles because of the difference in the heat addition method to the cycles. For closed Brayton cycles, the thermal efficiency is high especially with a heat regenerator incorporated into the design, which reduces the amount of heat input to the cycle. However, when the heat input is done by an external heat source, the heat source will have to be maintained at a higher temperature than that required by the cycle, with a large amount of unrecovered waste heat, especially when the cycle operates at a high turbine inlet temperature for a high thermal efficiency as reported. For open air Brayton cycles, where the combustion gas is used to drive the expander, fuel can be mixed with air for combustion directly, which translate to a relatively lower amount of waste heat, and thus a higher net efficiency.

In this paper, the choice of an open air Brayton cycle as topping cycle is due to the high temperature that can be achieved by the combustion process. For the bottoming cycle, a closed nitrogen Brayton cycle is chosen because of its ability to be cooled to near the boiling temperature of LNG, thus effectively reducing the compression power required. An LNG direct expansion cycle is also included to harvest the kinetic energy of LNG. The flow diagram of the LNG assisted power cycle is shown in Fig. 4 .

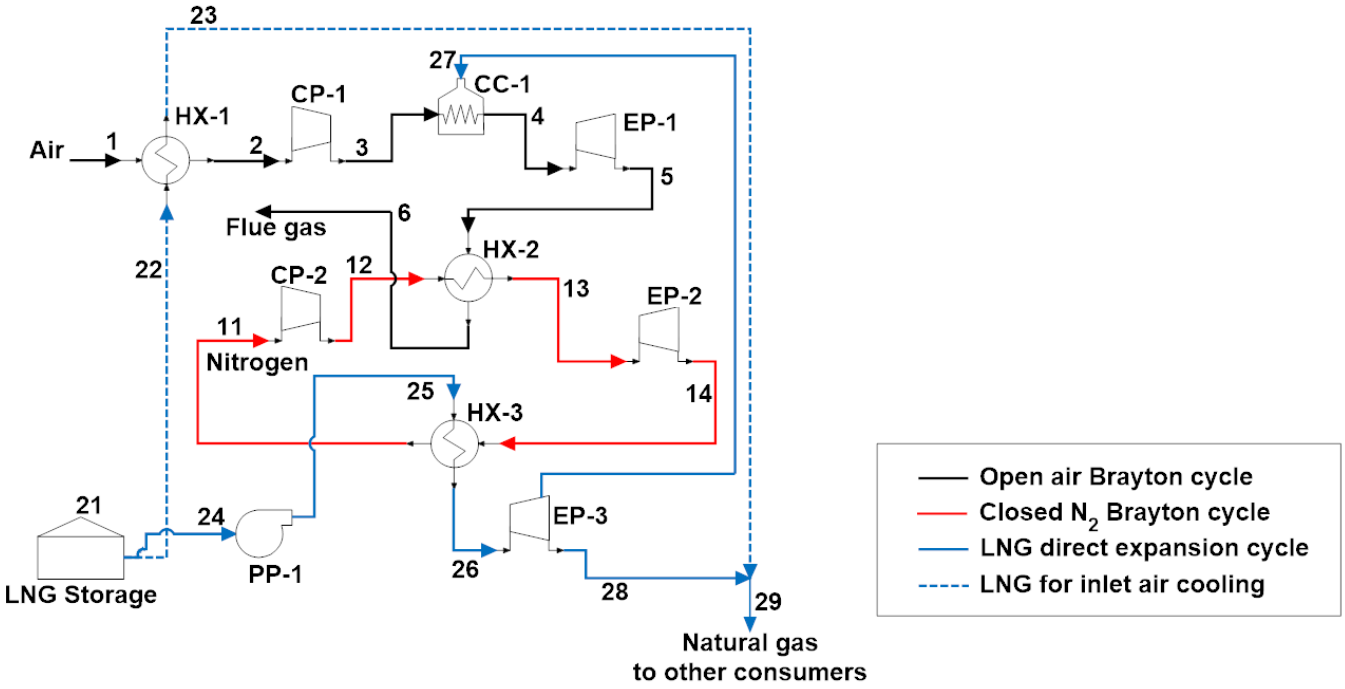

Fig. 4. Schematic diagram of an LNG assisted power cycle

The open air Brayton cycle is indicated by state points (1)-(6). The inlet air is first pre-cooled to 5°C (HX-1) by using ≈ 8.6% of LNG before being compressed to high pressure (CP-1). The compressed air is then mixed with ≈ 9.7% of natural gas from the LNG direct expansion cycle (EP-3) and heated to 1400°C in the combustion chamber (CC-1). The high temperature gas will pass through an expander (EP-1) before rejecting heat to the compressed nitrogen (HX-2).

The closed nitrogen Brayton cycle is indicated by state points (11)-(14) where the cooled nitrogen at -129°C is compressed (CP-2) and heated to ≈ 620°C utilizing the waste heat from the flue gas of the air Brayton cycle (HX-2); the heated nitrogen is then passed through an expander (EP-2) before being cooled in HX-2 by the LNG exiting the pump of direct expansion cycle.

The LNG from the storage tank is split into two streams. One branch (22)-(23) is utilized to precool the inlet air of the open air Brayton cycle, and the other branch (24)-(28) represents the LNG direct expansion cycle. In this second stream, LNG from the storage tank is first pumped to high pressure (PP-1) before heated to about 250°C (HX-3) using the turbine exhaust (EP-2) of nitrogen Brayton cycle. The heated natural gas is then passed through an expander (EP-3) to generate electric energy; part of the natural gas (27) is sent to the open air Brayton cycle, while the rest (28) together with stream (23) will be supplied to the rest of the natural gas consumers.

Table 5
Main parameters and performance for the LNG assisted power cycle

OPERATING PARAMETERS	VALUES
Air BC pressure ratio - (CP-1)	21
Air turbine inlet temperature (°C) - (EP-1)	1400
Pressure drop across heat exchangers (%)- (HX-1, HX-2 & HX-3)	1-3
Compressor isentropic efficiency (%) - (CP-1 & CP-2)	85.0
Turbine isentropic efficiency (%) - (EP-1, EP-2 & EP-3)	90.0
Nitrogen BC pressure ratio - (CP-2)	8.7
Pump isentropic efficiency (%) - (PP-1)	85.0
LNG mass flow rate (kg/s)	2.37
CYCLE EFFICIENCY	
Thermal efficiency (%)	66.5
Exergy efficiency (%)	51.1

The operating parameters used for the LNG assisted power cycle and its performance are shown in Table 5. Fig. 5 shows the exergy flows and the respective exergy destruction in each of the components.

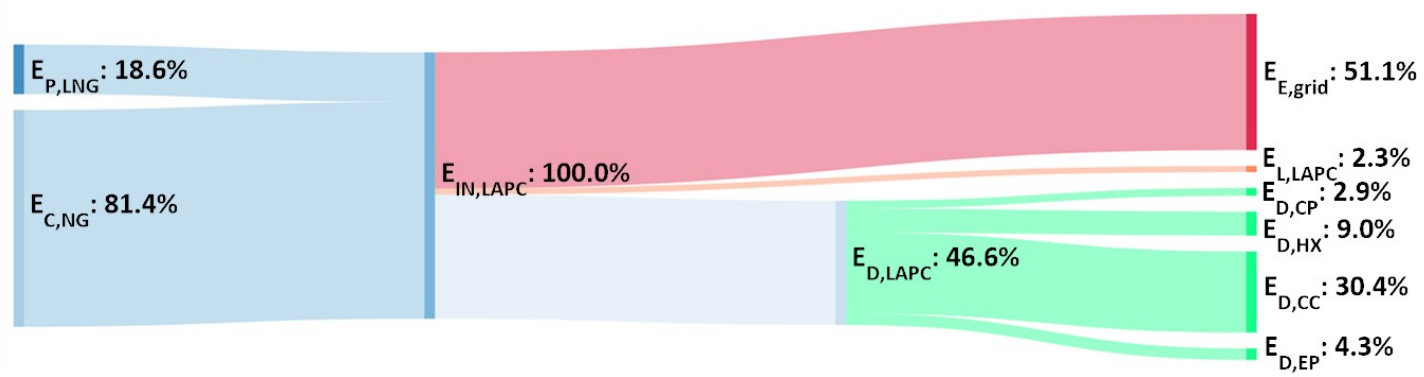

Fig. 5. Exergy flows for the LNG assisted power cycle

For the LNG assisted power cycle, the physical exergy (i.e. cold and mechanical exergy) of LNG ($E_{P,LNG}$) makes a significant contribution to the exergy input (≈ 18.6%) alongside the chemical exergy of the consumed natural gas ($E_{C,NG}$) compared to the baseline combined cycle. The exergy efficiency of the LNG assisted power plant is 51.1%, which is represented by the amount of electricity produced and delivered to the grid. The waste streams ($E_{L,LAPC}$), which mainly consist of the flue gas and regasified LNG, contains exergy amounts to 2.3% of the total exergy input. The exergy destroyed in this LNG assisted power cycle is 46.6%. Similar to the baseline combined cycle, the main exergy destruction occurs in the combustion chamber, mainly due to the chemical reactions and temperature mismatch inside the combustion chamber. Compared to the baseline combined cycle, the exergy destruction inside the heat exchangers is more significant due to the presence of HX-1, where LNG is used to precool the inlet air with more significant temperature mismatch.

3.3 Thermal Networks

In this section, working fluids are considered as cold energy vectors to recover and distribute the LNG cold. In the literature, as shown in Table 3, various hydrofluorocarbon or hydrocarbons have been used as working fluids. However, the interest towards natural working fluids and hydrofluoroolefins as alternative working fluids, especially for long distance downstream cold applications, has recently increased because of the concerns about the global warming potential of the hydrofluorocarbons and safety issues of the hydrocarbons. In [46], three working fluids are considered: water, carbon dioxide and hydrofluoroolefins R1234yf; water is used to provide heating/cooling using its sensible heat, while CO_2 and R1234yf provide heating/cooling using their latent heat. However, R1234yf is not considered in this paper because of its high cost [46].

In this paper, a dual-temperature thermal network is considered with liquid CO_2 and chilled water serving as the energy vectors for high-grade and low-grade cold. The liquid CO_2 will be pumped to the downstream cold applications and it will return in vapor state after the cold energy transfer. In a similar way, the chilled water will be pumped to the downstream cold applications and it will return as warm water. The central plant of the thermal network, where heat exchange between LNG and the working fluids takes place, is shown in Fig. 6. In this setup, the cold applications can choose the appropriate energy vector that suits them the most. For example, deep freezing and district cooling applications will only require cold from the liquid CO_2, whereas an air separation unit and dry ice generation require cold from both chilled water and liquid CO_2. These two classes are illustrated as cold applications X and Y in Fig. 6.

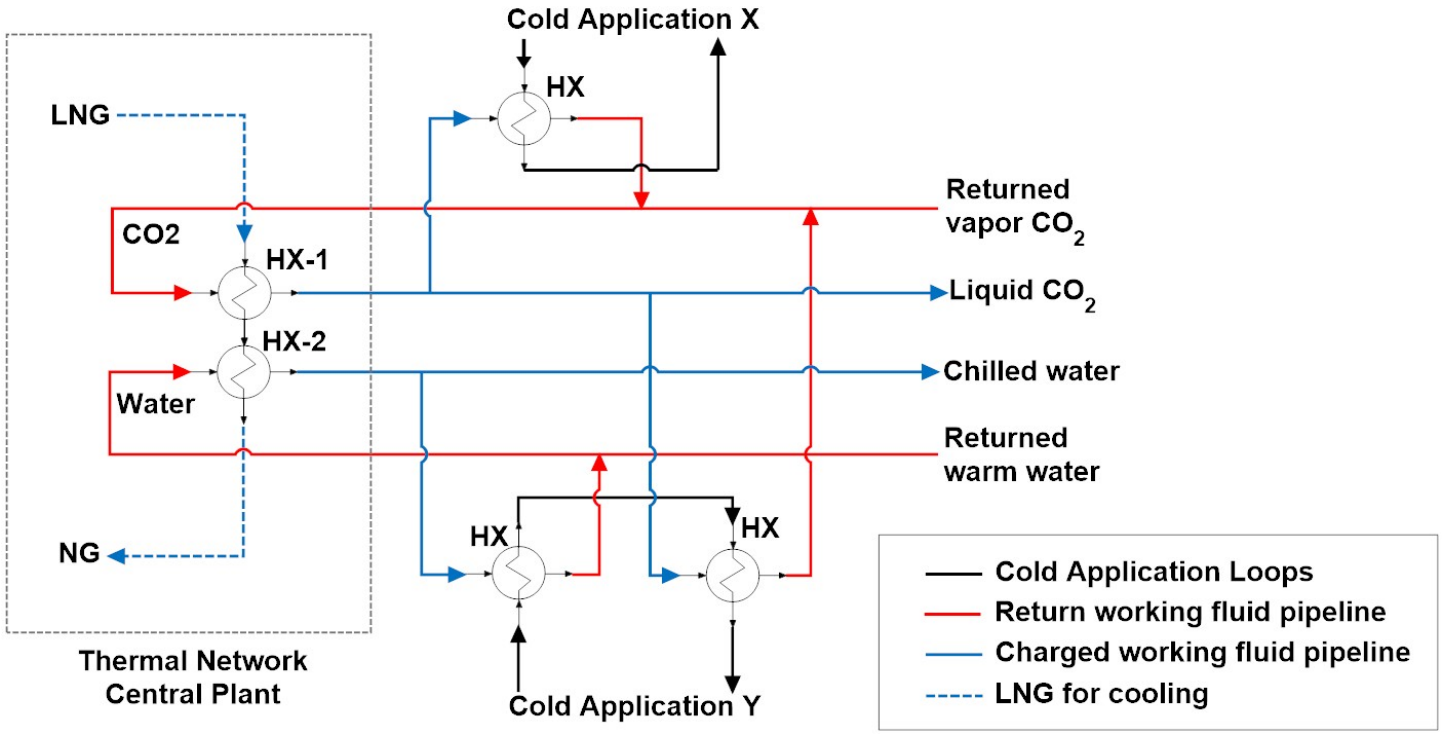

Fig. 6. Schematic diagram of the thermal network

The distribution parameters and required amounts of carbon dioxide and water is tabulated in Table 6 while Fig. *7* shows the exergy flows and exergy destruction in the thermal network central plant.

Table 6
Main parameters and performance for the thermal network

OPERATING PARAMETERS	CO_2	Water
Required mass flow rate (kg/s)	13.0	15.0
Supply temperature (°C)	-50 (liquid)	5
Return temperature (°C)	-50 (vapor)	50
LNG flow rate (kg/s)	7.7	
CYCLE EFFICIENCY		
Exergy efficiency (%)	29.2	

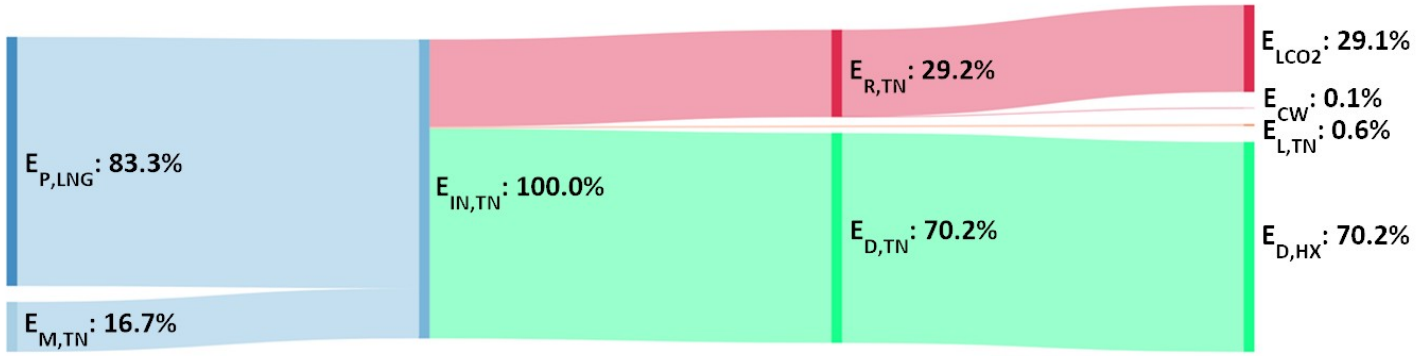

Fig. 7. Exergy flows for the thermal network central plant

In this paper, the pressure of the CO_2 network is set at ≈ 6.8 bar, which corresponds to the boiling temperature of the CO_2 at -50°C. This condition has been chosen as an optimum operating point, considering the triple point of CO_2 and the trade-off if we set higher operating temperature. In fact, when carbon dioxide is flowing at a higher temperature, there will

be a lower thermal loss due to smaller temperature difference with the surroundings. On the contrary, a higher operating temperature corresponds with a lower latent heat, thus resulting in higher mass flow rate of CO_2 required to satisfy the cooling demand. In addition to this, a higher operating temperature also causes a lower efficiency at the cold applications' side, causing the overall exergy efficiency to decrease.

The exergy flow inside the thermal network is shown in Fig. 7. It is found that LNG physical exergy ($E_{P,LNG}$) is the main exergy source, accounting for 83.3% of the total exergy input. The physical exergy of material streams (i.e. the returned vapor CO_2 and warm water) accounts for 16.7% of the total exergy input to the thermal network central plant. The exergy efficiency of the thermal network central plant is 29.2%, which also represents the exergy recovered in the charged energy vectors leaving the thermal network central plant (i.e. liquid CO_2 and chilled water). Waste streams, which include the regasified LNG, accounts for 0.6% of the total exergy input. The main exergy destruction (70.2%) comes from the heat exchangers, which are the only components inside the thermal network central plant. Here, large temperature mismatch occurs during heat exchange between LNG and the energy vectors, leaving high-grade cold exergy of LNG to be unutilized.

3.4 Thermal Storages

Thermal storage is advantageous over other energy vectors such as electricity, CO_2/chilled water due to the large availability of materials for different operating temperatures. This allows for a closer match of the temperature profiles during heat exchange between the thermal storage materials and the different downstream cold applications; in this way it is possible to reduce exergy destruction.

Thermal energy storage can be categorized into two main types: sensible and latent heat storage. Sensible heat is less advantageous compared to latent heat storage when it comes to storage capacity [47]; this means that for a given amount of thermal energy available, more space will be required for sensible heat storage than latent heat storage. Besides, for storage materials that involve solid state and must be transported by truck, a smaller storage capacity simply means that more truck hours are needed to distribute the cold.

In this paper, latent heat storage is used to store the LNG cold energy. Suitable PCMs are chosen from the work of Oro et al. [48]. As shown in Fig. 8, the LNG cold energy is recovered by four different PCMs which match better with the downstream cold applications. The thermo-physical properties of each PCM used are reported in Table 7. The first PCM chosen is a eutectic water salt solution, which is a composition of 24.8 wt.% HCl solution, with a phase change temperature of -86°C, which is the lowest phase change temperature reported in the literature [46].

The second PCM chosen is another eutectic water salt solution, which is a 24 wt.% LiCl solution with a phase change temperature of -67°C [48]. The last two PCMs chosen are two commercial PCM products dedicated for cold storage: SN33, which undergoes phase change at -33°C, and AN03, which undergoes phase change at -3°C [48, 49]. Both PCMs are made of a salt solution encapsulated with spherical molded capsules using blend of a few polyolefins.

Fig. 9 details the exergy flows and destruction inside the thermal storage central plant, where heat exchange between LNG and the PCMs occurs. The LNG will be delivered through a set of heat exchangers, exchanging heat with the four PCMs chosen for the cold storage process. Then the charged PCM will be delivered to the respective cold applications by truck. Upon unloading of the insulation tank containing the charged PCM to the cold applications, the truck will pick up the tank containing the utilized PCM.

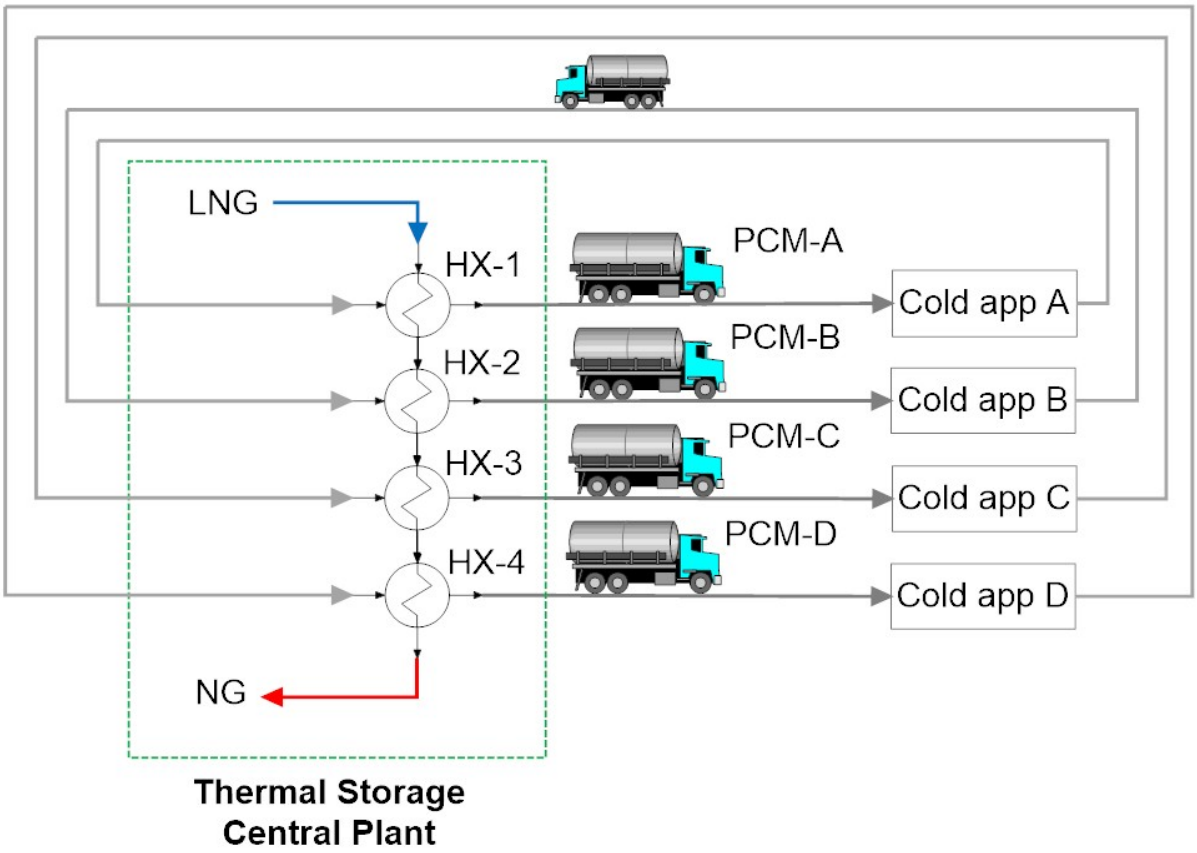

Fig. 8. Schematic diagram of the thermal storage system

Table 7
Main parameters and results for the LNG assisted thermal storage system

OPERATING PARAMETERS	PCM-A	PCM-B	PCM-C	PCM-D
Name / Composition	24.8 wt% HCl	24.0 wt% LiCl	SN33	AN03
Phase Change Temperature (°C)	-86	-67	-33	-3
Latent Heat (kJ/kg)	810	364	245	328
PERFORMANCE PARAMETERS				
Mass Rate (kg/s)	1.7	2.2	12.1	3.1
LNG Flow Rate (kg/s)	7.4			
Exergy Efficiency (%)	24.0			

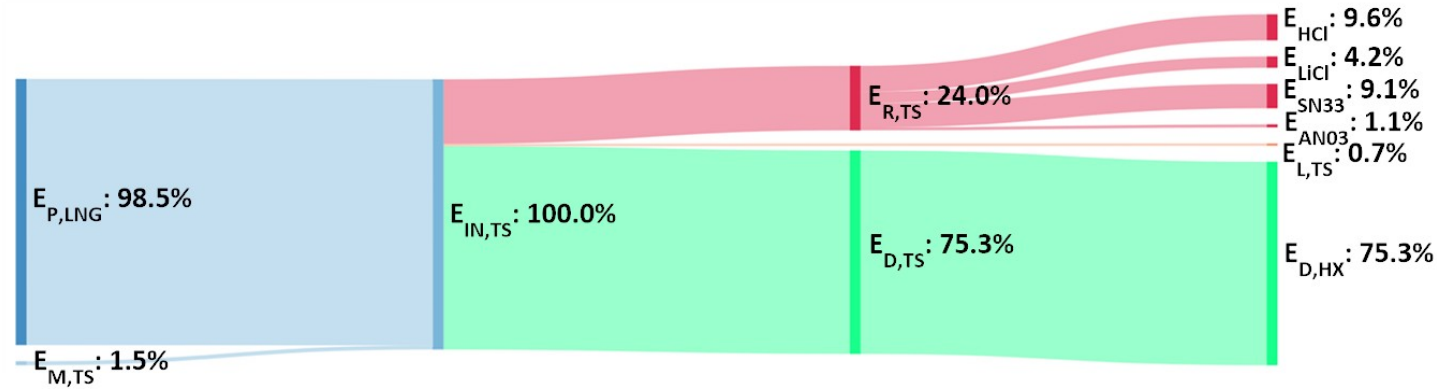

Fig. 9. Exergy flows for the thermal storage central plant

Similar to the thermal network, as shown in Fig. 9, most of the exergy input (98.5%) comes from the physical exergy of the LNG ($E_{P,LNG}$), to be regasified by releasing cold to the PCMs. The inlet material stream consists of exergy of the PCMs to be charged. Similar to the thermal network, due to the unutilized high-grade cold exergy contained in the LNG due to the limitation of the operating temperature of the PCMs, 75.3% of the exergy input is destroyed in the various heat exchangers. The waste stream ($E_{L,TS}$) leaving the thermal storage central plant is the regasified LNG delivered to the consumers. The rest of the exergy (24%) is recovered by the PCMs. The pressure loss in heat exchangers is too small to be shown in the exergy flow diagram (< 0.05%).

3.5 LNG Assisted Air Separation

Liquid air as energy vector is a relatively novel methodology for cogeneration applications. Air is liquefied at -196ºC at ambient pressure. By using liquid air, it is possible to generate both mechanical and cooling power at the same time. The former can be generated by means of isothermal expanders such as reciprocating engines [50] and/or turbines; the latter is generated by recovering the cold energy coming from the regasification of the liquid air (in a similar way as for the LNG) and/or at the exit of the expanders. Liquid air and liquid nitrogen hold very similar thermo-physical properties and often liquid nitrogen is preferred to liquid air as energy vector since it is a byproduct of cryogenic air separation plants.

With the cold input from LNG, it is possible to avoid using the conventional setting of Linde's double separation column to produce liquid air products. In some conventional double column setups, the inlet air is compressed to a high pressure of ≈ 12 MPa [43]. There have been multiple papers discussing air separation operations with cold input from LNG. Innovative layouts have been considered such as single-column [51, 52] and double column processes [53, 54] aimed at reducing the level of compression required below that of the typical air separation plants.

In this paper, a modified version of a double column process will be used to generate the required amount of liquid air products needed (refer to Fig. 10). The inlet air (1) is first compressed (CP-1) to slightly above the pressure of the high-pressure column (HPC) at ≈ 6 bar. The compressed air (2) is then precooled (HX-1) using cooling water (27-28) before passed through a multi stream heat exchanger (MSHE) where the air is cooled by streams of unwanted air products and cold released from LNG regasification. The cooled feed air (4) is then delivered to the HPC and separated into a gaseous high-purity nitrogen stream (7) and an oxygen-enriched stream (5) which is delivered to the low-pressure column (LPC) (6). The gaseous nitrogen stream (7) is then compressed (CP-2) to ≈ 3 MPa (8), before being cooled to its liquid state (9) by the LNG cold energy (23-24) in HX-2. It should be noted that for usage of liquid nitrogen as an energy vector, a high pressure liquid nitrogen corresponds to a lower amount of latent heat. Thus, in this setup, the required amount of liquid nitrogen (LN_2) is extracted (10) and pressure-relieved (11) before being separated into the liquid (12) and vapor nitrogen product (13). The amount of liquid nitrogen produced will depend on the downstream cold applications. The vapor nitrogen generated is sent to the MSHE for feed air cooling purpose. The rest of the high-pressure liquid nitrogen (15) is pressure-relieved and delivered to the low-pressure column (LPC) (16). From the LPC, pure liquid oxygen (17) and waste nitrogen (21) will be produced. As mentioned in Section 1, 1 kg/s of liquid oxygen required will be extracted (18) while the rest (19), together with the waste nitrogen stream (21) will be delivered to the MSHE for feed air cooling. Feed air cooling will also be carried out by the LNG regasification process (25-26).

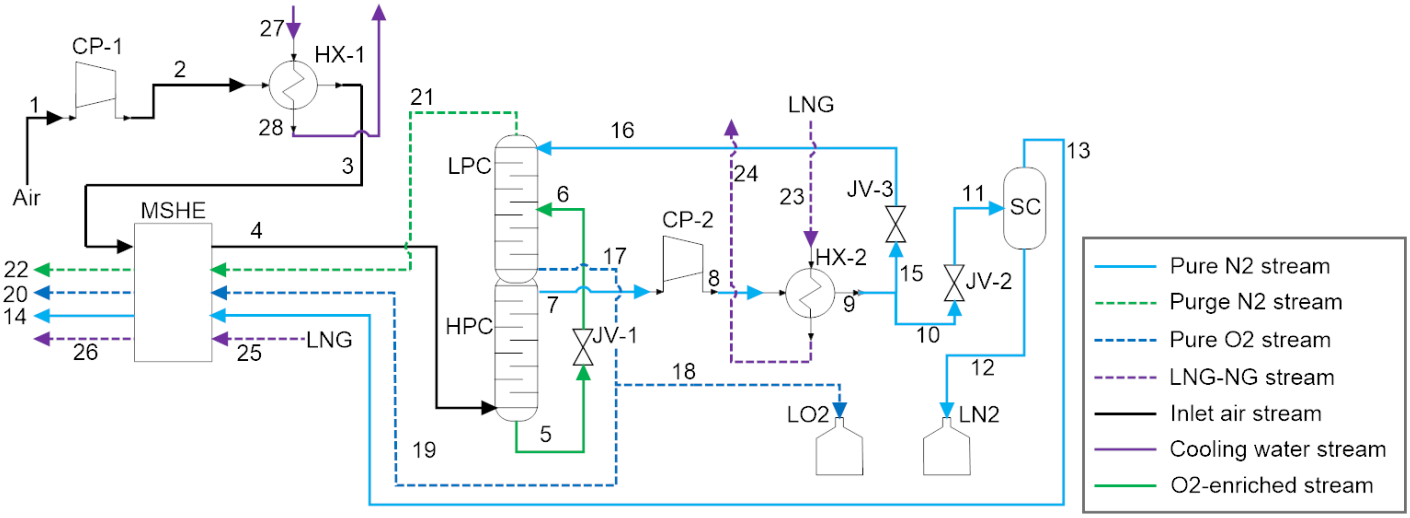

Fig. 10. Schematic diagram of an LNG assisted air separation unit

The parameters and the results of the abovementioned LNG assisted air separation unit is tabulated in Table 8. Fig. 11 details the exergy flows and exergy destruction in the LNG assisted air separation unit.

Table 8
Main parameters and performance for the LNG assisted air separation unit

MAIN PARAMETERS	Value
Pressure of HPC (bar)	5.5
Pressure of LPC (bar)	1.0
Compressor outlet pressure of CP-2 (bar)	30.0
Mass rate of liquid nitrogen produced (kg/s) (12)	5.5
Mass rate of liquid oxygen produced (kg/s) (18)	1.0
LNG flow rate (kg/s)	5.3
PERFORMANCE PARAMETERS	
Exergy efficiency (%)	33.1

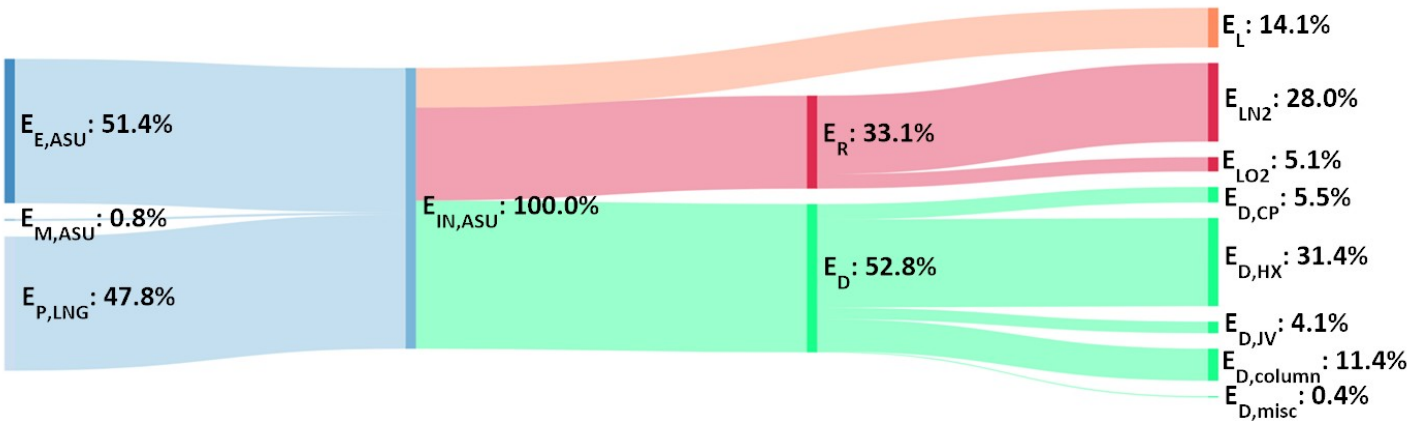

Fig. 11. Exergy flows for the LNG assisted air separation unit

For the LNG assisted air separation unit, the electricity assumed to be supplied from the baseline combined cycle power plant ($E_{E,ASU}$) is the main source of exergy input to drive the two compressors (i.e. inlet air compressor and nitrogen compressor), accounting for 51.4% of the total exergy input. LNG physical exergy ($E_{P,LNG}$) is the second largest exergy source at 47.8%, in which its thermal exergy is used for inlet air cooling in the MSHE and nitrogen liquefaction in HX-2. Material exergy (i.e. cooling water and inlet air) accounts for the rest of exergy input at 0.8%. The exergy efficiency of

the plant is evaluated as 33.1%, which represents the exergy recovered by the liquid nitrogen and liquid oxygen products. Waste stream exergy (E_L), which includes the exergy of cooling water, regasified LNG and side products of the air separation unit (i.e. gaseous nitrogen and gaseous oxygen), accounts for 14.1% of the total exergy input. The total exergy destruction (E_D) of the process is 52.8%, where a substantial amount of 31.4% occurs in heat exchangers (i.e. MSHE, HX-1 and HX-2) where temperature mismatch is the main cause of exergy destruction. Exergy destruction in the separation columns amounts to 11.4%, mainly due to exergy destruction in the distillation column where there is heat exchange in trays, the reflux sections and the distill sections; exergy destruction in other components is 10.0%.

4. Distribution of Energy Vectors

4.1 Electricity Grid

Distribution and transmission losses of electricity via electricity grid is obtained from averaged values over ten years from 2006 - 2015 [55]. The averaged transmission losses via electricity grid is about 5.5%, which directly indicates that the exergy efficiency for the electricity grid is 94.5%.

4.2 Pipeline for CO_2/chilled water

In this paper, insulated pipes are used to distribute liquid CO_2 at -50°C and water at 5°C over a distance of 5 km. The pipes are insulated using fiber glass with thermal conductivity of about 0.04 W/mK [56]. The formulas for calculation of the friction loss and thermal loss are shown in Appendix A.1. Table 9 shows the main parameters and the performance of the liquid CO_2 and chilled water pipelines, respectively.

Table 9
Main parameters and results for the pipeline distribution of liquid CO_2 and water

	Liquid CO_2 pipe	Water pipe
MAIN PARAMETERS		
Velocity of working fluid (m/s)	0.8	1
Inner diameter of pipe (m)	0.134	0.138
Insulation thickness (m)	0.08	0.04
Temperature difference (K)	80	25
PERFORMANCE PARAMETERS		
Pressure loss per length (Pa/m)	52.4	68.7
Friction loss for 5 km pipe (kW)	2.9	5.2
Thermal loss for 5 km pipe (kW)	115.1	61.9

4.3 Trucks for PCMs/liquid nitrogen

As shown in Fig. 8, trucks are being used to distribute the PCMs from the LNG regasification site to the cold applications. Trucks are needed as it is not possible to pump PCMs as they exist in solid and liquid phase.

For the liquid nitrogen energy vector, trucks are used as distribution method because pumping the liquid nitrogen over long distances would likely require an insulation container to prevent high thermal losses and boil-off due to the high temperature difference between the liquid nitrogen and the outer environment. In this case, a semi-trailer truck weighing 40 tons with 20 tons payload is selected as the energy vector carrier. The road transport loss information is obtained from US Environmental Protection Agency [57] and is reported in Table 10.

Table 10
Road transport requirement for a 5 km transportation distance and CO_2 emission [57]

MAIN PARAMETERS	Value
Distance travelled (km)	5.0
Total weight (tonnes)	40.0
PERFORMANCE PARAMETERS	
Diesel consumed (litre)	7.0
CO_2 emission (kg)	18.3

Specially designed containers are used to accommodate the PCMs and the liquid nitrogen. Liquid nitrogen container details are obtained from Linde Engineering [58], while the PCMs in this paper will be transported using tanks with similar parameters.

Table 11
Liquid nitrogen and PCM cryogenic containers information

MAIN PARAMETERS	Value
Payload Weight (tonnes)	20.0
Boil off rate (% per day)	0.3

5. Cold Applications

In this section, the setups of different cold applications with different energy vectors inputs are discussed. The performance of each cold application coupled with its respective energy vector and energy vector generation and distribution is analyzed and discussed. In Sections 5.1 to 5.4, each cold application is assumed to be a stand-alone application and is not part of the same industrial cluster. In Section 5.5, the overall performance of all the cold applications, assumed as parts of a cluster receiving input from different energy vectors, is reported.

5.1 Liquid Air Products Generation

For conventional liquid air products such as liquid nitrogen and liquid oxygen obtained by using electricity as the main exergy input, a modified Linde's double-column system named Heylandt's system is generally used [43].

As shown in Fig. 12a, the inlet air is compressed (CP-1, CP-2, CP-3, CP-4) to ≈ 12 MPa with intercooling using cooling water (HX-1, HX-2, HX-3) (1-9) and aftercooled by cooling water (HX-4) and an R134a heat pump (HX-5) (10). Streams (3) to (5) and (5) to (7) are exact replicates of (1) to (3) and represent the second-stage and third stage compression and intercooling section; hence are not shown. The compressed air is then split into two streams: (11) is passed through an expander (EP-1) and delivered to the high-pressure column (HPC) (12); (13) is cooled with a multi stream heat exchanger (MSHE) to (14) using the waste nitrogen stream (29) and unwanted oxygen stream (26) before being pressure-relieved (15). From the HPC, an oxygen-enriched stream is produced (16) and pressure-relieved (17). Stream (15) then mixes with (17) and is delivered to the low-pressure column (LPC) (18). Another stream produced by the HPC is the high purity liquid nitrogen stream (19), in which the amount required by the market is extracted (20) and the rest (21) is further cooled down (22) in HX-6 using the waste nitrogen stream (28) before being pressure-relieved and delivered to the LPC as reflux stream (23). From the LPC, high purity liquid oxygen stream is produced (24), in which the 1 kg/s market need is extracted (25) while the rest (26) is sent to the MSHE for feed air cooling. The LPC also produces a purge gaseous nitrogen stream (28) which is used to cool (21) before being delivered to the MSHE (29).

Fig. 12b shows the setup of an air separation unit with electricity input (assumed to be obtained from the baseline combined cycle) assisted by cold energy vectors from the thermal network or the thermal storage. The setup is similar to the air separation unit utilizing electricity as the main source of exergy input, with main changes in the four-stage compression and intercooling section. The energy vectors mentioned here can be chilled water/liquid CO_2 if cold is

obtained from the thermal network or PCMs of SN-33 together with 24.8 wt% HCl if cold is obtained from the thermal storage.

The inlet air (1) is compressed (2) and intercooled using chilled water in HX-1 and liquid CO_2 in HX-2 (SN-33 and HCl solution respectively if energy vectors are obtained from thermal storage). Streams (4) to (7) are exact replicates of (1) to (4) and represent the second-stage compression and intercooling section; hence that is not shown. After the third stage of compression (8), the intercooling is carried out using chilled water (or SN-33) in HX-5 and unwanted product streams from the air separation in MSHE-1 to (10), to reduce exergy loss and improve the efficiency of the air separation unit. Upon the last stage of compression (11), aftercooling (11)-(13) is carried out using chilled water and liquid CO_2 (SN-33 and HCl solution) again. The compressed air (13) is then split into two streams, (14) is passed through an expander (EP-1) and delivered to the high-pressure column (HPC) (15); (16) is cooled inside MSHE-2 using waste nitrogen stream (33) and unwanted oxygen stream (29) before being pressure-relieved to (18). From the HPC, oxygen-enriched stream (19) is produced and pressure-relieved (20) before mixed with (18) and delivered to a low-pressure column (LPC) (21). High purity liquid nitrogen stream (22) is produced from the top of the HPC, in which the required 1 kg/s amount required by the market is extracted (23) and the rest (24) is cooled using waste nitrogen stream (32) generated from the LPC in HX-8 to (25) before being pressure-relieved and delivered to the LPC as reflux (26). From the LPC, high purity liquid oxygen stream is produced (27), where 1 kg/s of market need is extracted (28) while the rest is sent to MSHE-2 for feed air cooling purpose (29). Gaseous purge nitrogen stream (32) is generated at the top of the LPC, and is used to cool stream (24) before delivered to MSHE-2 (33). The cooling streams exiting MSHE-2, (30) and (34), which are still at a sub-ambient temperature due to temperature limitation of stream (16), are delivered to MSHE-1 for intercooling purpose.

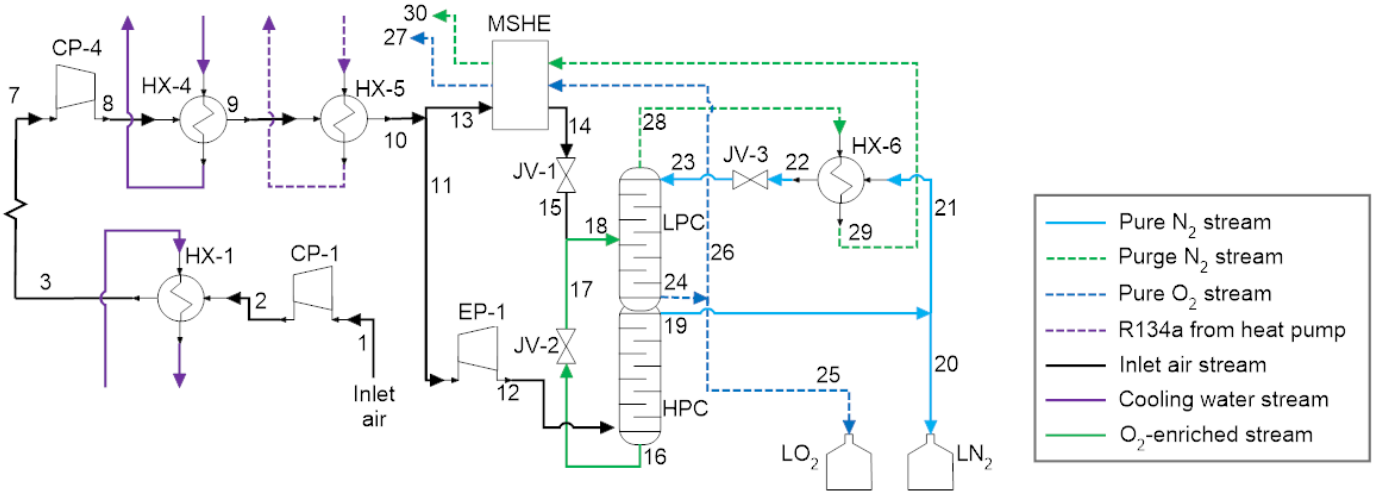

(a)

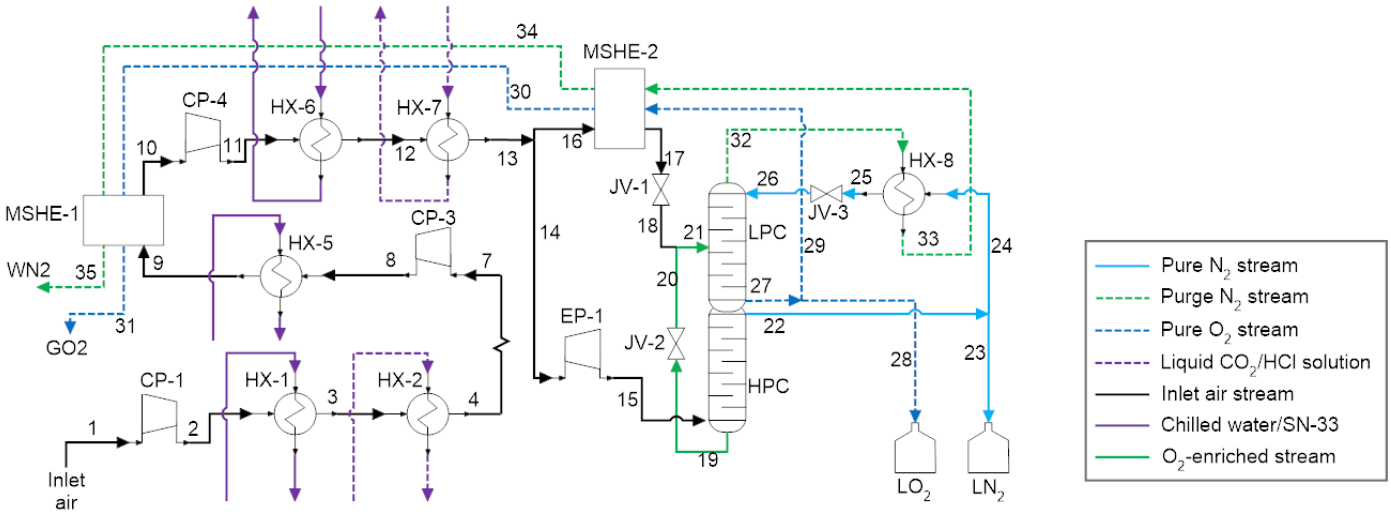

(b)

Fig. 12. Schematic diagram of an air separation unit using energy input of (a) electricity only (b) electricity assisted by liquid CO_2/chilled water/PCM

The results are tabulated in Table 12, which reports the comparison of the performance of the air separation unit using different energy vectors as their main energy input source, and in Fig. **13** which details the exergy flows inside each of the air separation processes.

Table 12
Exergy amounts and performance of air separation units utilizing different energy vectors to produce 1 kg/s liquid nitrogen and 1 kg/s liquid oxygen

Energy Vector	Electricity	Liquid CO_2/water	PCM
SOURCE OF EXERGY INPUT (MW)			
Electricity Exergy, E_E	4.64	3.62	3.59
Exergy of Cold Vectors, $E_{CW}/E_{LCO2}/E_{PCM}$	0.00	0.89	1.12
PERFORMANCE PARAMETER			
Exergy Efficiency (%)	25.61	26.86	25.69

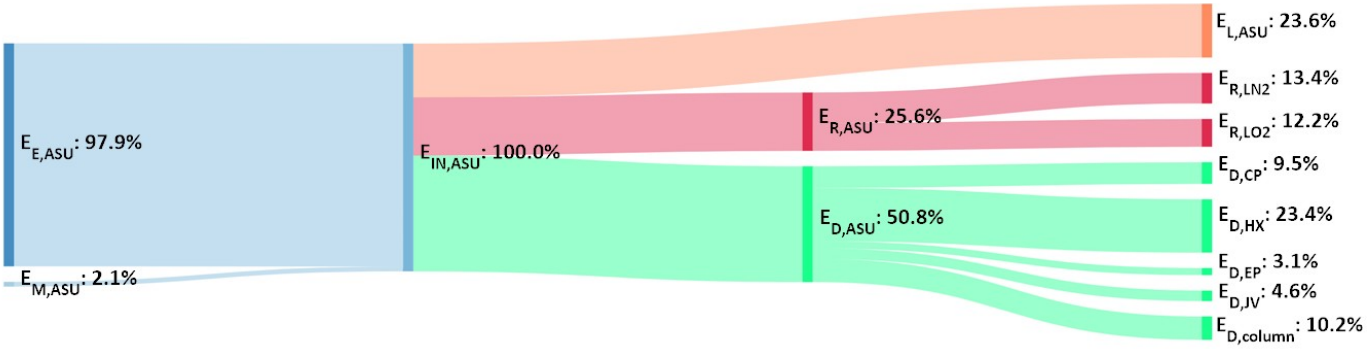

(a)

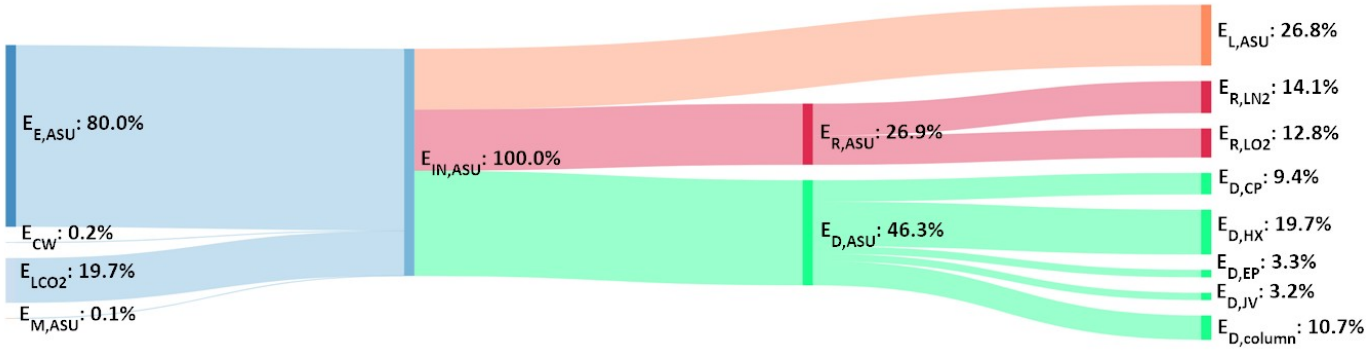

(b)

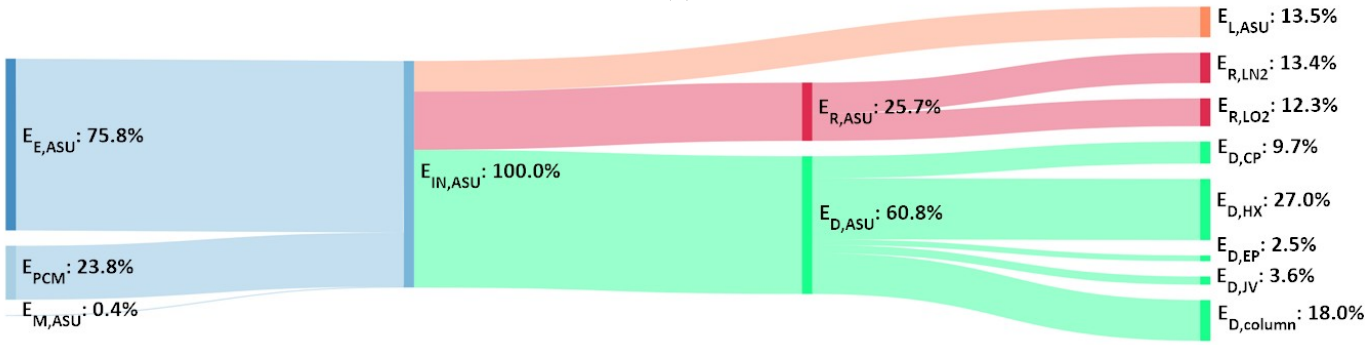

(c)

Fig. 13. Exergy flows for air separation process using (a) electricity input (b) electricity assisted by cold from liquid CO_2/chilled water (c) electricity assisted by cold from PCM

Fig. 13a shows that to produce 1 kg/s of liquid nitrogen and liquid oxygen each by using an air separation unit with mainly electricity input, the major exergy input source comes from the electricity which corresponds with 97.9% of the total exergy input (≈ 4.6 MW) to the air separation unit. Exergy of the waste stream leaving the air separation process is 23.6%, which mainly consists of the heated cooling water for the intercooling of the compressed air and by-products of the air separation process. The total amount of exergy destruction in the air separation unit is 50.8%, which is mainly attributed to the heat exchangers, compressors and the distillation columns. The exergy recovered for the air separation process, which are exergy contained in the liquid air products, is 25.6% of the total exergy input.

Fig. 13b shows the exergy flows inside the air separation unit using cold from liquid CO_2/chilled water as part of the exergy input. Electricity is still needed to drive the compressor work, it can be seen from Table 12 that the dependency on electricity has been significantly reduced to 3.6 MW, which is equivalent to 80.0% of the total exergy input to the air separation unit. The significantly reduced electricity input is due to the more efficient intercooling process when using liquid CO_2/chilled water at a far lower temperature than cooling water, thus allowing the compression work to be reduced. Around 19.7% (or ≈ 0.9 MW) of the total exergy input now comes from the physical exergy contained in the liquid CO_2/chilled water. Exergy of the waste stream is 26.8%, which consists of the heated energy vectors and the unused by-products leaving the air separation process. The total amount of exergy destruction is 46.3%, and is mainly contributed by the heat exchangers, compressors and the distillation column; the exergy recovered by the liquid air products is 26.9%.

Fig. 13c shows the exergy flows inside the air separation unit using cold from PCMs as part of the exergy input. Around 75.8% (≈ 3.6 MW) of the total exergy input comes from electricity which is used to drive the compressors, while 23.8% (≈ 1.1 MW) of the total exergy input comes from the physical exergy of PCMs which provide cold for intercooling. The amount exergy lost via waste streams, which mainly consist of unused by-products of air separation process, is 13.5% of the total exergy input. The amount of exergy destruction is ≈ 60.8%, and is mainly contributed by the heat exchangers, the separation column and the compressors. The amount of exergy recovered by the liquid nitrogen and liquid oxygen is 25.7%.

The results shown in Table 12 and Fig. **13** are the amount of exergy flows inside the air separation unit, in which the input exergy is mainly electricity. In order to understand the performance of the overall process such as the carbon emission reduction of the air separation setup assisted by the cold energy vectors, the amount of electricity consumed needs to be converted to the amount of primary fuel consumed in the baseline combined cycle/LNG assisted power cycle. Similarly, the amount of carbon emission during distribution of PCM by truck also needs to be considered. In Table 13 the amount of primary fuel consumed and the amount of LNG cold energy consumed are reported. The exergy efficiency and the carbon emission of the overall process going from the generation (or charging) of the energy vectors all the way down to their consumption in the cold applications, are also reported; the exergy flows of this process is shown in Fig. 14.

Table 13
Overall exergy input and overall performance of air separation units coupled to different energy vectors

	Baseline	LNG Thermal Cycle	Thermal Network	Thermal Storage
SOURCE OF EXERGY INPUT (MW)				
NG Chemical Exergy, $E_{C,NG}$	9.59	7.83	7.07	7.00
LNG Physical Exergy, $E_{P,LNG}$	0.00	1.79	3.59	4.41
Diesel Fuel Exergy, E_{fuel}	0.00	0.00	0.00	0.12
PERFORMACE PARAMETERS				
Overall Exergy Efficiency (%)	12.4	12.5	10.3	10.1
Overall Carbon Emission (kTPA)	16.64	13.59	12.26	12.41

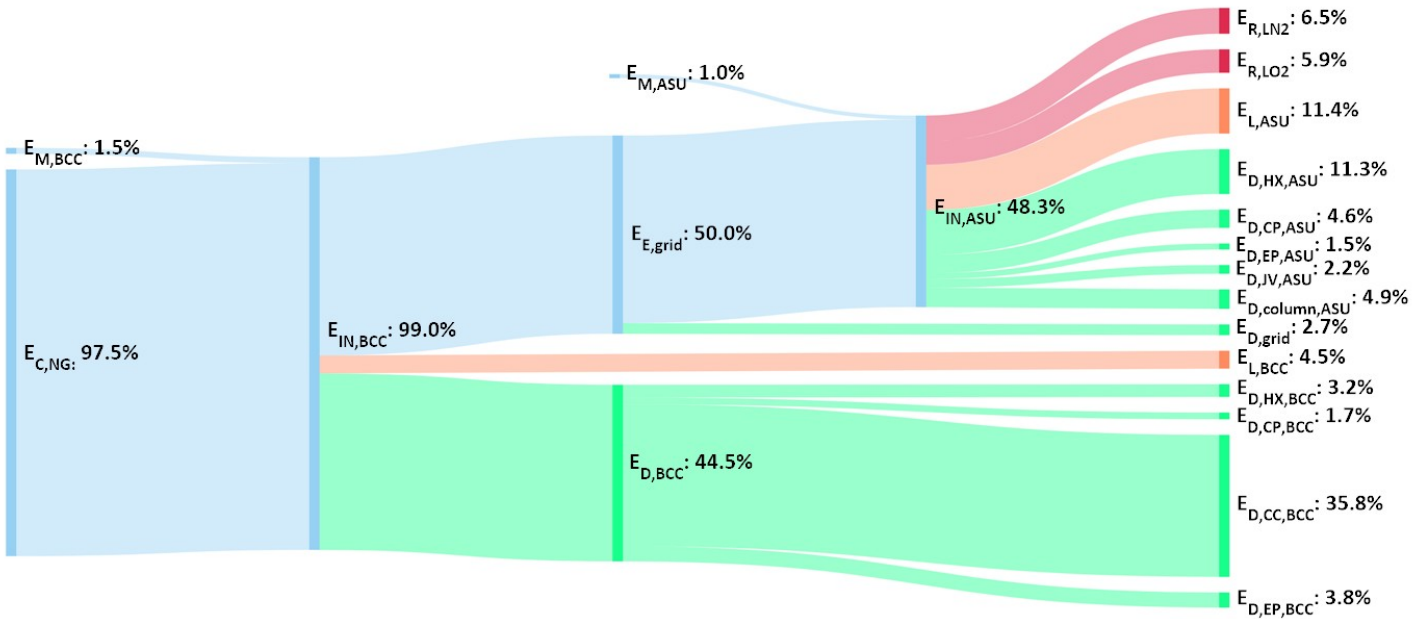

(a)

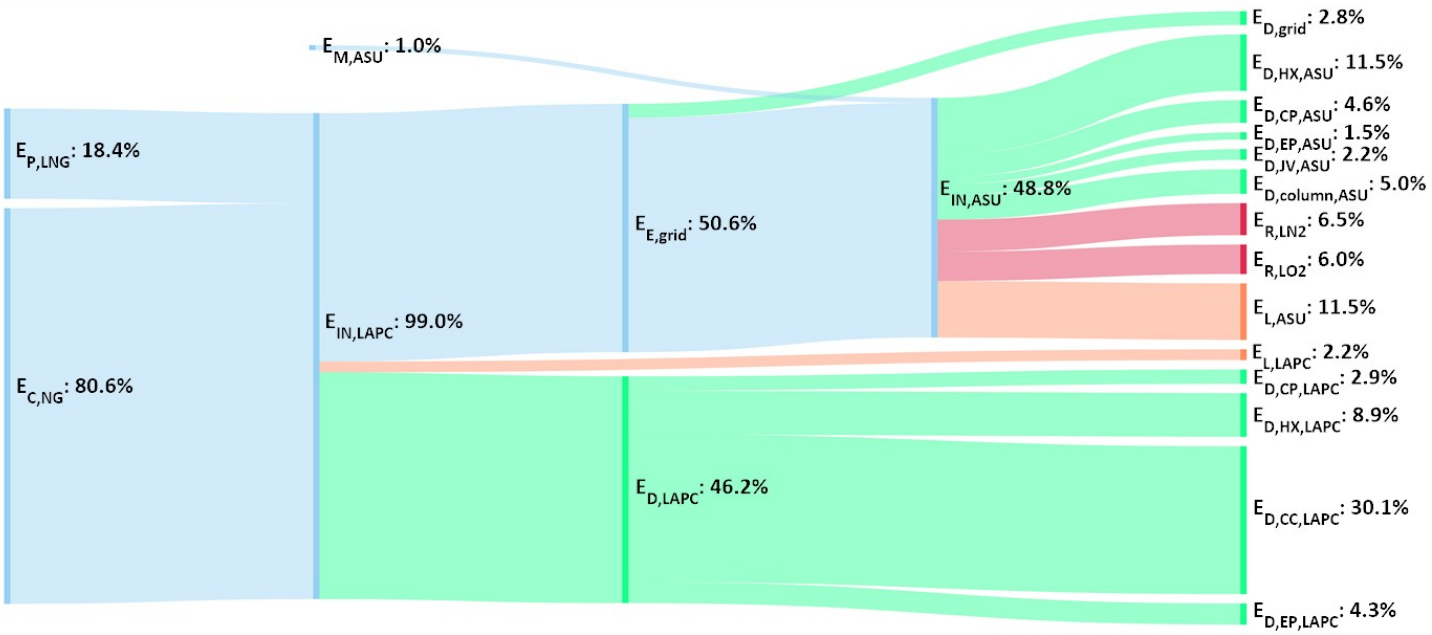
E_M,ASU: 1.0%
E_P,LNG: 18.4%
E_C,NG: 80.6%
E_IN,LAPC: 99.0%
E_E,grid: 50.6%
E_D,LAPC: 46.2%
E_IN,ASU: 48.8%
E_D,grid: 2.8%
E_D,HX,ASU: 11.5%
E_D,CP,ASU: 4.6%
E_D,EP,ASU: 1.5%
E_D,JV,ASU: 2.2%
E_D,column,ASU: 5.0%
E_R,LN2: 6.5%
E_R,LO2: 6.0%
E_L,ASU: 11.5%
E_L,LAPC: 2.2%
E_D,CP,LAPC: 2.9%
E_D,HX,LAPC: 8.9%
E_D,CC,LAPC: 30.1%
E_D,EP,LAPC: 4.3%

(b)

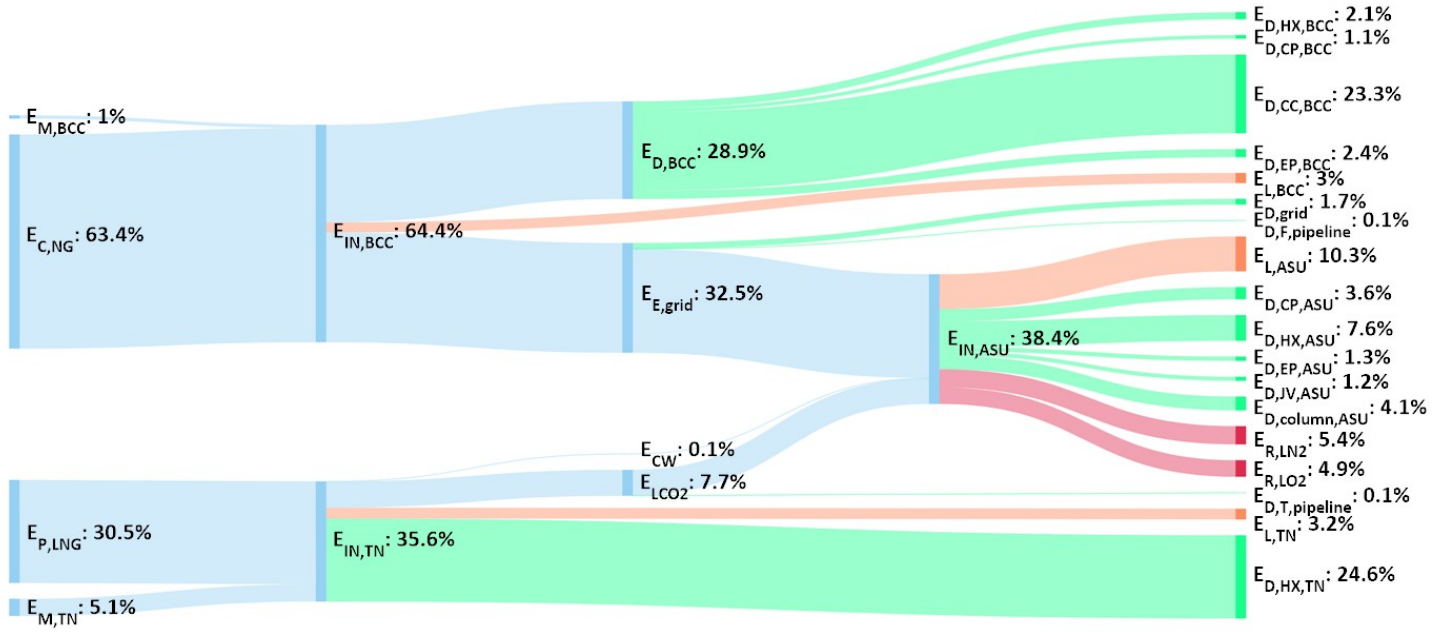
E_M,BCC: 1%
E_C,NG: 63.4%
E_P,LNG: 30.5%
E_M,TN: 5.1%
E_IN,BCC: 64.4%
E_IN,TN: 35.6%
E_D,BCC: 28.9%
E_E,grid: 32.5%
E_CW: 0.1%
E_LCO2: 7.7%
E_IN,ASU: 38.4%
E_D,HX,BCC: 2.1%
E_D,CP,BCC: 1.1%
E_D,CC,BCC: 23.3%
E_D,EP,BCC: 2.4%
E_L,BCC: 3%
E_D,grid: 1.7%
E_D,F,pipeline: 0.1%
E_L,ASU: 10.3%
E_D,CP,ASU: 3.6%
E_D,HX,ASU: 7.6%
E_D,EP,ASU: 1.3%
E_D,JV,ASU: 1.2%
E_D,column,ASU: 4.1%
E_R,LN2: 5.4%
E_R,LO2: 4.9%
E_D,T,pipeline: 0.1%
E_L,TN: 3.2%
E_D,HX,TN: 24.6%

(c)

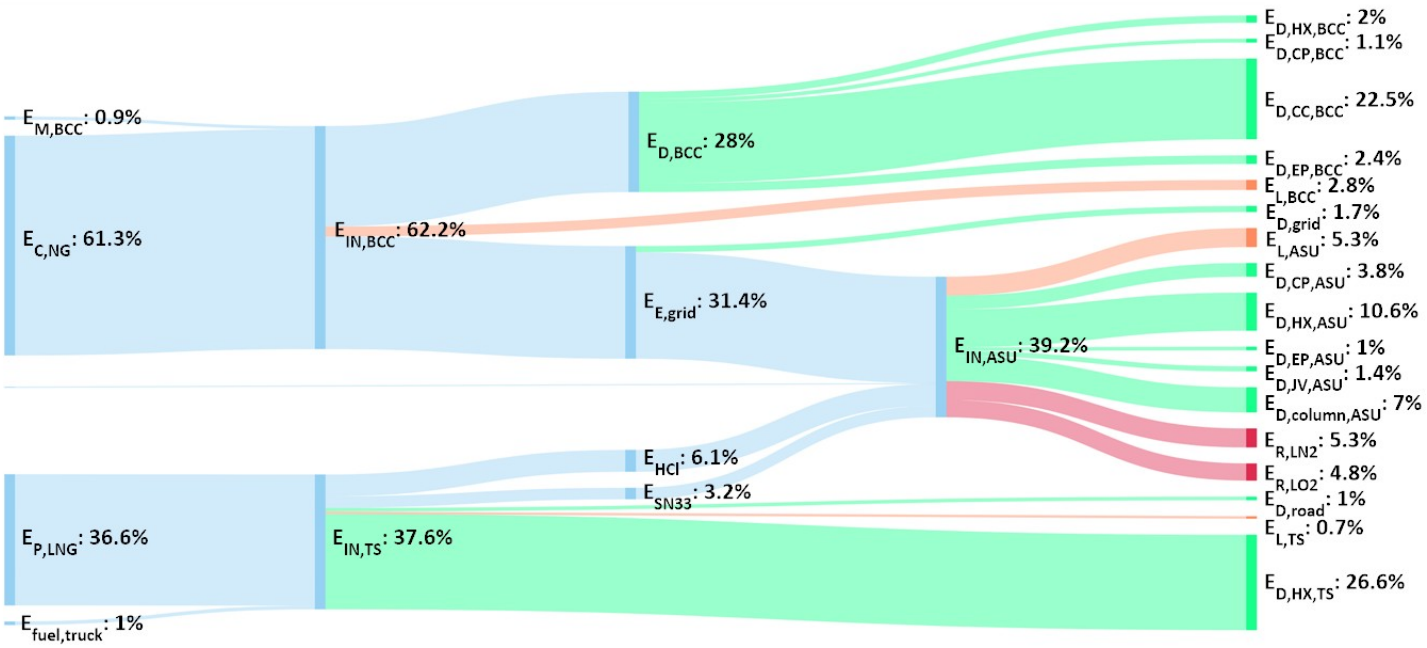

(d)

Fig. 14. Overall exergy flows for air separation process downstream of (a) baseline combined cycle (b) LNG assisted power cycle (c) thermal network (d) thermal storage

Fig. 14a shows the overall exergy flows for an air separation unit coupled to the baseline combined cycle for the stated amount of liquid air products. Around 97.5% (or ≈ 9.6 MW) of the entire exergy input to the whole system (i.e. combined cycle for electricity generation and air separation unit where liquid air products are generated), comes from the chemical exergy contained in the natural gas fuel, while 1.5% of the total exergy input comes from the physical exergy of materials input (i.e. inlet air and cooling water) into the combined cycle, and the rest comes from the physical exergy of materials input to the air separation unit. As discussed in Section 0, the exergy efficiency of the baseline combined cycle is 50.5%, generating electricity amounts to 50.0% of the total exergy input which is subsequently delivered to the grid. Exergy of the waste stream in the combined cycle accounts for 4.5% of the total exergy input, while the total exergy destruction in the combined cycle accounts for 44.5% of the total exergy input, with the main source of exergy destruction from the combustion chamber, which accounts for 35.8% of the total exergy input. Exergy destruction due to transmission and distribution losses accounts for 2.7% of the total exergy input to the system. Thus, the electricity exergy that reaches the air separation unit is 47.3% of the total exergy input. Inside the air separation unit, the exergy destruction accounts for 24.5% of the total exergy input, with the main sources of exergy destruction (11.3% of total exergy input) in the heat exchangers and the MSHE. The waste streams leaving the air separation unit account for 11.4% of the total exergy input, while the liquid air products (i.e. liquid nitrogen and liquid oxygen) account for 12.4% of the total exergy input.

For an air separation unit coupled to the LNG assisted power cycle for generation of the stated amount of liquid air products, as shown in Fig. 14b, 18.4% (or ≈ 1.8 MW) of the total exergy comes from the physical exergy of LNG to be regasified in the LNG assisted power cycle. Exergy contained in other material streams (i.e. inlet air) is too small to be shown in the exergy diagram. Around 80.6% (or ≈ 7.8 MW) of the total exergy input to the system comes from the chemical exergy of the natural gas consumed by the power cycle. The exergy efficiency of the LNG assisted power cycle is 51.1%, with the main source of exergy destruction in the combustion chamber, which accounts for 30.0% of the total exergy input. Due to existence of larger temperature mismatch, the amount of exergy destruction in the heat exchangers is significantly higher compared to the air separation unit coupled to the baseline combined cycle, and is around 8.9%. Exergy destruction for the rest of the components in the LNG assisted power cycle accounts for 2.9% of the total exergy input. Thus, the total exergy destruction amounts to 46.1% of the total exergy input while the exergy of the waste streams leaving the LNG assisted power cycle accounts for 2.3% of the total exergy input. Theexergy distribution and destruction/losses in the air separation unit are very similar to the air separation unit discussed earlier.

For an air separation unit coupled to the thermal network, alongside the cold energy obtained from the thermal network, electricity from the baseline combined cycle is required as energy input to drive the compressors. As shown in Fig. 14c, 63.4% (or ≈ 7.1 MW) of the total exergy input is obtained from the chemical exergy of the natural gas consumed in the baseline combined cycle to generate electricity, and exergy of the material streams input to the baseline combined cycle accounts for 1.0% of the total exergy input. The baseline combined cycle produces electricity which is distributed by the grid along the same assumed distance of 5 km before reaching the air separation unit, and the detailed exergy flows and destruction inside the baseline combined cycle are similar to that explained in Section 3.1. The amount of electricity entering the air separation unit accounts for 30.7% of the total exergy input. Around 30.5% (or ≈ 3.6 MW) of the total exergy input comes from the physical exergy of LNG regasified in the thermal network central plant. The rest of the exergy input comes from the material streams input to the thermal network (i.e. vapor CO_2 and warm water). Inside the thermal network central plant, due to the large temperature mismatch and thus wastage of high-grade exergy contained in the LNG, the amount of exergy destruction in the heat exchangers is high and accounts for 24.6% of the total exergy input. Exergy of the waste stream leaving the thermal network is ≈ 3.2% of the total exergy input, and is mainly contributed by the physical exergy contained in the regasified LNG. The exergy contained in the liquid CO_2 and chilled water leaving the thermal network central plant and entering the pipeline accounts for 7.8% of the total exergy input. During the pipeline distribution, the exergy destruction due to thermal and friction losses accounts for 0.1% of the total exergy input each. The exergy of the liquid CO_2 and chilled water entering the air separation unit accounts for 7.7% of the total exergy input. Inside the air separation unit, the total exergy destruction is 17.8%, where the main source of exergy destruction is in the heat exchangers and the MSHEs. Exergy of the waste streams leaving the air separation unit is 10.3% of the total exergy input, in which 5.1% of the total exergy input is contained in the consumed energy vectors (i.e. vapor CO_2 and warm water) which will be returned to the thermal network central plant as material stream. The exergy contained in the useful air products (i.e. liquid oxygen and liquid nitrogen) accounts for 10.3% of the total exergy input, which means that the overall exergy efficiency investigated here is at 10.3%.

Fig. 14d shows the exergy flows of an air separation unit coupled to the thermal storage. Similar to the air separation coupled to the thermal network, electricity will be obtained from the baseline combined cycle to drive the compressors. Around 61.3% (or ≈ 7.0 MW) of the total exergy input comes from the chemical exergy contained in the natural gas consumed by the combined cycle. With 0.9% of the exergy input from material streams to the combined cycle, electricity, representing 29.7% of the total exergy input, is supplied to the air separation unit. Around 36.6% (or ≈ 4.4 MW) of the total exergy input to the system comes from the physical energy contained in the LNG to be regasified in the thermal storage central plant. Exergy of the waste stream leaving the thermal storage central plant, which is mainly contributed by the regasified LNG, amounts to 0.7% of the total exergy input. The exergy destruction in the thermal storage mainly occurs in the heat exchangers, and amounts to 26.6%. The PCMs leaving the thermal storage contain 9.3% of the total exergy input. For distribution of the PCMs by truck, 1.0% of the total exergy is destroyed due to transport loss, and is compensated by the chemical exergy contained in the diesel fuel consumed by trucks. Due to the good thermal insulating properties of the cryogenic tanks, the thermal loss during distribution is negligible. Inside the air separation unit, the total exergy destruction accounts for 23.8% of the total exergy input, with the main source of exergy destruction from the heat exchangers. Exergy of waste stream leaving the air separation unit amounts to 5.3% of the total exergy input, while the useful air products accounts for 10.1% of the total exergy input.

It is observed from Table 13 and Fig. 14 that the air separation unit coupled to the LNG assisted power cycle has the highest overall exergy efficiency among all the air separation units coupled to different energy vectors. This is because of the advantage over the air separation unit coupled to the baseline combined cycle by significantly reducing the amount of natural gas consumed by the power cycle. However, the advantage is not considerable as it is taking in a significant amount of exergy from the physical exergy contained in the LNG, which is originally meant to be wasted if not utilized. For air separation unit coupled to a thermal network or a thermal storage, the dependency on cold exergy contained in the LNG has significantly increased, thus reducing the overall exergy efficiency of these setups. For the comparison of the overall carbon emission for the different setups of air separation units, due to the large consumption of natural gas, air separation unit coupled to the baseline combined cycle yields the highest overall carbon emission, followed by air separation unit coupled to the thermal network. Due to similarity in the setups, air separation units coupled to the thermal storage and

thermal network yield the least carbon emission due to their significantly reduced compression work, which is caused by the presence of the sub-ambient temperature energy vectors that provide cold energy for intercooling process.

5.2 Dry Ice Production

Four different setups have been considered according to the energy vectors utilized by the dry ice production. Fig. 15a shows the setup of a conventional dry ice production using electricity as the main energy vector input described by Arora [44]. Inlet CO_2 (1) is firstly mixed with recycled CO_2 from the snow chamber (12) to lower its temperature. The mixed stream is then compressed to a pressure slightly above the triple point of CO_2 (3) before being cooled using cooling water to (4). Then it is mixed with another recycled stream from the separation column (13) before being further compressed to ≈ 20 bar (6). The compressed CO_2 is then cooled by a water cooler (7) and an R134a heat pump (represented by state (21)-(24)) to liquid state (8), before being pressure-relieved to a pressure slightly above its triple point (9). Here the liquid CO_2 is separated from its vapor state; the vapor state is recycled (12) and the liquid CO_2 is sent to the snow chamber (10), where dry ice is collected as the output product (11). For the snow chamber, the entering liquid CO_2 is at a pressure slightly above the triple point; the liquid CO_2 will be pressure-relieved in this specially designed snow chamber.

The dry ice production using liquid CO_2/chilled water as assistive source of energy input is shown in Fig. 15b. The process is similar to the conventional dry ice production process, but modified with a few more cooling steps to reduce the amount of compression work. Inlet CO_2 (1) is first precooled using liquid CO_2 from the thermal network to about -40^{0}C (2). It is then mixed with recycled CO_2 from the snow chamber (15) to reduce temperature (3) and compression work. The mixed stream is then compressed to slightly above the CO_2 triple point pressure (4) before being cooled by chilled water in HX-2 and liquid CO_2 in HX-3 respectively to state (6). Then it is mixed with the recycled CO_2 from the separation column (13) before being further compressed to ≈ 10 bar (8). Further cooling is done by chilled water in HX-4 (9) and liquid CO_2 from thermal network in HX-5 (10). The liquefied CO_2 is then pressure-relieved (11) and separated into its liquid (12) and vapor phase (13). Liquid CO_2 from the separation column is then delivered to the snow chamber to be processed into dry ice while the vapor phase is recycled for cooling purposes.

The dry ice production mechanisms using electricity as main energy input or that using electricity with chilled water/liquid CO_2 exergy input require two stage compression because of the high CO_2 liquefaction pressure due to unavailability of cold source at suitable low temperature. Two-stage compression with intercooling will thus minimize the required compression power.

With availability of lower temperature cold sources such as PCMs, which operate at low enough temperatures, the CO_2 compressor outlet pressure can be further reduced, simplifying the whole setup into a single compression process as shown in Fig. 15c. In this setup, a salt solution [48] consisting of 24 wt% LiCl is used as the PCM with phase change temperature of -67°C. The input CO_2 (1) is first precooled using cold released from the PCM (2), before being mixed with the recycled CO_2 from the snow chamber (3). The mixed CO_2 is then compressed to a pressure just above the triple point (4) and is cooled using cooling water (5) and PCM (6) to its liquid state before delivered to the snow chamber.

With liquid nitrogen as energy vector, as shown in Fig. 15d, dry ice production is also a simple compression process. The inlet CO_2 (1) is mixed with recycled CO_2 (8) from the snow chamber (2), before being compressed to ≈ 8.5 bar (3) using mechanical power generated during the expansion of liquid nitrogen. The compressed CO_2 is then cooled to state (4) by using cooling water and state (5) using a mix of water-glycol and boiling nitrogen (13) exitiing the isothermal expander (EP-1), before being delivered to the snow chamber. In this case the CO_2 compressor outlet pressure is set at 8.5 bar, which is optimized based on the amount of liquid nitrogen needed and the availability of mechanical energy in the liquid nitrogen supplied to the expander. Inside the isothermal expander (EP-1), the liquid nitrogen (12) is mixed with water-glycol solution (11) and is evaporated, generating mechanical power. The mixture (13) is then delivered to HX-2 to liquefy the CO_2 prior to be discharged (14).

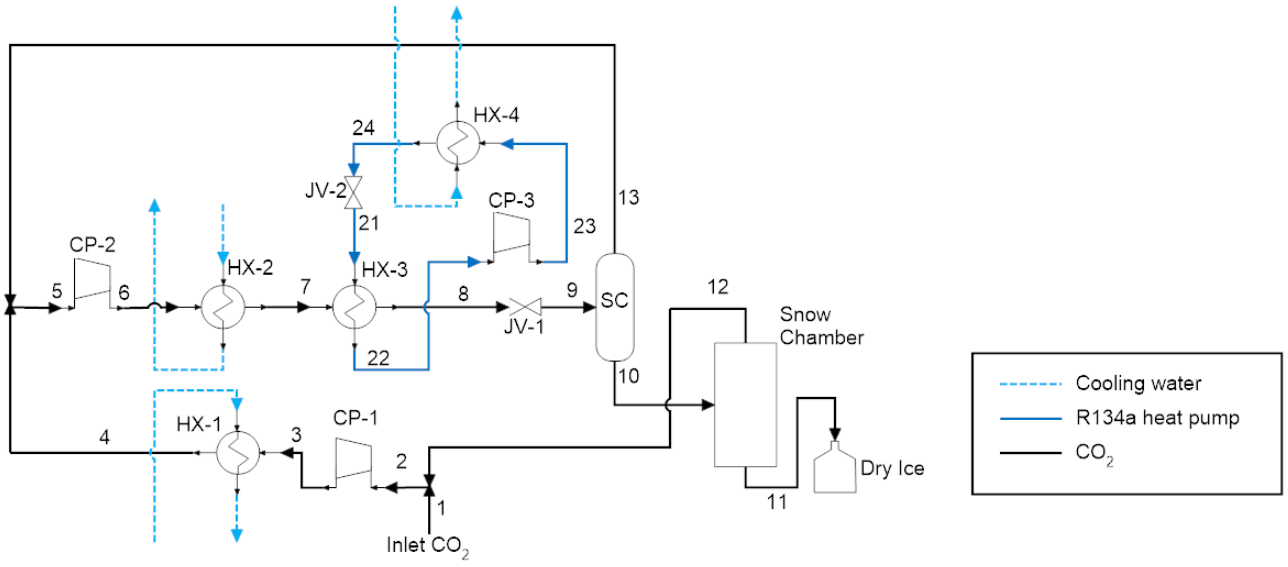
HX-4
24
JV-2
21
CP-3
23
13
CP-2
5
6
HX-2
7
HX-3
8
9
SC
12
Snow
Chamber
JV-1
22
10
HX-1
4
3
CP-1
2
1
Inlet CO_2
Dry Ice
11
Cooling water
R134a heat pump
CO_2

(a)

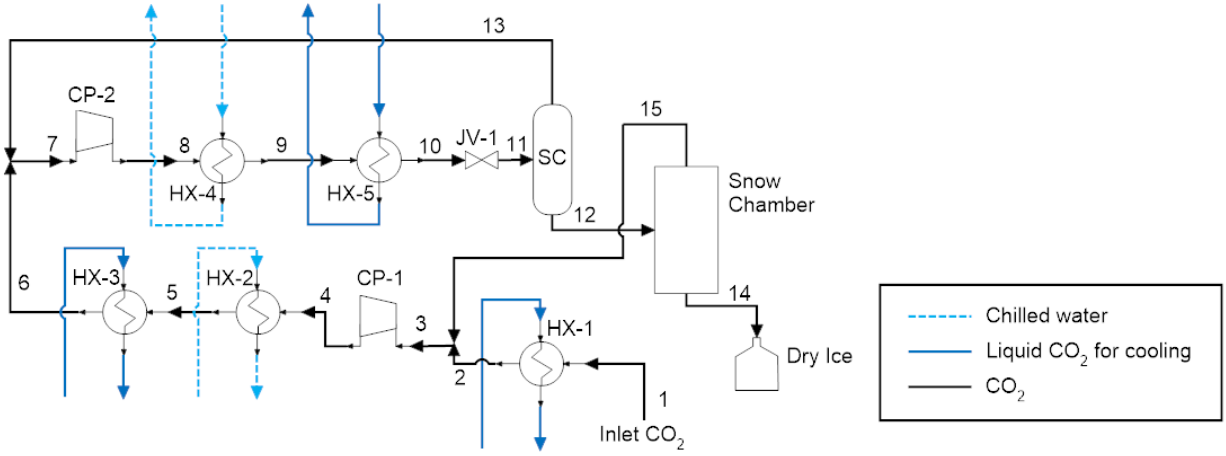
13
CP-2
7
8
9
10
JV-1
11
SC
15
Snow
Chamber
HX-4
HX-5
12
6
HX-3
5
HX-2
4
CP-1
3
HX-1
2
1
Inlet CO_2
14
Dry Ice
Chilled water
Liquid CO_2 for cooling
CO_2

(b)

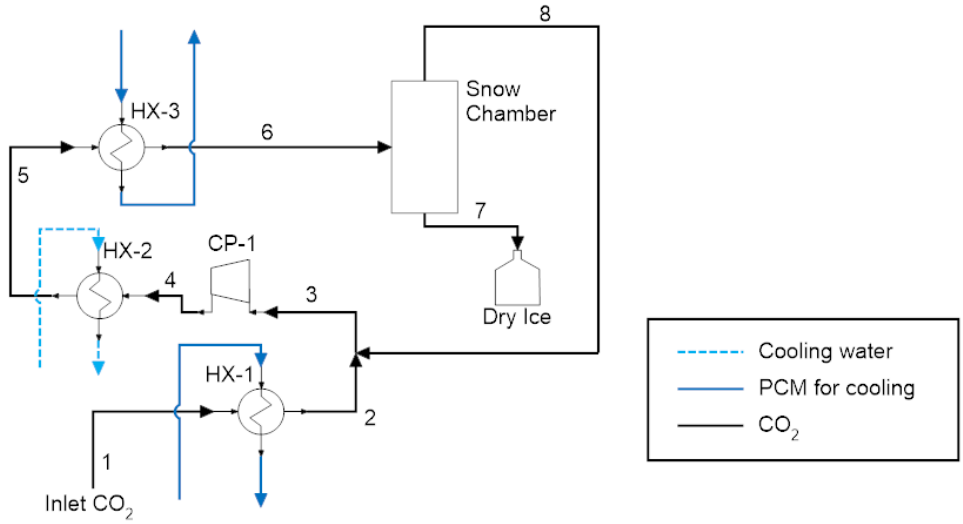
8
HX-3
Snow
Chamber
6
5
7
HX-2
CP-1
4
3
Dry Ice
HX-1
2
1
Inlet CO_2
Cooling water
PCM for cooling
CO_2

(c)

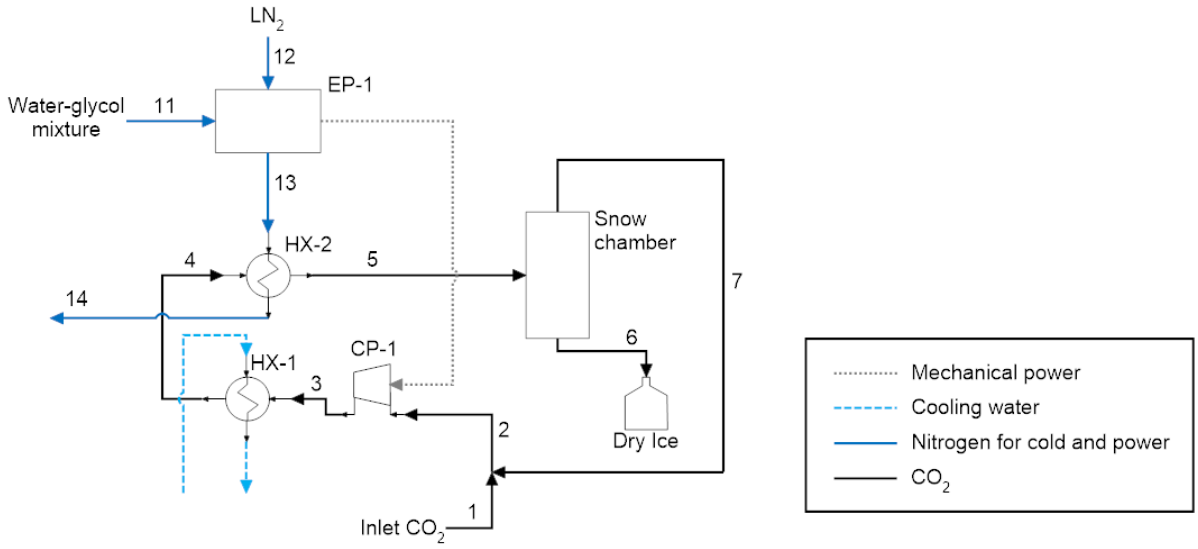

(d)

Fig. 15. Schematic diagram of the dry ice production using energy input of (a) electricity only (b) electricity and liquid CO_2/chilled water (c) electricity and thermal storage (d) liquid nitrogen only

Table 14
Input exergy amounts and performance by utilizing different energy vectors to produce 1 kg/s dry ice

Energy vector	Electricity	Liquid CO_2/water	PCM	LN_2
SOURCE OF EXERGY INPUT (MW)				
Electricity Exergy, E_E	0.79	0.24	0.18	0.00
Exergy of Cold Vectors, $E_{CW}/E_{LCO2}/E_{PCM}/E_{LN2}$	0.00	0.49	0.32	1.22
PERFORMANCE PARAMETER				
Exergy Efficiency (%)	32.99	39.98	58.27	23.84

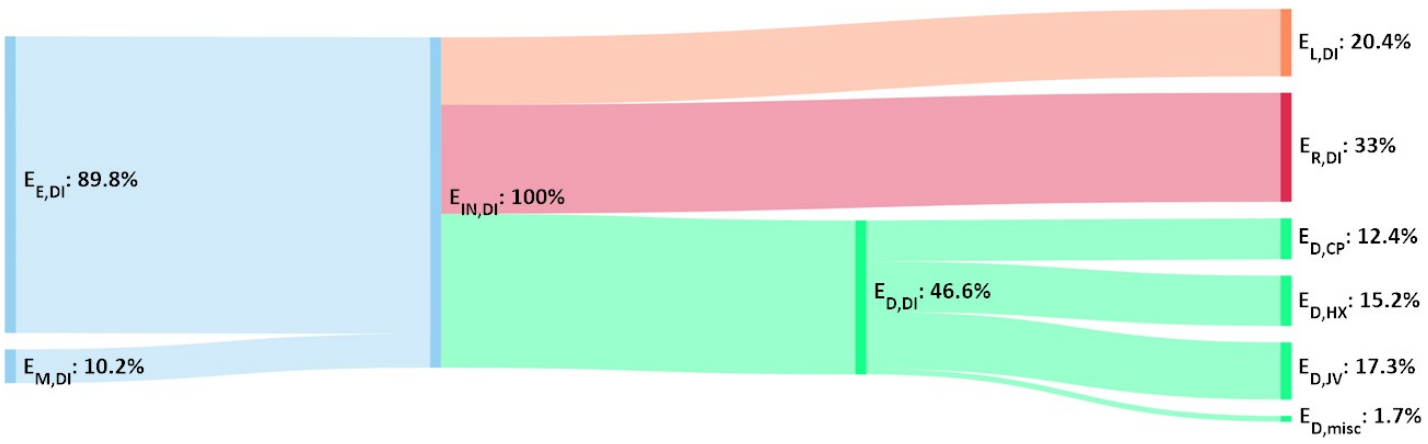

(a)

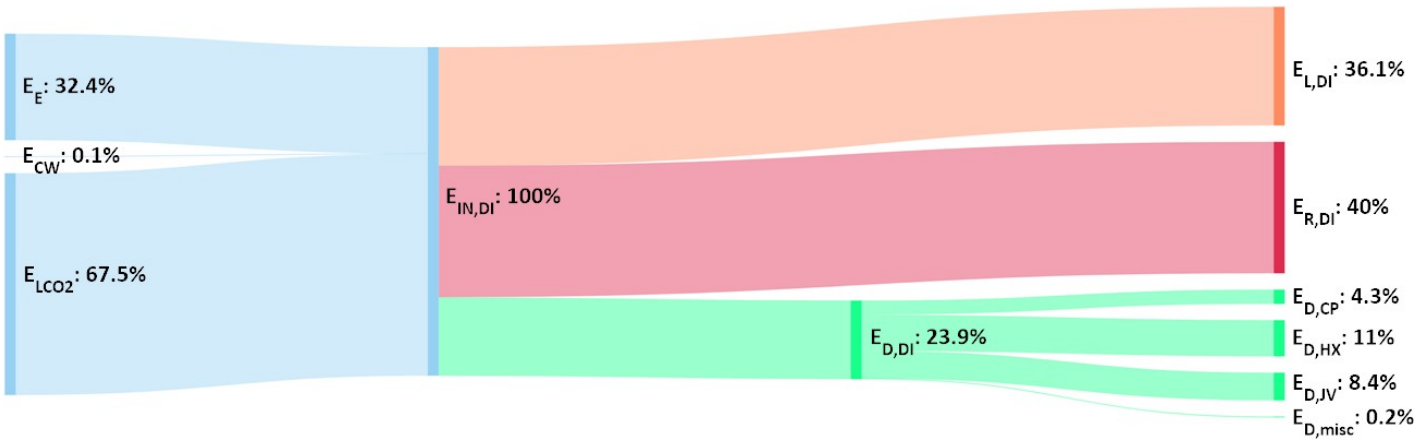

(b)

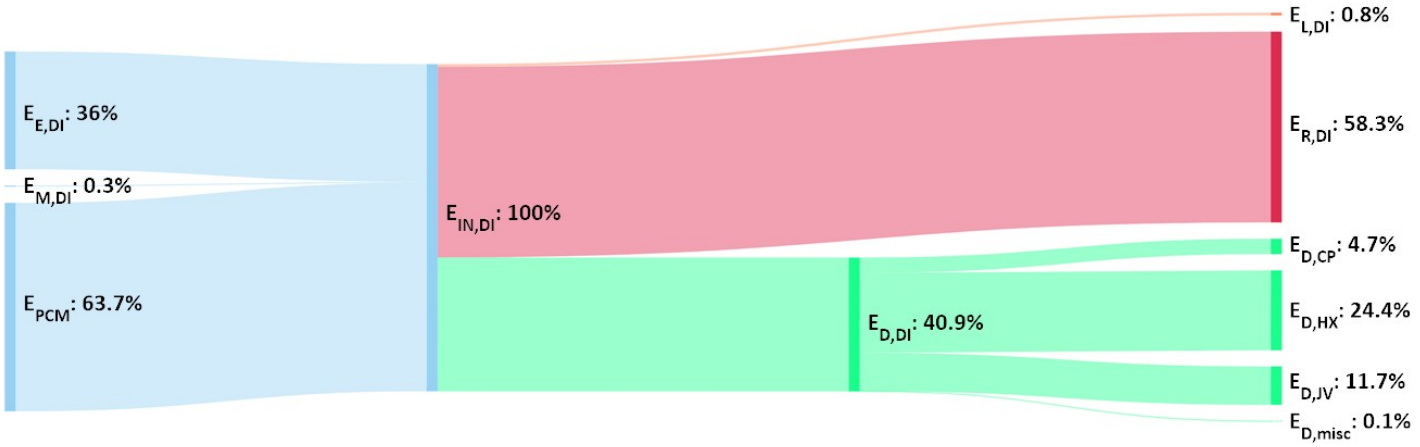

(c)

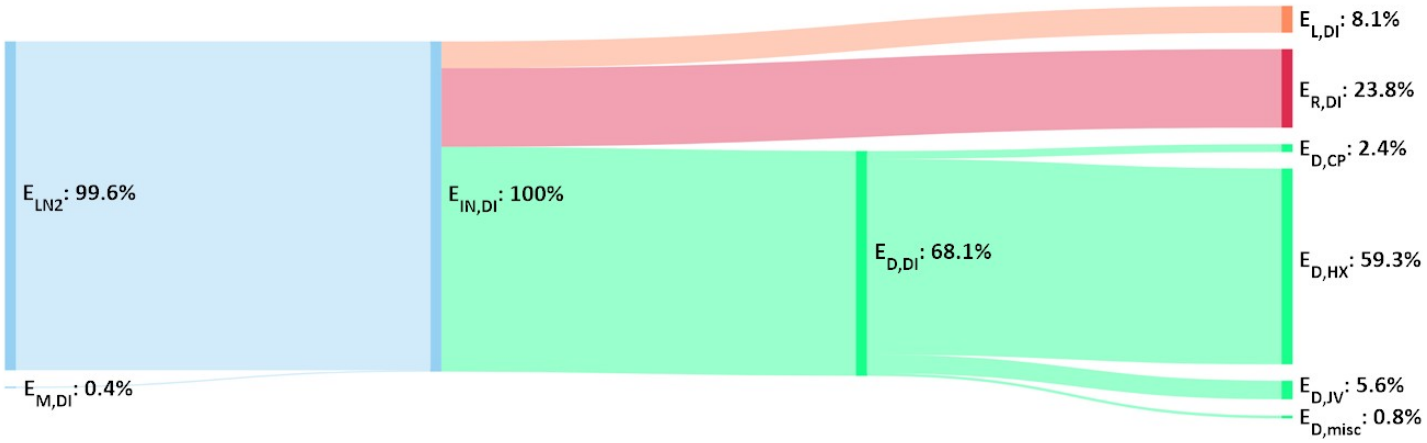

(d)

Fig. 16. Exergy flows for the dry ice production using (a) electricity input (b) electricity assisted by cold from liquid CO_2/chilled water (c) electricity assisted by cold from PCM (d) energy from liquid nitrogen

To produce 1 kg/s of dry ice, Fig. 16a shows that for dry ice production using electricity to drive the compressors, the main source of exergy input (≈ 0.79 MW) comes from the electricity and contributes to 89.8% of the total exergy input. Exergy of the waste stream (i.e. the heated cooling water) makes 20.4% of the total exergy input. The total exergy

destruction in the process is 46.6%, with the main location of exergy destruction in the compressors, heat exchangers and the valves.

Fig. 16b shows the exergy flows for dry ice production using cold from liquid CO_2 and chilled water as exergy input to assist in the dry ice production. Due to the presence of low temperature liquid CO_2/chilled water for the intercooling process, the electricity required to drive the compressors is significantly reduced to ≈ 0.24 MW which is equivalent to 32.4% of the total exergy input. The major exergy input comes from the physical exergy of the liquid CO_2/chilled water, which contributes to 67.5% of the total exergy input to the system. Waste streams leaving the dry ice production process are mainly the heated water and vapor CO_2 that represents 36.1% of the total exergy input. The exergy recovered by the dry ice produced is 40.0% of the total exergy input. The total exergy destroyed is 23.9%, and is mainly contributed by heat exchangers and Joule-Thompson valves. Compared to the case with electricity as main exergy input, the exergy destruction in the compressors is less due to the reduced pressure ratio and thus reduced compressor work.

Fig. 16c shows the exergy flows in the dry ice production utilizing cold from thermal storage as part of the exergy input together with electricity. Similar to the dry ice production process with liquid CO_2/chilled water input, the electricity input is 36.0% (or ≈ 0.18 MW) of the total exergy input. Physical exergy of the PCM contributes 63.7% of the total exergy input. The exergy recovered by the dry ice is 58.3%, while the exergy destruction is 40.9%, mainly due to the heat exchangers and the valves.

The exergy flows for the dry ice production using liquid nitrogen as energy vector are shown in Fig. 16d. The mechanical power, which is part of the physical exergy of the liquid nitrogen energy vector, is used to drive the compressor. The physical exergy of the liquid nitrogen, which also includes the cold exergy, contributes to about 99.6% of the total exergy input. The waste stream leaving the dry ice production, which mainly consists of the vapor nitrogen, contains exergy of 8.1% of the total exergy input. The exergy recovered by the dry ice is 23.8%. The exergy destruction in the process is 68.1%, and is mainly due to the heat exchangers operating with the high-grade exergy contained in the unutilized liquid nitrogen.

Table 15
Overall exergy input and overall performance of dry ice production coupled to different energy vectors

Energy Vector	Baseline	LNG Power Cycle	Thermal Network	Thermal Storage	LNG ASU
SOURCE OF EXERGY INPUT (MW)					
NG Chemical Exergy, $E_{C,NG}$	1.73	1.41	0.49	0.37	4.62
LNG Physical Exergy, $E_{P,LNG}$	0.00	0.32	1.46	1.18	2.08
Diesel Exergy, E_{fuel}	0.00	0.00	0.00	0.03	0.02
PERFORMANCE PARAMETERS					
Exergy Efficiency (%)	15.70	15.88	13.08	18.42	4.26
Carbon Emission (kTPA)	3.00	2.45	0.85	0.71	8.07

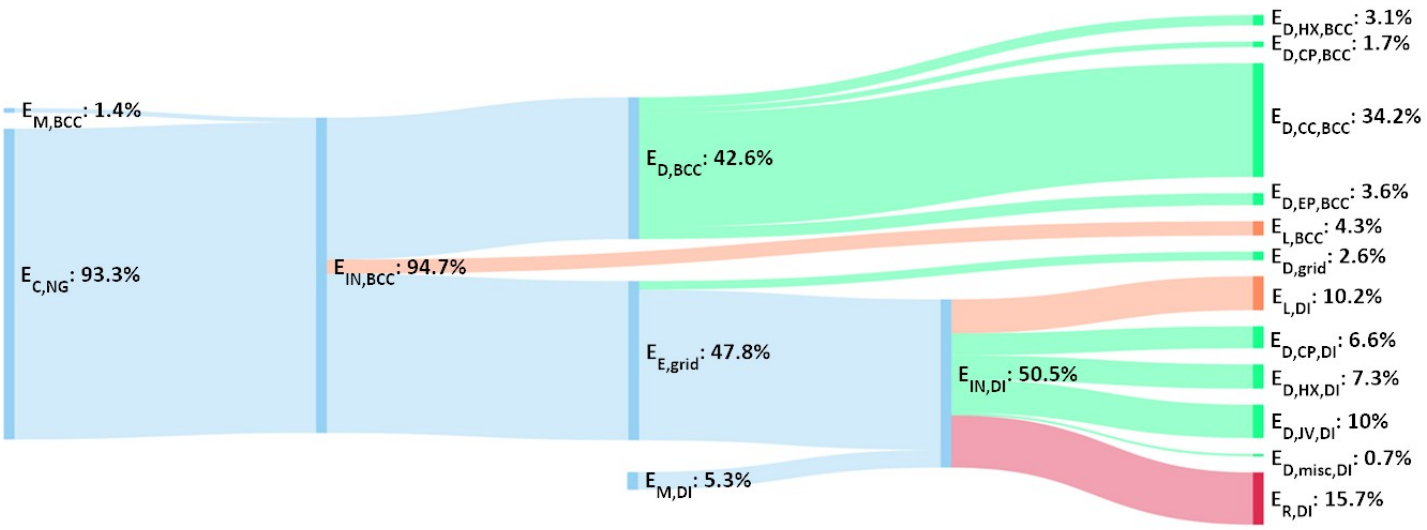
$E_{M,BCC}$: 1.4%
$E_{C,NG}$: 93.3%
$E_{IN,BCC}$: 94.7%
$E_{D,BCC}$: 42.6%
$E_{E,grid}$: 47.8%
$E_{M,DI}$: 5.3%
$E_{IN,DI}$: 50.5%
$E_{D,HX,BCC}$: 3.1%
$E_{D,CP,BCC}$: 1.7%
$E_{D,CC,BCC}$: 34.2%
$E_{D,EP,BCC}$: 3.6%
$E_{L,BCC}$: 4.3%
$E_{D,grid}$: 2.6%
$E_{L,DI}$: 10.2%
$E_{D,CP,DI}$: 6.6%
$E_{D,HX,DI}$: 7.3%
$E_{D,JV,DI}$: 10%
$E_{D,misc,DI}$: 0.7%
$E_{R,DI}$: 15.7%

(a)

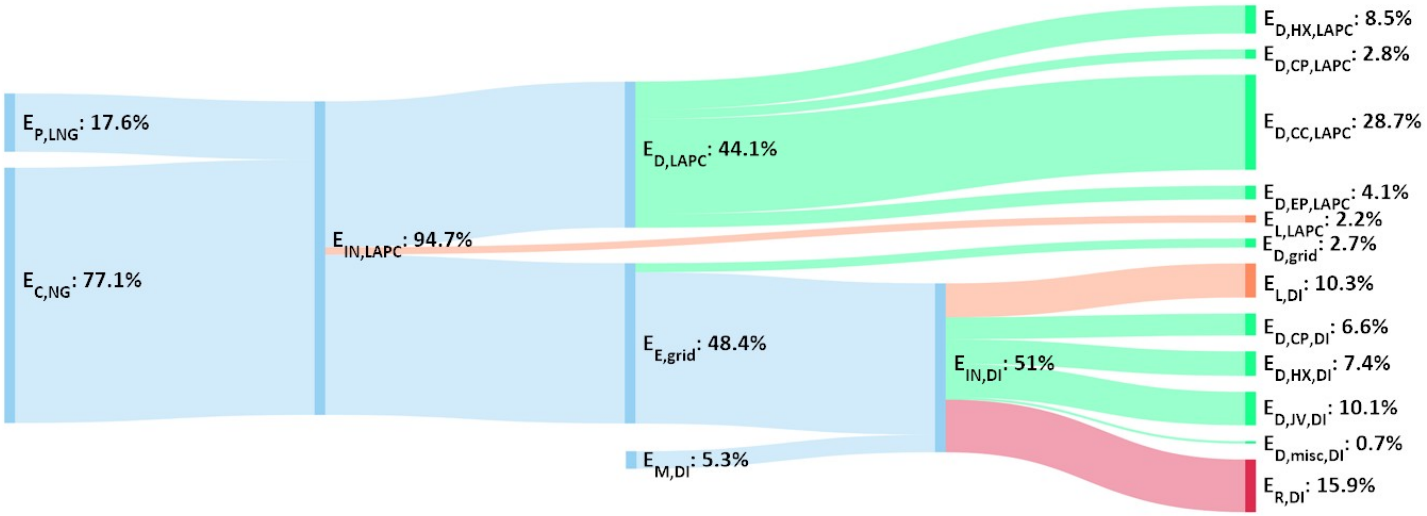
$E_{P,LNG}$: 17.6%
$E_{C,NG}$: 77.1%
$E_{IN,LAPC}$: 94.7%
$E_{D,LAPC}$: 44.1%
$E_{E,grid}$: 48.4%
$E_{M,DI}$: 5.3%
$E_{IN,DI}$: 51%
$E_{D,HX,LAPC}$: 8.5%
$E_{D,CP,LAPC}$: 2.8%
$E_{D,CC,LAPC}$: 28.7%
$E_{D,EP,LAPC}$: 4.1%
$E_{L,LAPC}$: 2.2%
$E_{D,grid}$: 2.7%
$E_{L,DI}$: 10.3%
$E_{D,CP,DI}$: 6.6%
$E_{D,HX,DI}$: 7.4%
$E_{D,JV,DI}$: 10.1%
$E_{D,misc,DI}$: 0.7%
$E_{R,DI}$: 15.9%

(b)

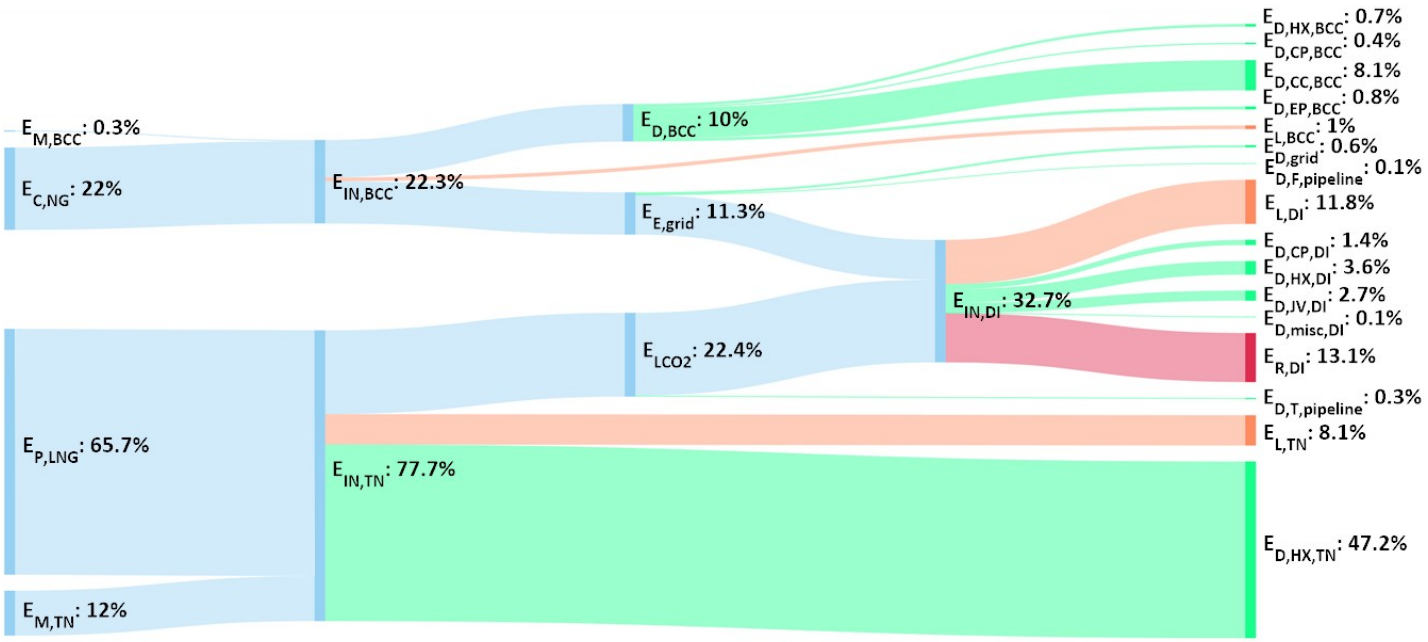
E_M,BCC: 0.3%
E_C,NG: 22%
E_P,LNG: 65.7%
E_M,TN: 12%
E_IN,BCC: 22.3%
E_IN,TN: 77.7%
E_D,BCC: 10%
E_E,grid: 11.3%
E_LCO2: 22.4%
E_IN,DI: 32.7%
E_D,HX,BCC: 0.7%
E_D,CP,BCC: 0.4%
E_D,CC,BCC: 8.1%
E_D,EP,BCC: 0.8%
E_L,BCC: 1%
E_D,grid: 0.6%
E_D,F,pipeline: 0.1%
E_L,DI: 11.8%
E_D,CP,DI: 1.4%
E_D,HX,DI: 3.6%
E_D,JV,DI: 2.7%
E_D,misc,DI: 0.1%
E_R,DI: 13.1%
E_D,T,pipeline: 0.3%
E_L,TN: 8.1%
E_D,HX,TN: 47.2%

(c)

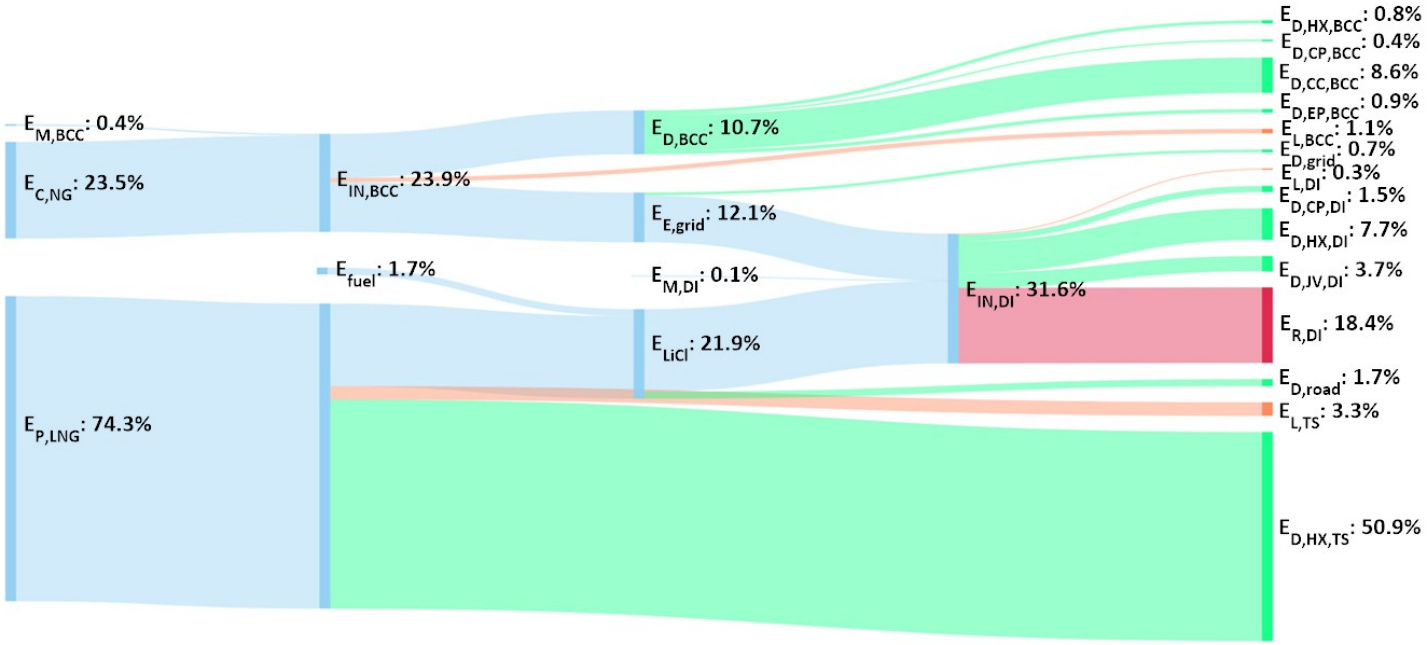
E_M,BCC: 0.4%
E_C,NG: 23.5%
E_P,LNG: 74.3%
E_fuel: 1.7%
E_IN,BCC: 23.9%
E_IN,TN: 77.7%
E_D,BCC: 10.7%
E_E,grid: 12.1%
E_M,DI: 0.1%
E_LiCl: 21.9%
E_IN,DI: 31.6%
E_D,HX,BCC: 0.8%
E_D,CP,BCC: 0.4%
E_D,CC,BCC: 8.6%
E_D,EP,BCC: 0.9%
E_L,BCC: 1.1%
E_D,grid: 0.7%
E_L,DI: 0.3%
E_D,CP,DI: 1.5%
E_D,HX,DI: 7.7%
E_D,JV,DI: 3.7%
E_R,DI: 18.4%
E_D,road: 1.7%
E_L,TS: 3.3%
E_D,HX,TS: 50.9%

(d)

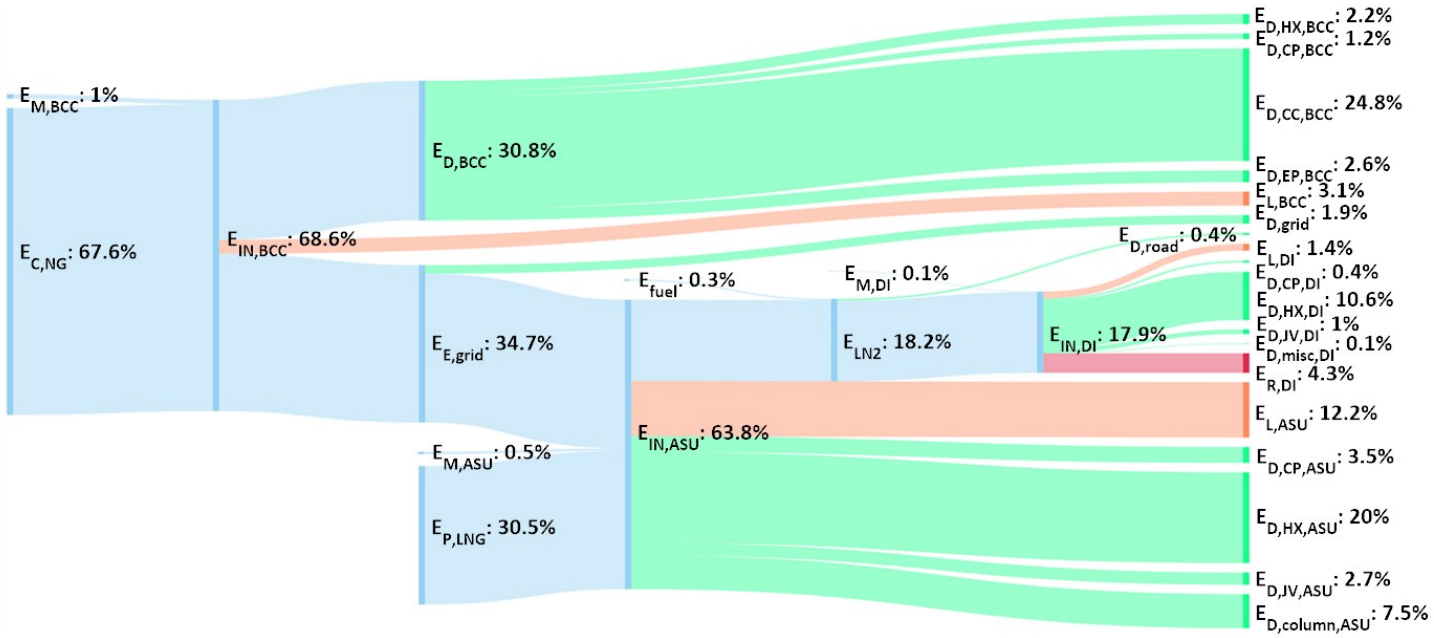

(e)

Fig. 17. Overall exergy flows for dry ice production downstream of (a) baseline power plant (b) LNG assisted power plant (c) thermal network (d) thermal storage (e) LNG assisted air separation

As shown in Fig. 17a, for conventional dry ice production which is coupled to the baseline combined cycle, the main source of exergy input (93.3% of the total exergy input or ≈ 1.7 MW) is the chemical exergy contained in the natural gas consumed by the combined cycle. The exergy flows and destruction inside the baseline combined cycle are similar to that discussed in Section 3.1, in which the total exergy destruction amounts to 42.6% of the total exergy input, with the main exergy destruction occurring in the combustion chamber. Upon grid distribution, the electricity that reaches the dry ice production amounts to 45.2% of the total exergy input to the system. With the amount of electricity, together with the exergy of material streams input to the dry ice production (i.e. cooling water and carbon dioxide), which is at 5.3% of the total exergy input, dry ice is produced at an overall exergy efficiency of 15.7%. The exergy of waste stream leaving the dry ice production process amounts to 10.2%, and consists mainly of exergy contained in the heated cooling water. The main occurrence of exergy destruction is in the valves, which included JV-1 and JV-2, and in the snow chamber (as shown in Fig. 15a) where the liquid CO_2 is pressure-relieved again to atmospheric pressure to facilitate the production of dry ice. The exergy destruction in the heat exchangers amounts to 7.3%, due to the temperature mismatch in the various heat exchangers; the exergy destruction due to the isentropic efficiency of the compressors amounts to 6.6%.

For dry ice production coupled to the LNG assisted power cycle, the exergy flows are shown in Fig. 17b. Compared to the dry ice production using electricity generated from the baseline combined cycle, the chemical exergy of the natural gas consumed is reduced to ≈ 1.4 MW, which is equivalent to 77.1% of the total exergy input. Around 17.6% (or ≈ 0.3 MW) of the total exergy comes from the physical exergy of the regasified LNG in the power cycle. The exergy of other material streams is too small to be included in the exergy flow diagram. The exergy flows inside the LNG assisted power cycle are similar to that discussed in Section 3.2, with exergy destruction at 44.1% of the total exergy input: the main source of exergy destruction is the combustion chamber and the heat exchangers. The electricity used in the dry ice production amounts to 45.7% of the total exergy input, while 5.3% of the total exergy coming from the material streams entering the process. Dry ice is produced with an overall efficiency of 15.9%. The exergy flows and destructions in the dry ice production process are similar to that shown in Fig. 17a.

Exergy flows for dry ice production coupled to the thermal network are shown in Fig. 17c. The electricity used to drive the CO_2 compressor is assumed to be obtained from the baseline combined cycle, with exergy flows similar to that in Section 3.1. Chemical exergy of the natural gas consumed in the baseline combined cycle amounts to 22.0% (or ≈ 0.5

MW) of the total exergy input to the system. The amount of electricity that enters the dry ice production process upon grid distribution amounts to 10.6%. Around 65.7% (or ≈ 1.5 MW) of the total exergy input to the system comes from the physical exergy of LNG, which acts as the cold source to charge the liquid CO_2/chilled water energy vector. The remaining 12.0% of the total exergy input is contributed by the material streams entering the thermal network central plant (i.e. warm water and vapor CO_2). Due to large temperature mismatch in the heat exchangers, the exergy destruction in the thermal network central plant is 47.2%. Around 8.1% of the total exergy input is lost in the waste streams leaving the thermal network central plant, which mainly consist of the regasified LNG. Around 22.4% of the total exergy input is converted into liquid CO_2 in the thermal network central plant. Due to the small amount of chilled water needed for the dry ice production, the exergy of chilled water is negligible (<0.05%) and thus not shown in the exergy flow diagram. Along the pipeline, the exergy destruction due to the thermal loss is 0.3%, while the exergy destroyed due to friction loss (0.1% of total exergy input) is covered by the electricity input to the pump. With electricity and the cold from liquid CO_2/chilled water as main exergy sources for dry ice production, dry ice is produced with an overall exergy efficiency of 13.1%. Waste streams exiting the dry ice production process, which mainly consist of the warm water and vapor CO_2 that will be returned to the thermal network central plant, account for 11.8% of the total exergy input. Compared to the dry ice production coupled to electricity as the energy vector, the exergy destruction in the dry ice production process is significantly reduced and only accounts for 7.8% of the total exergy input.

Fig. 17d shows the exergy flows for dry ice production coupled to the thermal storage. Electricity will still be obtained from the baseline combined cycle to drive the compressors. Thus, 23.5% of the total exergy input is the chemical exergy of natural gas consumed by the combined cycle, producing electricity (11.4% of total exergy input) entering the dry ice production. The main source of exergy input to the system (74.5% of the total exergy input) comes from the physical exergy of LNG to be regasified in the thermal storage central plant. However, the exergy destruction in the heat exchangers of the central plant is large (50.9% of the total exergy input) due to temperature mismatch and the waste of LNG high-grade exergy which is not utilized in the process. For the dry ice production, the amount of exergy destruction in the process is 12.9%, with the main source of exergy destruction in the heat exchangers. The overall exergy efficiency of the process is 18.4%.

Exergy flows for the dry ice production process coupled to the liquid nitrogen energy vector are shown in Fig. 17e. Liquid nitrogen is produced using the LNG assisted air separation process, and is used as energy vector to drive the dry ice production. For the air separation process, electricity is assumed to be obtained from the baseline combined cycle, thus the main source of exergy input coming from the chemical exergy of natural gas consumed by the combined cycle (67.6% of the total exergy input or ≈ 4.6 MW). The exergy flows inside the combined cycle are similar to that described earlier. Electricity produced and delivered to the air separation unit is 32.8% of the total exergy input. Another major exergy source is the physical exergy of LNG to be regasified in the air separation unit (30.5% of the total exergy input or ≈ 2.1 MW), providing cold energy for the air separation process. For the air separation process, the exergy contained in the waste streams (i.e. the cooling water and unused side-product) is around 12.2% of the total exergy input. The total amount of exergy destruction in the air separation process is 33.7%, with the main sources of exergy destruction in the MSHE and the heat exchangers. The liquid nitrogen supplied to drive the dry ice production contains 17.9% of the total exergy input. The road transport loss represents 0.4% of the total exergy input, and is covered by the fuel consumed by the trucks. The thermal loss is negligible. The exergy going into the dry ice production is 18.0% and mainly comes from the physical exergy contained of the liquid nitrogen. For the dry ice production process, due to the large temperature mismatch in heat exchangers, a large amount of high-grade thermal exergy in the liquid nitrogen is not utilized, resulting in the exergy destruction in the heat exchangers to be the largest and amounts to 10.6% of the total exergy input. The exergy destruction in the rest of the components (i.e. valves, compressor and separation column) amounts to 1.5%. The waste streams leaving the dry ice production, mainly consisting of the physical exergy of vaporized air leaving the process and unused mechanical work, contain 1.5% of the total input exergy. Due to the large amount of exergy destruction in the baseline combined cycle, in the air separation process and in the heat exchangers during dry ice production, the overall exergy efficiency is only ≈ 4.3%.

From Fig. 17 and

Table *15*, it can be noticed that the cleanest and most exergy efficient energy vector for dry ice production is the PCM. This is because with suitable PCM to assist in the dry ice production, the dry ice production setup can be simplified from two-stage compression to single stage, significantly reducing the amount of compression work required for the process and thus increasing its exergy efficiency; this reduces the dependency on electricity input, subsequently reducing the carbon emission. Usage of liquid CO_2 and chilled water as energy vectors, is the second cleanest option for dry ice production due to large reduction in compression work compared to the dry ice production depending solely on electricity. Liquid nitrogen as energy vector has the lowest performance despite only a single stage compression is required for the dry ice production. This is due to the large amount of exergy destruction alongside the electricity generation and the air separation process. Besides, the high-grade cold contained in the liquid nitrogen cannot be utilized completely by the dry ice production, causing large amount of exergy destruction in the process, thus further reducing the overall exergy efficiency.

5.3 Deep freezing

For deep freezing purposes, 1 MW_t of cold is needed and supplied to an amount of air that is cooled from -10°C to -20°C. Conventional deep freezing processes utilize an R134a heat pump to provide the amount of cold required, with a COP of ≈ 2.0 (Fig. 18a). The returned air at -10^{0}C (1) is cooled to -20^{0}C (2) via HX-1 using R134a, in which (11)-(14) represents the heat pump cycle. When energy vectors such as liquid CO_2 or PCM (e.g. SN33 [46]) are considered, heat exchangers will be used to exchange cold with the air to be cooled down, as shown in Fig. 18b.

Liquid nitrogen is known to be able to generate cold and mechanical power at the same time when used to drive an isothermal expander. As shown in Fig. 18c, in the isothermal expander (EP-1), liquid nitrogen (22) is mixed with a liquid-glycol solution (21) to be evaporated, generating mechanical power in the process, which will be delivered to the R134a heat pump cycle (11)-(14) with COP of ≈ 2.0 for heat extraction from the inlet air stream (2) via HX-2. The mixture of liquid nitrogen and water-glycol solution (23) exiting EP-1 at a low temperature, will be used for heat extraction from another stream of inlet air (4) via HX-1.

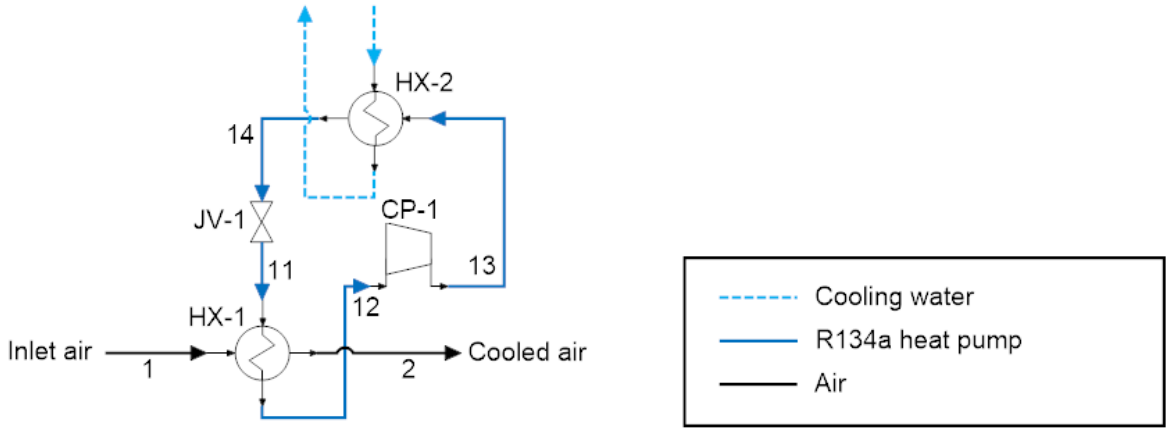

(a)

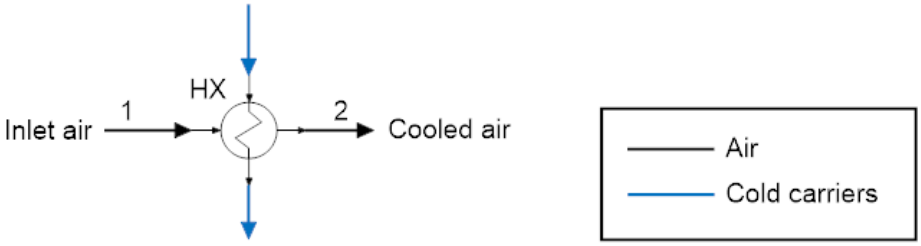

(b)

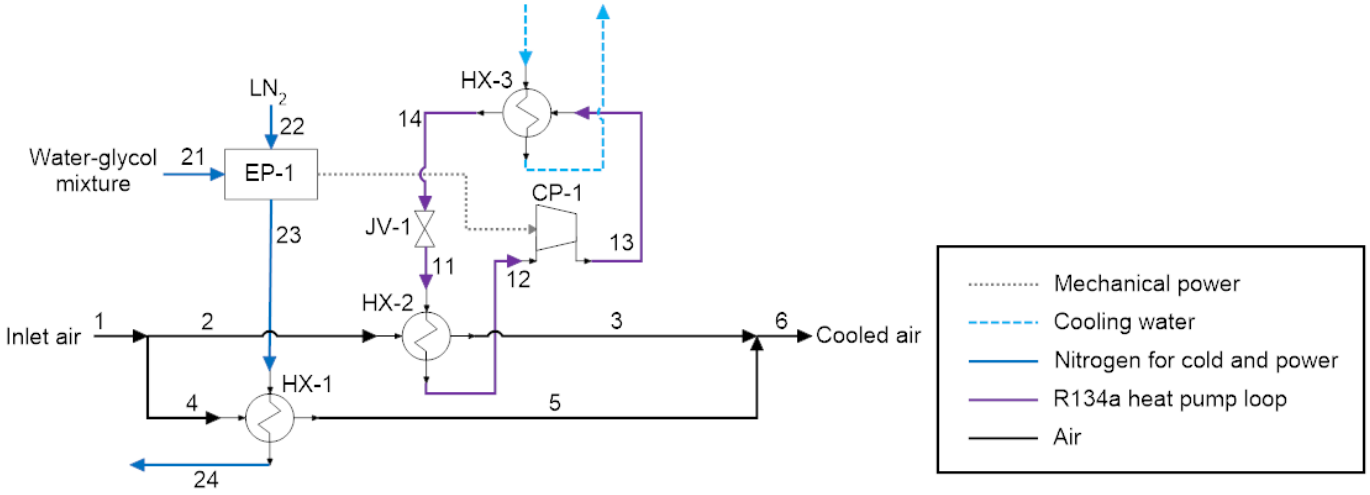

(c)

Fig. 18. Schematic diagram for deep freezing process/cooling of water returned from district cooling using energy input of (a) electricity only (b) liquid CO_2/PCM (c) liquid nitrogen only

Table 16
Input exergy amounts and performance of deep freezing process utilizing different energy vectors

Energy Vector	Electricity	Liquid CO_2	PCM	LN_2
SOURCE OF EXERGY INPUT (MW)				
Electricity Exergy, E_E	0.49	0.00	0.00	0.00
Exergy of Cold Vectors, $E_{CW}/E_{LCO2}/E_{PCM}/E_{LN2}$	0.00	0.61	0.34	0.81
PERFORMANCE PARAMETER				
Exergy Efficiency (%)	32.79	31.72	55.95	23.75

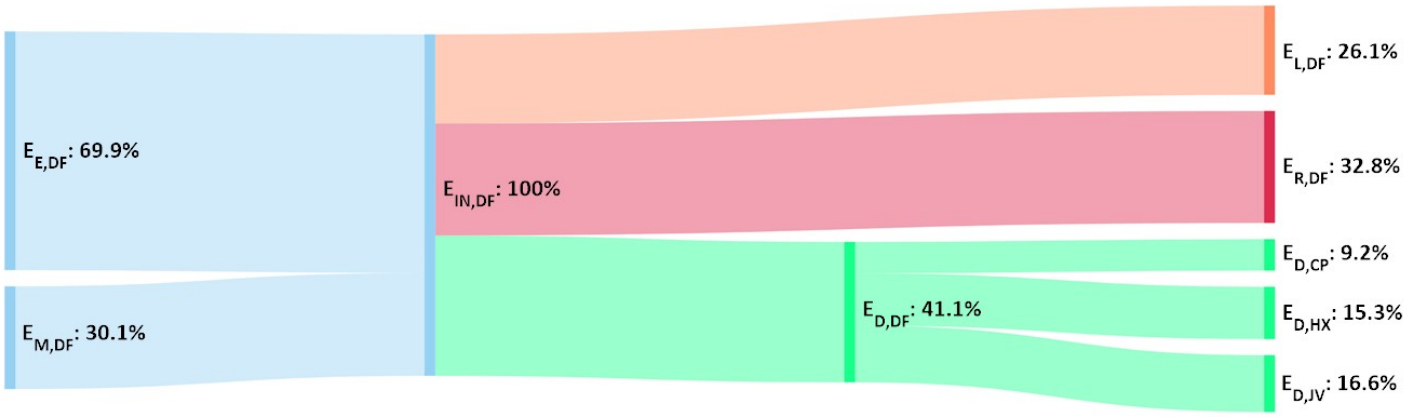
$E_{E,DF}$: 69.9%
$E_{M,DF}$: 30.1%
$E_{IN,DF}$: 100%
$E_{L,DF}$: 26.1%
$E_{R,DF}$: 32.8%
$E_{D,CP}$: 9.2%
$E_{D,DF}$: 41.1%
$E_{D,HX}$: 15.3%
$E_{D,JV}$: 16.6%

(a)

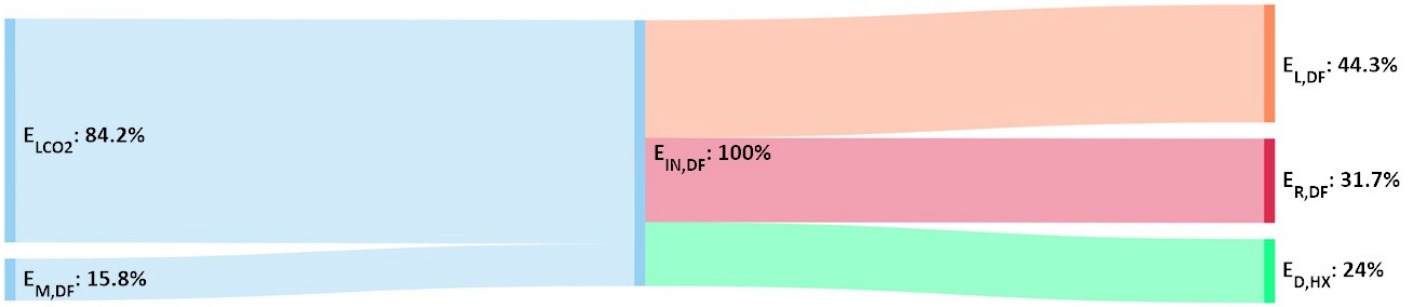
E_{LCO2}: 84.2%
$E_{M,DF}$: 15.8%
$E_{IN,DF}$: 100%
$E_{L,DF}$: 44.3%
$E_{R,DF}$: 31.7%
$E_{D,HX}$: 24%

(b)

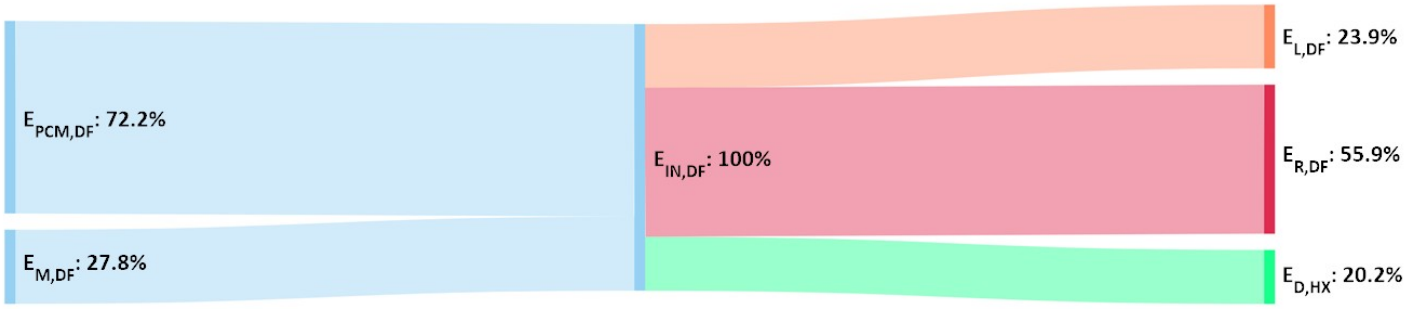
$E_{PCM,DF}$: 72.2%
$E_{M,DF}$: 27.8%
$E_{IN,DF}$: 100%
$E_{L,DF}$: 23.9%
$E_{R,DF}$: 55.9%
$E_{D,HX}$: 20.2%

(c)

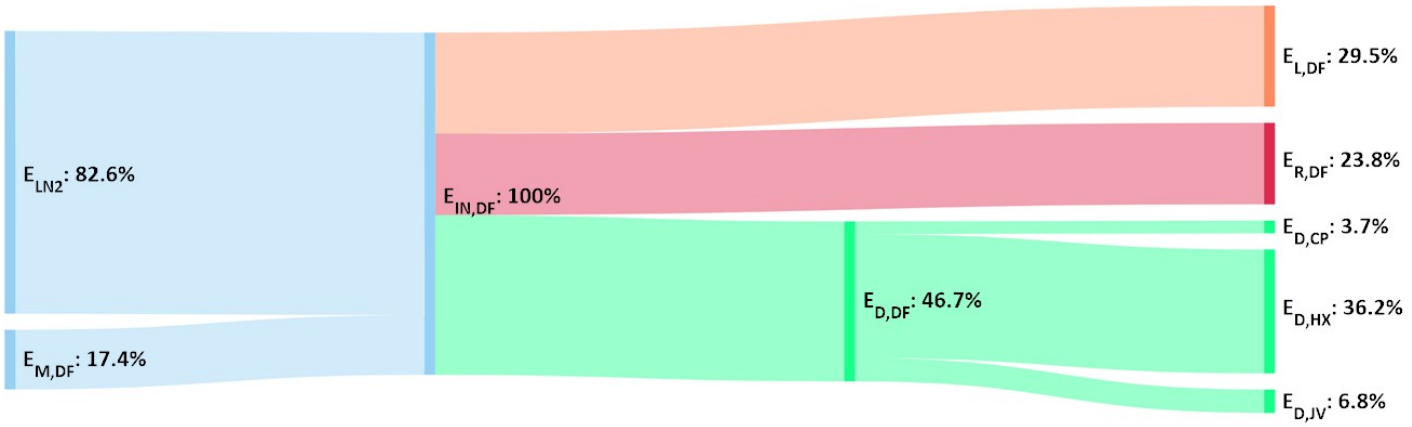
E_{LN2}: 82.6%
$E_{M,DF}$: 17.4%
$E_{IN,DF}$: 100%
$E_{L,DF}$: 29.5%
$E_{R,DF}$: 23.8%
$E_{D,CP}$: 3.7%
$E_{D,DF}$: 46.7%
$E_{D,HX}$: 36.2%
$E_{D,JV}$: 6.8%

(d)

Fig. 19. Exergy flows for the deep freezing process using (a) electricity input (b) cold from liquid CO_2 (c) cold from PCM (d) energy from liquid nitrogen

Fig. 19a shows the exergy flows of the deep freezing process using a heat pump. Electricity represents 69.9% of the total exergy input (or ≈ 0.5 MW) and is used to drive the compressor of the heat pump cycle to generate cooling power. The rest of exergy input comes from the cooling water going into the heat pump and the exergy contained in the inlet air to be cooled, which are labelled as the material streams into the deep freezing process. The waste stream, which mainly consists of the heated cooling water leaving the heat pump, contains 26.1% of the total exergy input. Exergy recovered by the cooled air for the deep freezing process is 32.8% of the total exergy input. Exergy destruction occurs in the main component of the setup, which is the heat pump. The components of the heat pump (compressor, heat exchangers and valve) account for most of the exergy destruction and amount to 41.1% of the total exergy input.

Fig. 19b and Fig. 19c show the deep freezing process using liquid CO_2 and PCM as the main energy vectors for cold energy input. The main exergy input source is now the physical exergy from these energy vectors. The waste stream mainly consists of the energy vector leaving the cold application after exchanging heat with the inlet air. The main location of exergy destruction is in the heat exchangers, where the heat transfer and temperature mismatch occur. The amount of exergy destruction is reduced compared to the case with using electricity as the main exergy input due to the reduced number of components. When the setup using liquid CO_2 as the main exergy input is compared to that using PCM as energy vector, the analysis shows that the setup with PCM has significantly higher exergy efficiency (55.9% compared to 31.7%) due to good selection of material and thus a good temperature profile match and less amount of waste of high-grade cold exergy.

Fig. 19d shows the exergy flows of the deep freezing process using liquid nitrogen as cold energy vector; the physical exergy of liquid nitrogen (i.e. cold exergy and mechanical exergy) makes 82.6% of the total exergy input. The waste streams mainly consist of the used nitrogen and the cooling water leaving the heat pump, with their physical exergy values at 29.5% of the total exergy input. The exergy recovered by the cooled air is 23.8%, while the exergy destruction of the process is 46.7%. The exergy destruction in the heat exchangers for this deep freezing setup is higher compared to the deep freezing process using other exergy input (i.e. electricity, liquid CO_2 and PCM) because of the increased number of heat exchangers in the overall setup and also the unutilized high-grade cold of the liquid nitrogen.

Table 17
Overall exergy input and overall performance for deep freezing process coupled to different energy vectors

	Baseline	LNG Thermal Cycle	Thermal Network	Thermal Storage	LNG ASU
SOURCE OF EXERGY INPUT (MW)					
NG Chemical Exergy, $E_{C,NG}$	1.02	0.83	0.00	0.00	3.06
LNG Physical Exergy, $E_{P,LNG}$	0.00	0.19	1.96	1.33	1.38
Diesel Exergy, E_{fuel}	0.00	0.00	0.00	0.05	0.02
PERFORMANCE PARAMETERS					
Exergy Efficiency (%)	18.57	18.75	9.49	15.96	4.94
Carbon Emission (kTPA)	1.77	1.44	0.01	0.12	5.34

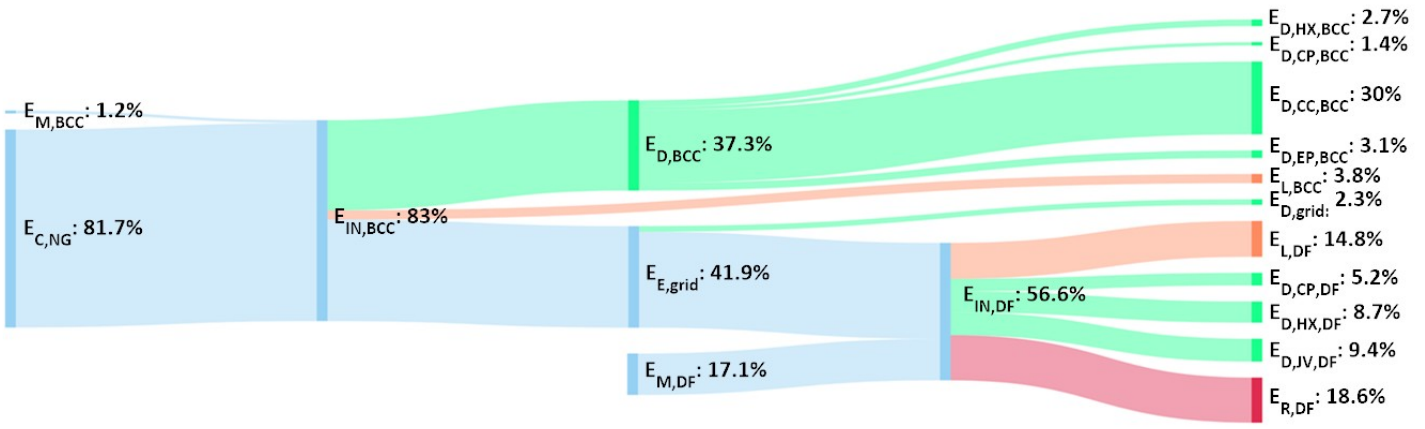
E_M,BCC: 1.2%
E_C,NG: 81.7%
E_IN,BCC: 83%
E_D,BCC: 37.3%
E_E,grid: 41.9%
E_M,DF: 17.1%
E_IN,DF: 56.6%
E_D,HX,BCC: 2.7%
E_D,CP,BCC: 1.4%
E_D,CC,BCC: 30%
E_D,EP,BCC: 3.1%
E_L,BCC: 3.8%
E_D,grid: 2.3%
E_L,DF: 14.8%
E_D,CP,DF: 5.2%
E_D,HX,DF: 8.7%
E_D,JV,DF: 9.4%
E_R,DF: 18.6%

(a)

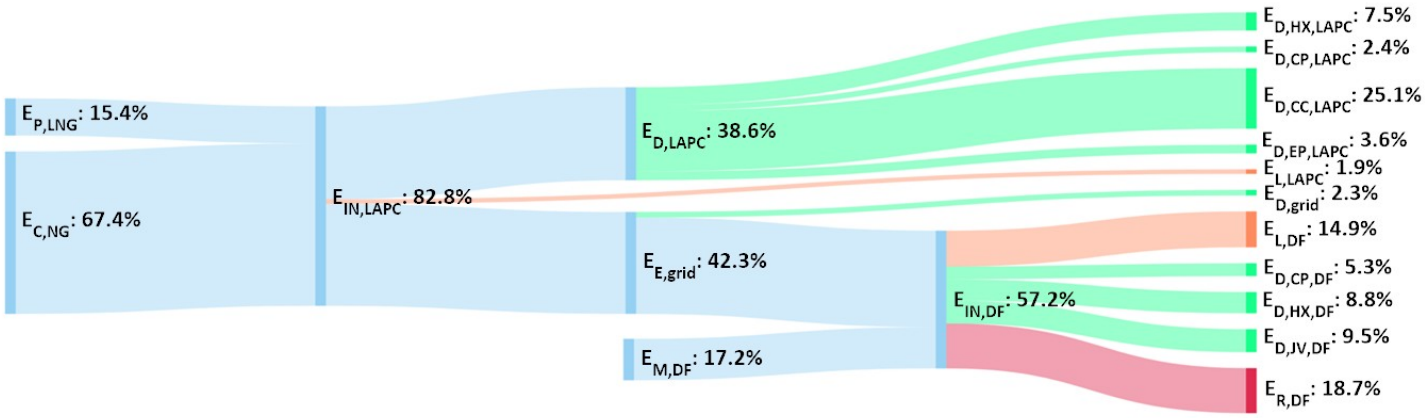
E_P,LNG: 15.4%
E_C,NG: 67.4%
E_IN,LAPC: 82.8%
E_D,LAPC: 38.6%
E_E,grid: 42.3%
E_M,DF: 17.2%
E_IN,DF: 57.2%
E_D,HX,LAPC: 7.5%
E_D,CP,LAPC: 2.4%
E_D,CC,LAPC: 25.1%
E_D,EP,LAPC: 3.6%
E_L,LAPC: 1.9%
E_D,grid: 2.3%
E_L,DF: 14.9%
E_D,CP,DF: 5.3%
E_D,HX,DF: 8.8%
E_D,JV,DF: 9.5%
E_R,DF: 18.7%

(b)

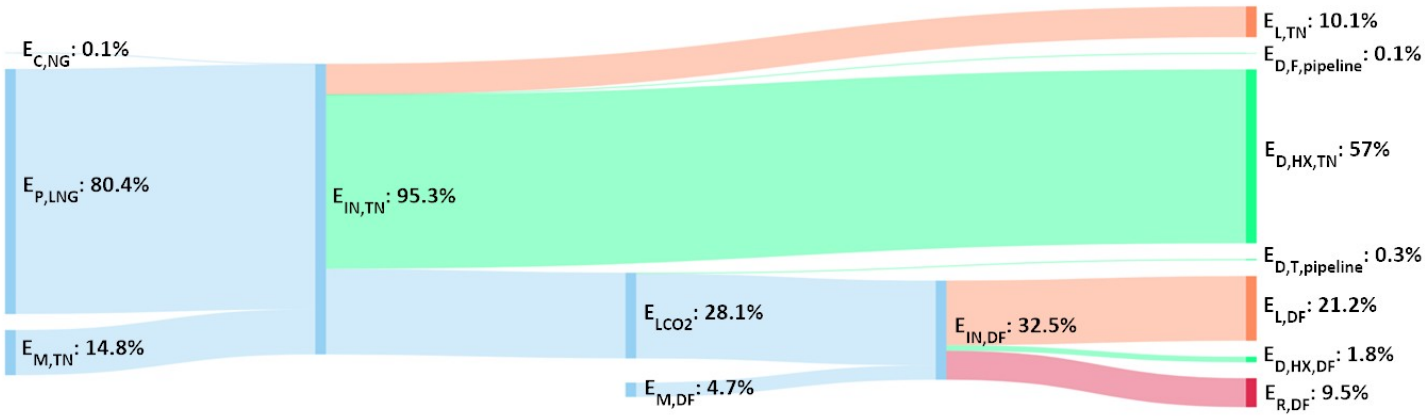
E_C,NG: 0.1%
E_P,LNG: 80.4%
E_M,TN: 14.8%
E_IN,TN: 95.3%
E_LCO2: 28.1%
E_M,DF: 4.7%
E_IN,DF: 32.5%
E_L,TN: 10.1%
E_D,F,pipeline: 0.1%
E_D,HX,TN: 57%
E_D,T,pipeline: 0.3%
E_L,DF: 21.2%
E_D,HX,DF: 1.8%
E_R,DF: 9.5%

(c)

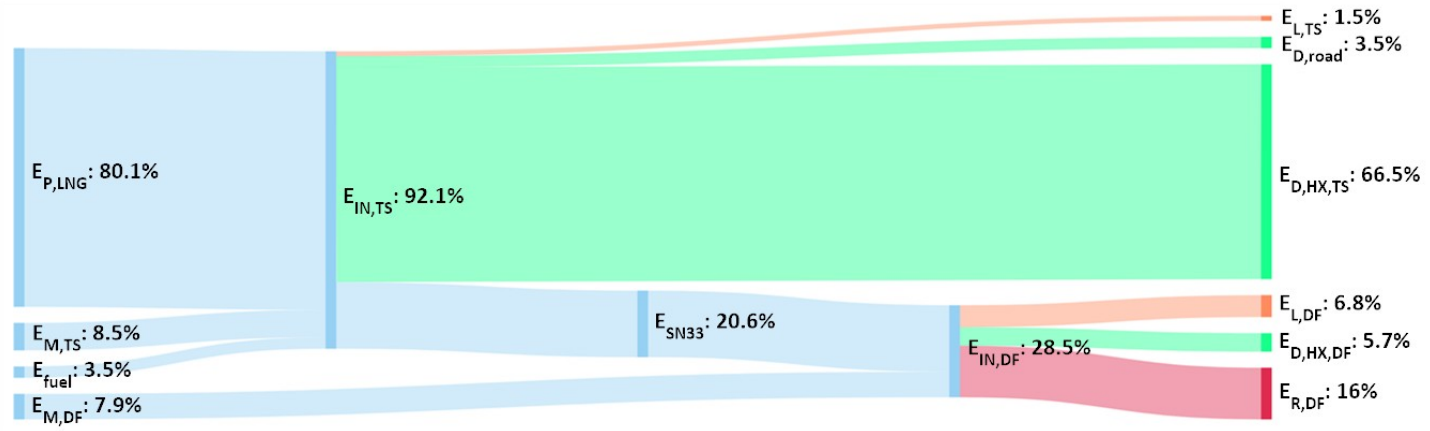

(d)

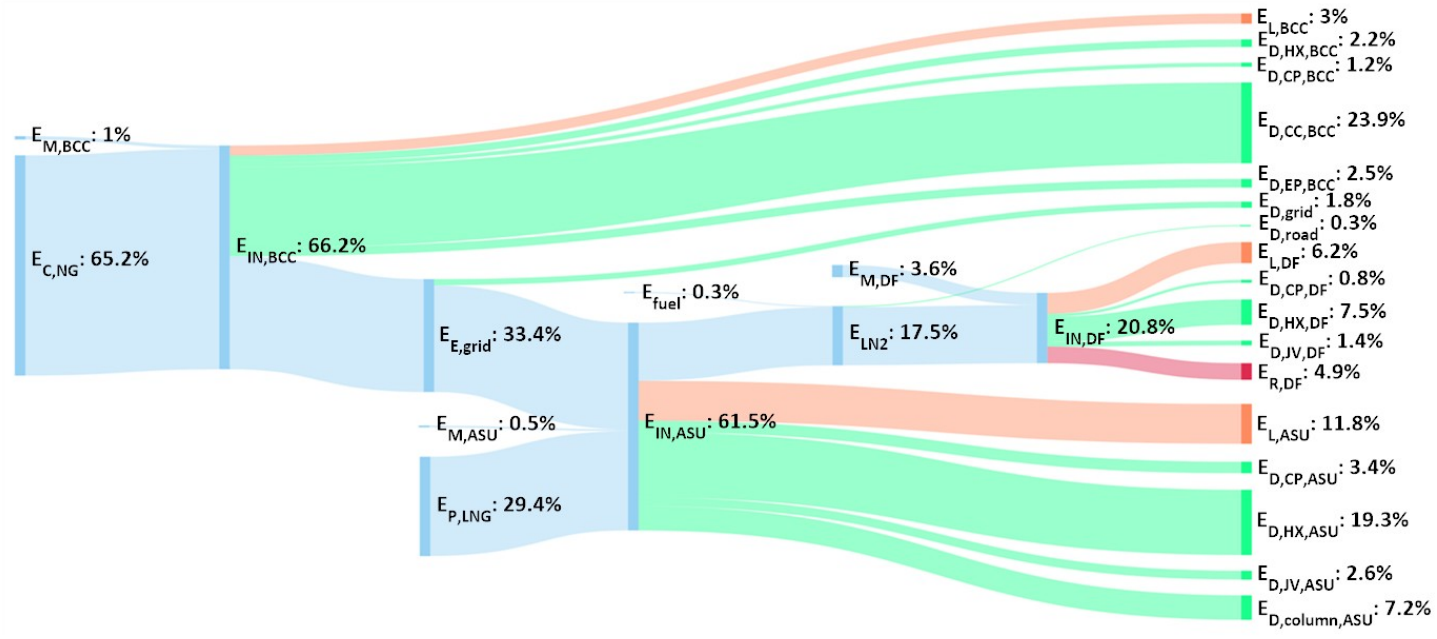

(e)

Fig. 20. Overall exergy flows for the deep freezing process downstream of (a) baseline power plant (b) LNG assisted power plant (c) thermal network (d) d thermal storage (e) LNG assisted air separation unit

Fig. 20a shows the overall exergy flows from a baseline combined cycle to the deep freezing process. It can be seen that the main source of exergy input (81.7% of total exergy input or ≈ 1.0 MW) is the chemical exergy contained in the natural gas to be consumed by the combined cycle. In the baseline combined cycle, the total amount of exergy destruction is 37.2%, mainly occurring in the combustion chamber. The electricity produced and used in the deep freezing process makes 39.6% of the total exergy input. For the deep freezing process, the exergy flows are similar to those shown in Fig. 19a, and the total exergy destruction is 23.3% of the total exergy input; the overall exergy efficiency is 18.6%.

From Fig. 20b, which shows the exergy flows from an LNG assisted power cycle to the deep freezing process, the amount of natural gas chemical exergy input is reduced to ≈ 0.83 MW (or 67.4%) of the total exergy input. Around 15.4% (or ≈ 0.2 MW) of the total exergy input comes from the physical exergy of LNG to be regasified in the power cycle. The total exergy destruction is 38.6%, and is mainly due to the combustion chamber. After the transmission process, the electricity reaching the deep freezing process is 40.0% of the total exergy input. In the deep freezing process, the amount of exergy destruction is 23.6% and the amount of exergy for the waste streams is 14.9%; the overall exergy efficiency is 18.7%.

Fig. 20c shows the exergy flows from the thermal network central plant to the deep freezing process. The main exergy input comes from the physical exergy of LNG to be regasified (80.4% of the total exergy input or ≈ 2.0 MW). Other main exergy input to the thermal network central plant comes from the material stream (i.e. exergy of the vapor CO_2). The exergy destruction is large at the central plant where the heat exchange between LNG and the working fluids occur (as shown in Fig. 6) due to the large amount of unutilized high-grade cold from LNG. The exergy of liquid CO_2 is 28.1% of the total exergy input. The pressure loss in the pipes is almost negligible, and the exergy destruction due to the thermal loss is 0.3% of the total exergy input, yielding liquid CO_2 entering the deep freezing process with an exergy of 27.8% of the total exergy input. A large amount of exergy is lost through the waste stream, which in the CO_2 leaving the deep freezing process at a still low temperature, due to the requirement to maintain the operating condition of the CO_2 pipeline. The amount of exergy destruction during the heat exchange for deep freezing process is low at 1.8%, due to a better temperature profile matching in the heat exchanger. This yields the overall exergy efficiency of 9.5%.

The exergy flows from the thermal storage to the deep freezing process, as shown in Fig. 20d, are very similar to the deep freezing process coupled to the thermal network. Around 80.1% of the exergy input comes from the LNG physical exergy, in which a large amount is destroyed in the thermal storage central plant where the heat exchange between LNG and the PCM energy vector occurs due to poor temperature profile match and thus loss of high-grade cold exergy. Inside the deep freezing process, due to a good selection of the PCM, which has a good temperature match with the deep freezing process, the exergy loss due to the waste stream (which mainly consist of the PCM leaving the heat exchange process) and the exergy destruction in the heat exchanger is significantly reduced compared to the deep freezing process coupled to the thermal network, yielding a significantly higher overall exergy efficiency of 16.0%.

For the deep freezing process coupled to the liquid nitrogen produced by the LNG assisted air separation unit (Fig. 20e), the main exergy input comes from the chemical exergy of the natural gas consumed by the baseline combined cycle to produce electricity, which is subsequently used to drive the compressors in the LNG assisted air separation unit. The amount of chemical exergy consumed is 65.2% of the total exergy input (or ≈3.1 MW), and the exergy flows in the baseline combined cycle are similar to those discussed in Section 3.1. The electricity entering the air separation unit has 31.6% amount of the total exergy input, combined with the physical exergy provided by the LNG entering the air separation process, liquid nitrogen is produced, containing exergy amounts to 17.5% of the total exergy input. The distribution loss of liquid nitrogen is ≈ 0.3% of the total exergy input, which is mainly contributed by the road transport loss; the thermal loss is negligible due to the good tank insulation and short distribution distance. The exergy destruction due to road transport loss is assumed to be obtained from the diesel fuel input to the truck. For the deep freezing process, as discussed in Fig. 19d, the main cause of exergy destruction is in the heat exchangers. The total amount of exergy wasted and destruction is 6.2% and 9.7% respectively, yielding an overall efficiency of 4.9%.

From the overall exergy efficiency point of view, deep freezing utilizing electricity (from both the baseline combined cycle and LNG assisted power cycle) as main energy input is the most advantageous because of the relatively smaller amounts of the total exergy input to the overall process, as compared with deep freezing processes acquiring other energy vector as exergy input, which require large amounts of cold energy input from the LNG regasification. However, it should be noted that the cold energy will be wasted if not utilized properly, and it has been shown that with the cold energy input, electricity input is no longer required for the deep freezing process, and in the case of deep freezing acquiring liquid CO_2 or PCM as cold energy source, it can be seen that the process has been significantly simplified. However, for deep freezing process utilizing liquid nitrogen, due to the presence of both mechanical and cold energy, the setup has become more complicated as two different loops will be required to recover both the mechanical and cold energy of the liquid nitrogen. Besides that, the exergy efficiency is extremely low due to the waste of energy to generate liquid nitrogen, which contains very high-grade cold energy that is subsequently unrecoverable by the deep freezing process alone. For the carbon emission part, for deep freezing processes using electricity as main source of exergy, the carbon emission is ≈ 1.8 kTPA for deep freezing using electricity generated by the baseline combined cycle and ≈ 1.4 kTPA for the deep freezing process using electricity generated by the LNG assisted power cycle. For deep freezing with liquid CO_2 as energy source, the carbon emission is almost negligible and the only cause of the carbon emission is the consumption of electricity for the small amount of pressure loss. The deep freezing using cold input from the PCM yields ≈ 0.12 kTPA and is mainly caused by

the transportation of PCM by truck. For the deep freezing using liquid nitrogen energy vector, the carbon emission is high at ≈ 5.3 kTPA due to high amount of electricity consumed in the air separation process.

5.4 District Cooling

It is assumed that the industrial district is cooled by using a district cooling concept to achieve energy savings compared to stand-alone cooling systems in each of the industrial facilities. For this cooling purpose, it is assumed that 1 MW_t of cooling is needed, and is supplied using water from a district cooling central plant to each of the facilities via a pipeline system that is already in-place. In this scenario, it is assumed that this district cooling central plant will receive the water returned from the industrial plant at ≈ 15°C and cool it to ≈ 5°C before supplying it to the district cooling network again.

In the conventional scenario of a district cooling process using electricity input, a heat pump cycle with a COP of ≈ 4.2 will be used to convert electricity to cooling energy to cool the water returned after the district cooling process. The scenario is very similar to the deep freezing process as shown in Fig. 18a, with streams (1) and (2) replaced with inlet water at 15°C and cooled water at 5°C respectively.

Using liquid CO_2 or PCM energy vectors to supply cold energy for district cooling, due to the availability of a cold source, the heat pump cycle can be replaced by a single heat exchange process, eliminating the dependence on electricity in the returned water cooling process. It is similar to the deep freezing process as shown in Fig. 18b, in which (1) and (2) are replaced with returned water and cooled water. In this case, for the usage of cold from the thermal network, liquid CO_2 alone will be utilized due to the very small temperature difference between the chilled water from the thermal network and the water returned to the district cooling central plant to be cooled. For the district cooling utilizing cold from the thermal storage, PCM AN03 with a phase change temperature of -3°C [48] will be used.

The district cooling can also be powered by liquid nitrogen, which is able to generate cold and mechanical power at the same time. The setup of this district cooling is similar to the deep freezing process shown in Fig. 18c, in which streams (1), (2) and (4) are replaced with returned water and streams (3), (5) and (6) replaced with cooled water. The heat pump cycle (11)-(14) has a COP of ≈ 4.2 and utilize mechanical energy produced by liquid nitrogen during the nitrogen evaporation process to drive the compressor. This heat pump cycle is used to cool the water through HX-2 while direct heat exchange occurs through HX-1 between the mixture of water-glycol with boiled nitrogen (23) and the returned water (4).

Table 18
Input exergy amounts and performance for cooling of returned water utilizing different energy vectors

Energy Vector	Electricity	Liquid CO_2	PCM	LN_2
SOURCE OF EXERGY INPUT (MW)				
Electricity Exergy, E_E	0.24	0.00	0.00	0.00
Exergy of Cold Vectors, $E_{CW}/E_{LCO2}/E_{PCM}/E_{LN2}$	0.00	0.61	0.07	0.49
PERFORMANCE PARAMETER				
Exergy Efficiency (%)	6.95	3.66	27.08	4.06

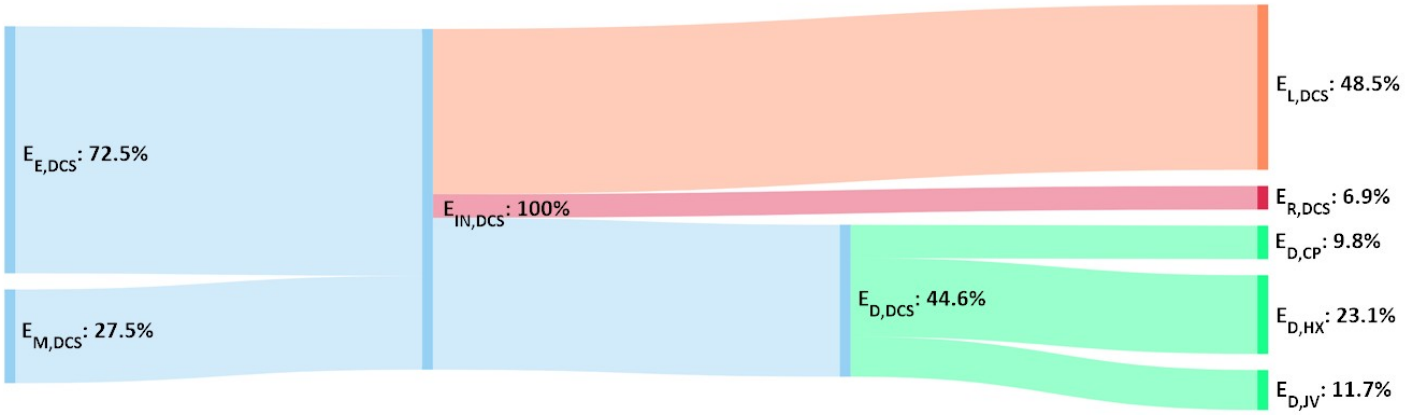
$E_{E,DCS}$: 72.5%
$E_{M,DCS}$: 27.5%
$E_{IN,DCS}$: 100%
$E_{L,DCS}$: 48.5%
$E_{R,DCS}$: 6.9%
$E_{D,CP}$: 9.8%
$E_{D,DCS}$: 44.6%
$E_{D,HX}$: 23.1%
$E_{D,JV}$: 11.7%

(a)

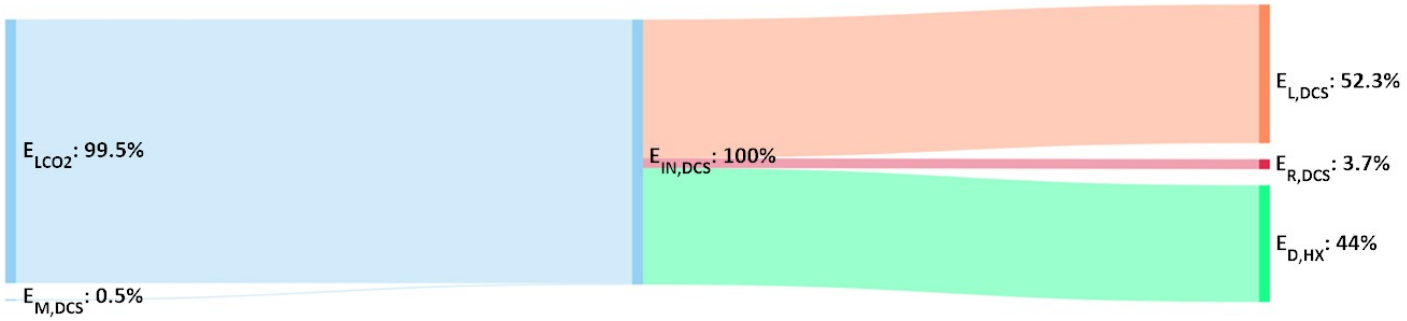
E_{LCO2}: 99.5%
$E_{M,DCS}$: 0.5%
$E_{IN,DCS}$: 100%
$E_{L,DCS}$: 52.3%
$E_{R,DCS}$: 3.7%
$E_{D,HX}$: 44%

(b)

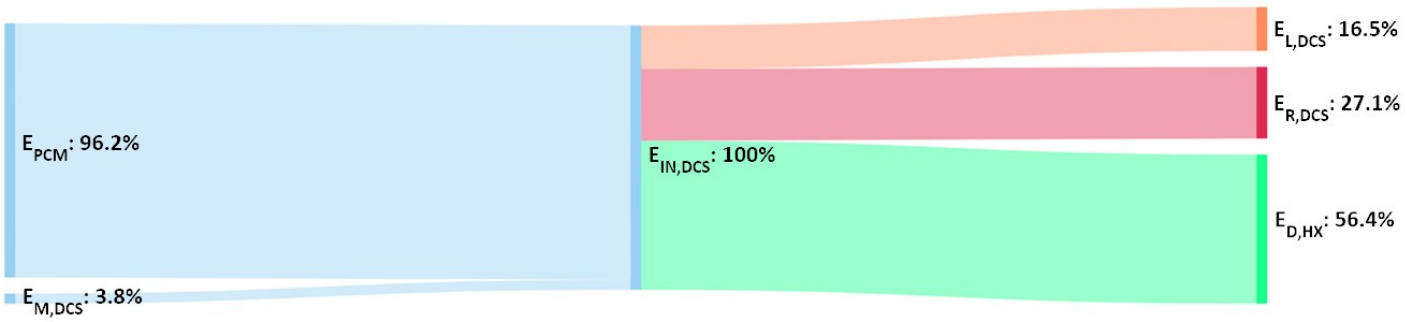
E_{PCM}: 96.2%
$E_{M,DCS}$: 3.8%
$E_{IN,DCS}$: 100%
$E_{L,DCS}$: 16.5%
$E_{R,DCS}$: 27.1%
$E_{D,HX}$: 56.4%

(c)

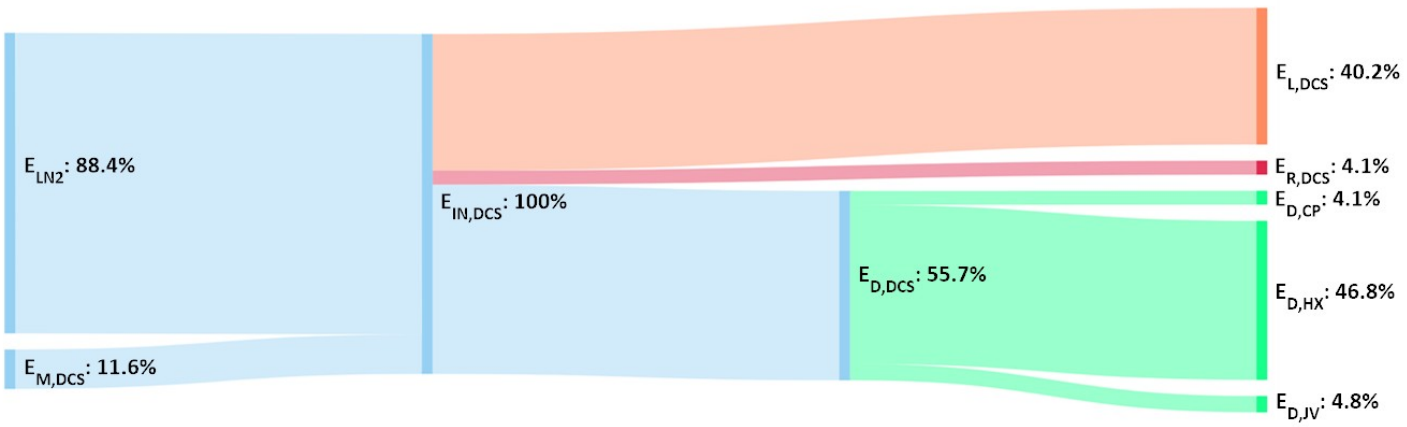
E_{LN2}: 88.4%
$E_{M,DCS}$: 11.6%
$E_{IN,DCS}$: 100%
$E_{L,DCS}$: 40.2%
$E_{R,DCS}$: 4.1%
$E_{D,CP}$: 4.1%
$E_{D,DCS}$: 55.7%
$E_{D,HX}$: 46.8%
$E_{D,JV}$: 4.8%

(d)

Fig. 21. Exergy flows for cooling of returned water using (a) electricity input (b) cold from liquid CO_2 (c) cold from PCM (d) energy from liquid nitrogen

Fig. 21 shows the exergy flows for the district cooling in which different energy vectors are converted to the cold energy contained in the cooling water to be distributed to the industrial facilities for district cooling purposes. The exergy flows are similar to that of the deep freezing process coupled to different energy vectors, which are shown in Fig. 19.

Fig. 21a shows the exergy flows for the district cooling using electricity as the main exergy input to cool the water returned from the district cooling process. Around 0.24 MW electricity (72.5% of the total exergy input) is needed by the heat pump cycle to generate the required 1 MWt cooling power. The waste stream mainly consists of the cooling water leaving HX-2 of the heat pump cycle and contributes to exergy loss of 48.5% of the total exergy input. Due to the low-grade cold acquired by the cooled water to be distributed to the district, the exergy efficiency is reduced to 6.9% compared to the deep freezing process. The exergy destruction is 44.6%, and is contributed mainly by the heat exchangers HX-1 and HX-2.

Fig. 21b and Fig. 21c show the exergy flows for cooling of the returned water from district cooling via single heat exchange process using liquid CO_2 (Fig. 21b) and PCM AN-03 (Fig. 21c). For usage of liquid CO_2, the main exergy input source comes from the physical exergy of the liquid CO_2 (99.5% of the total exergy input or ≈ 0.61 MW). The exergy efficiency is low, at 3.7%, which is mainly affected by the high loss of exergy (52.3% of the total exergy input) through the waste streams leaving the heat exchange process, which mainly consist of the vapor CO_2 at a below-ambient temperature and the large amounts of exergy destruction in the heat exchanger. For the cooling of returned water using PCM, the main exergy input source also comes from the physical exergy of the PCM (96.2% of the total exergy input) but at a far lower amount of 0.07 MW compared to that using liquid CO_2 energy vector. Thus, this process yields a higher exergy efficiency of 27.1%, with a much lower amount of exergy loss via waste streams (16.5% of the total exergy input), which mainly consist of the PCM at a closer-to-ambient condition.

Fig. 21d shows the exergy flows of the water cooling process using liquid nitrogen as input energy vector. The physical exergy of liquid nitrogen is 88.4% of the total exergy input. The waste streams of the process consist of the physical exergy of the cooling water leaving the condenser HX-3 of the heat pump cycle and the used nitrogen, which is at 49.2% of the total exergy input. The exergy efficiency of this process is 4.1% while the total exergy destruction is 55.7% (mainly due to three heat exchangers).

Table 19
Overall exergy input and overall performance for cooling of returned water from district cooling coupled to different energy vectors

	Baseline	LNG Thermal Cycle	Thermal Network	Thermal Storage	LNG ASU
SOURCE OF EXERGY INPUT (MW)					
NG Chemical Exergy, $E_{C,NG}$	0.49	0.40	0.00	0.00	1.87
LNG Physical Exergy, $E_{P,LNG}$	0.00	0.09	1.80	1.23	0.84
Diesel Exergy, E_{fuel}	0.00	0.00	0.00	0.04	0.01
PERFORMANCE PARAMETERS					
Exergy Efficiency (%)	3.87	3.91	1.06	1.77	0.80
Carbon Emission (kTPA)	0.85	0.69	0.01	0.09	3.27

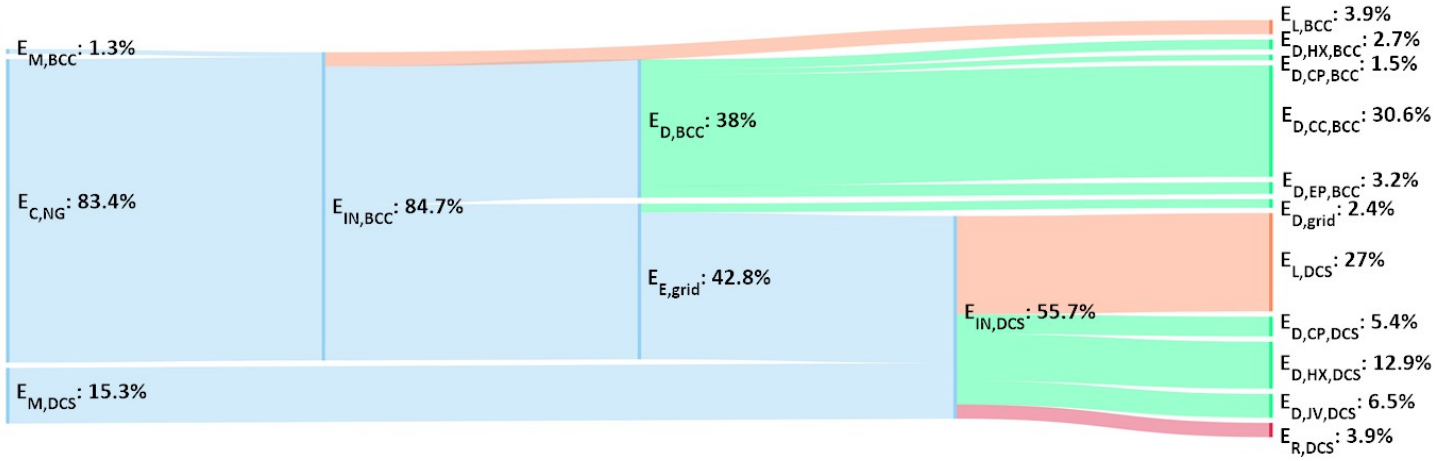
E_M,BCC: 1.3%
E_C,NG: 83.4%
E_M,DCS: 15.3%
E_IN,BCC: 84.7%
E_D,BCC: 38%
E_E,grid: 42.8%
E_IN,DCS: 55.7%
E_L,BCC: 3.9%
E_D,HX,BCC: 2.7%
E_D,CP,BCC: 1.5%
E_D,CC,BCC: 30.6%
E_D,EP,BCC: 3.2%
E_D,grid: 2.4%
E_L,DCS: 27%
E_D,CP,DCS: 5.4%
E_D,HX,DCS: 12.9%
E_D,JV,DCS: 6.5%
E_R,DCS: 3.9%

(a)

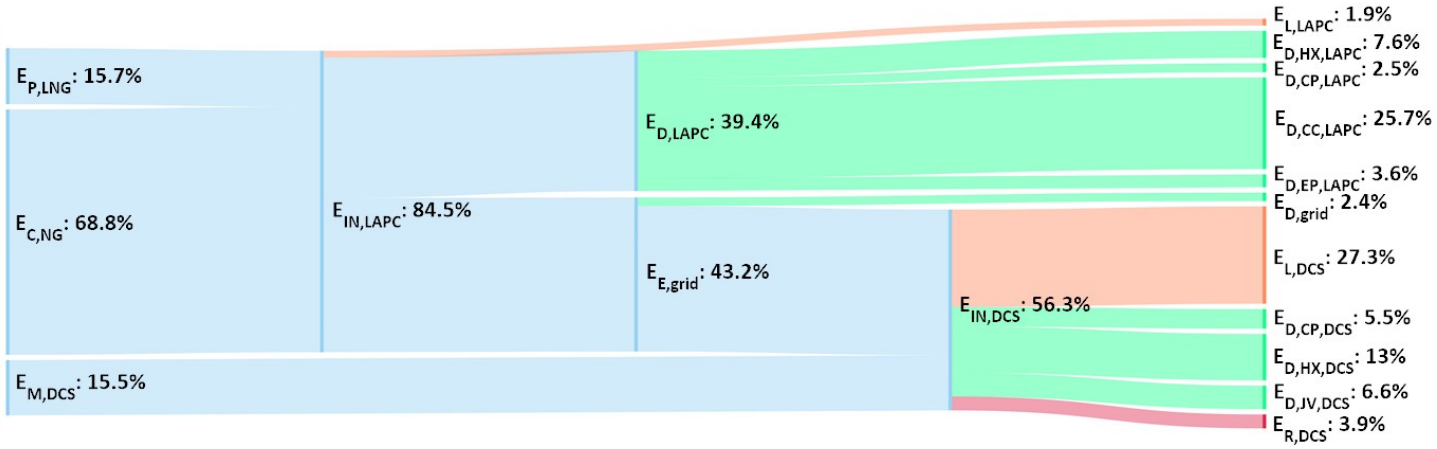
E_P,LNG: 15.7%
E_C,NG: 68.8%
E_M,DCS: 15.5%
E_IN,LAPC: 84.5%
E_D,LAPC: 39.4%
E_E,grid: 43.2%
E_IN,DCS: 56.3%
E_L,LAPC: 1.9%
E_D,HX,LAPC: 7.6%
E_D,CP,LAPC: 2.5%
E_D,CC,LAPC: 25.7%
E_D,EP,LAPC: 3.6%
E_D,grid: 2.4%
E_L,DCS: 27.3%
E_D,CP,DCS: 5.5%
E_D,HX,DCS: 13%
E_D,JV,DCS: 6.6%
E_R,DCS: 3.9%

(b)

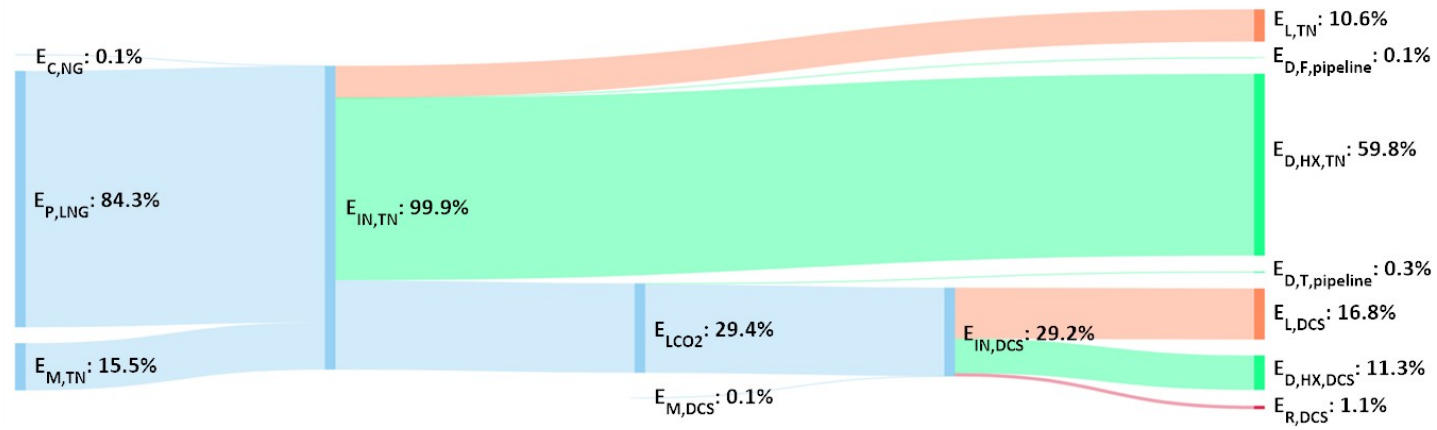
E_C,NG: 0.1%
E_P,LNG: 84.3%
E_M,TN: 15.5%
E_IN,TN: 99.9%
E_LCO2: 29.4%
E_M,DCS: 0.1%
E_IN,DCS: 29.2%
E_L,TN: 10.6%
E_D,F,pipeline: 0.1%
E_D,HX,TN: 59.8%
E_D,T,pipeline: 0.3%
E_L,DCS: 16.8%
E_D,HX,DCS: 11.3%
E_R,DCS: 1.1%

(c)

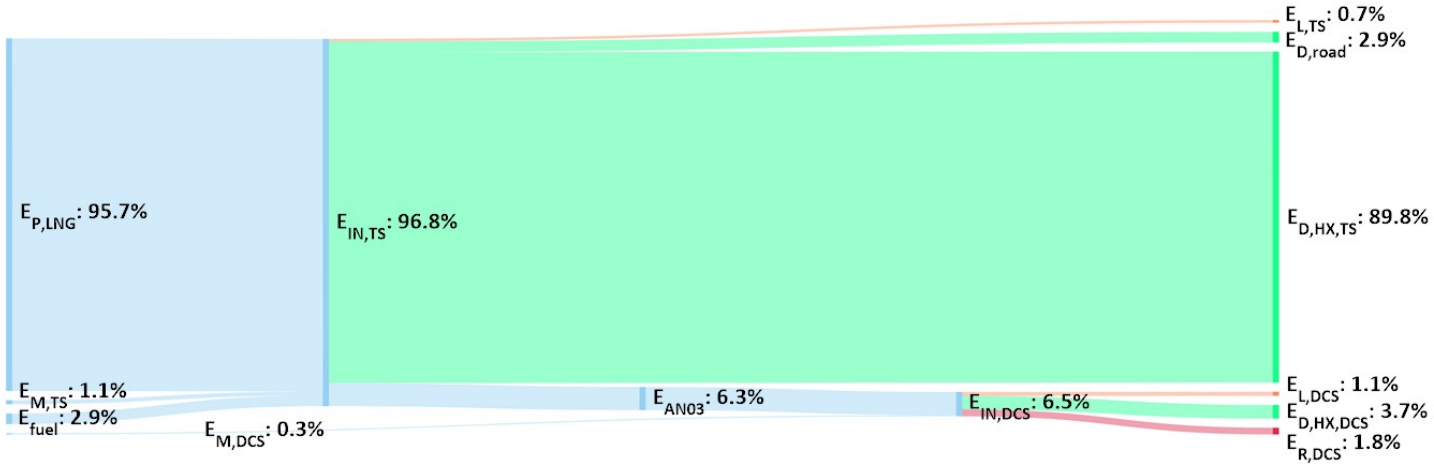

(d)

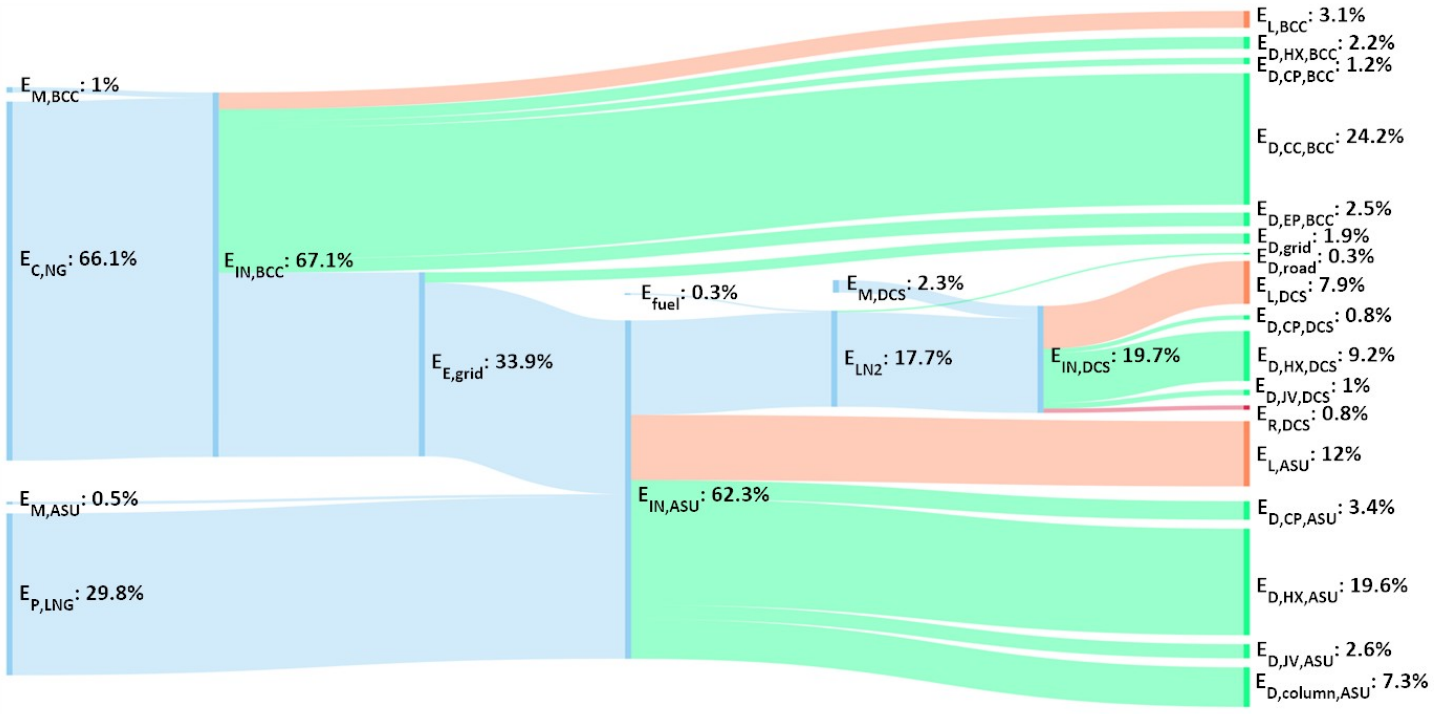

(e)

Fig. 22. Overall exergy flows for cooling of returned water using energy vectors generated from (a) baseline combined cycle (b) LNG assisted power cycle (c) thermal network (d) thermal storage (e) LNG assisted air separation unit

Fig. 22 shows the exergy flows of the overall process, from the generation of energy vector to the cold applications. Due to the similar setup for cooling of the water returned from district cooling with the deep freezing process, the exergy flows as shown in Fig. 22 is very similar to that shown in Fig. 20. For Fig. 22a and Fig. 22b, which show exergy flows for cooling of the returned water from district cooling using electricity, the main exergy source (>68% of the total exergy input) comes from the chemical exergy of the natural gas consumed by the power cycles to produce electricity (≥ 0.4 MW). With the main exergy destruction occurring in the combustion chamber of the power cycles and the components of the heat pump cycle, the overall exergy efficiency of the water cooling process using electricity from both baseline combined cycle and the LNG assisted power cycle is low, at ≈ 3.9%, which is caused by the low exergy content in the product cooling water.

Fig. 22c and Fig. 22d show the exergy flows for using energy vectors produced by the thermal network and thermal storage respectively for the similar water cooling process. In both cases, the main exergy input comes from the physical

exergy of the LNG to be regasified. Due to the unutilized high-grade cold of the LNG for these energy vectors, the exergy destruction inside the heat exchangers of the central plant for both the thermal network and the thermal storage is high. This is expected due to the large temperature difference between LNG and the cooled water which is the product of the cold application. This causes the low exergy efficiency as shown, which is ≈ 1.1% for that using liquid CO_2 energy vector and ≈ 1.8% for that using PCM energy vector.

Fig. 22e shows the exergy flows from the LNG assisted air separation unit for the water cooling process. The main exergy input (≈ 66% of the total exergy input) is the chemical exergy of the natural gas consumed by the baseline combined cycle, which is used to produce electricity to drive the compressors in the air separation unit. Another main exergy input is the physical exergy of the LNG assisting the air separation process. The total amount of exergy lost and destruction in the baseline combined cycle and air separation unit is 33.2% and 44.9% respectively. Due to the large amounts of exergy destruction and wastage, the overall exergy efficiency of the water cooling process using liquid nitrogen energy vector is only 0.8%.

From the overall exergy efficiency, the cooling of returned water from district cooling using electricity seems promising due to the high efficiency demonstrated. However, it should again be remembered that the cold energy is free and the charging process of energy vectors such as liquid CO_2 and PCMs is much cleaner compared to the electricity generation process. Due to the large amounts of energy consumed for the air separation process, the liquid nitrogen energy vector alone is not suitable for the district cooling process due to the low efficiency and waste of high-grade cold energy contained in the liquid nitrogen. For the carbon emission part, similar to the deep freezing process, the liquid CO_2 and PCM energy vectors are cleaner (almost zero carbon emission) compared to the liquid nitrogen and electricity energy vector as energy input due to the minimization of electricity usage. As aforementioned, during the production of liquid nitrogen energy vector, large amounts of electricity that is assumed to come from the baseline combined cycle is required as input to the air separation unit, resulting in a high carbon emission of ≈ 3.3 kTPA.

5.5 Compilation of cold applications

In this section, each of the energy vectors generation methods is analyzed by looking at the total exergy consumption, exergy efficiency and carbon emission when each of them is connected to all the downstream cold applications.

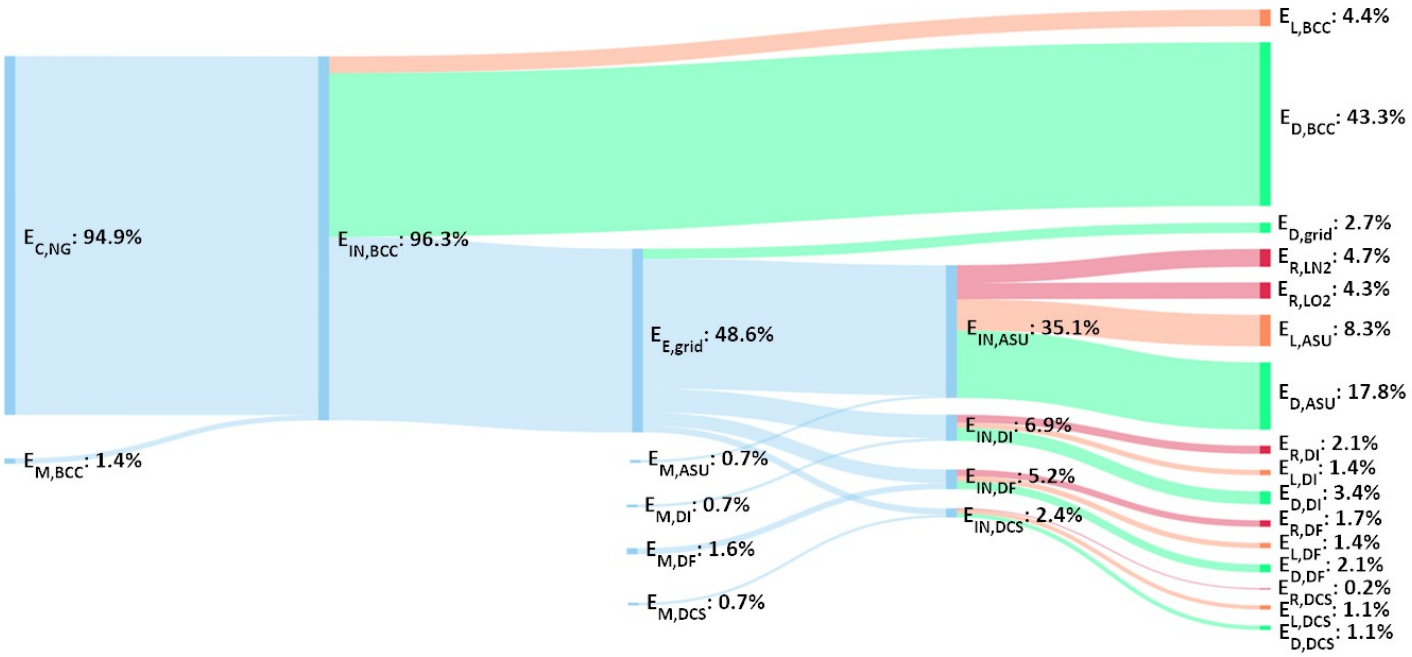

(a)

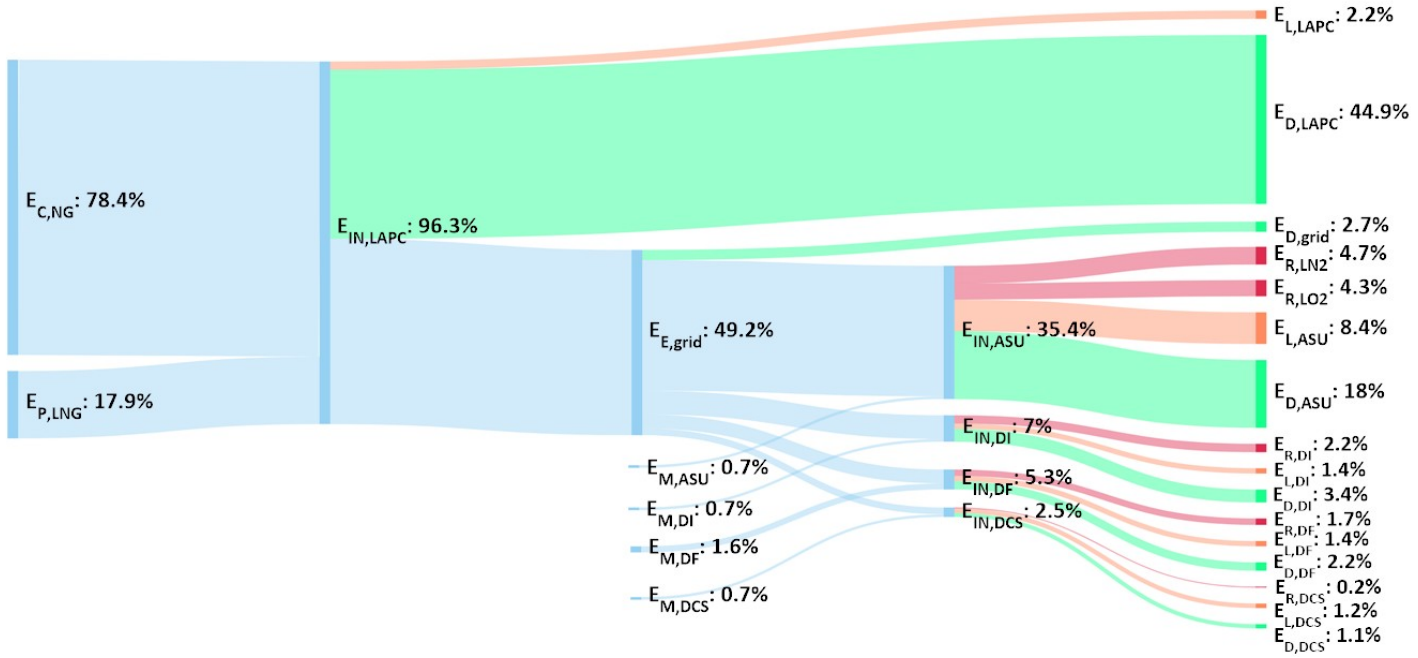
E_C,NG: 78.4%
E_P,LNG: 17.9%
E_IN,LAPC: 96.3%
E_E,grid: 49.2%
E_M,ASU: 0.7%
E_M,DI: 0.7%
E_M,DF: 1.6%
E_M,DCS: 0.7%
E_IN,ASU: 35.4%
E_IN,DI: 7%
E_IN,DF: 5.3%
E_IN,DCS: 2.5%
E_L,LAPC: 2.2%
E_D,LAPC: 44.9%
E_D,grid: 2.7%
E_R,LN2: 4.7%
E_R,LO2: 4.3%
E_L,ASU: 8.4%
E_D,ASU: 18%
E_R,DI: 2.2%
E_L,DI: 1.4%
E_D,DI: 3.4%
E_R,DF: 1.7%
E_L,DF: 1.4%
E_D,DF: 2.2%
E_R,DCS: 0.2%
E_L,DCS: 1.2%
E_D,DCS: 1.1%

(b)

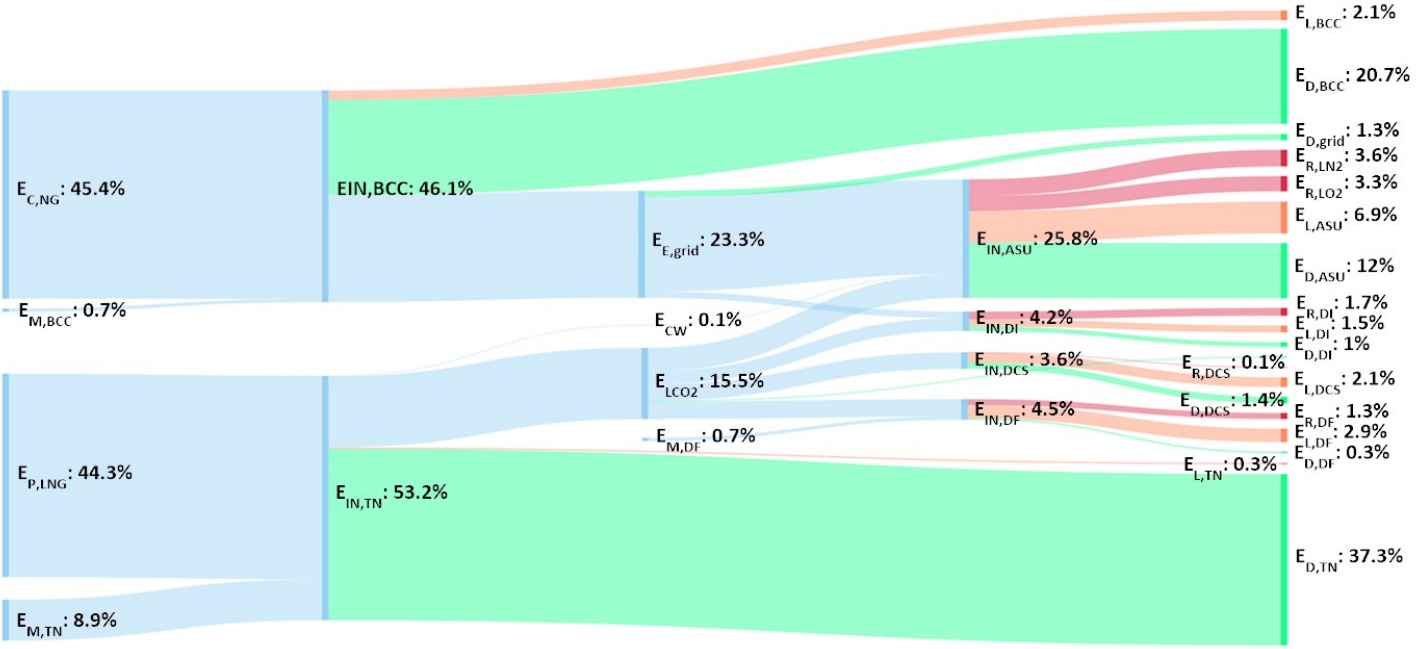
E_C,NG: 45.4%
E_M,BCC: 0.7%
E_P,LNG: 44.3%
E_M,TN: 8.9%
EIN,BCC: 46.1%
E_IN,TN: 53.2%
E_E,grid: 23.3%
E_CW: 0.1%
E_LCO2: 15.5%
E_M,DF: 0.7%
E_IN,ASU: 25.8%
E_IN,DI: 4.2%
E_IN,DCS: 3.6%
E_IN,DF: 4.5%
E_L,BCC: 2.1%
E_D,BCC: 20.7%
E_D,grid: 1.3%
E_R,LN2: 3.6%
E_R,LO2: 3.3%
E_L,ASU: 6.9%
E_D,ASU: 12%
E_R,DI: 1.7%
E_L,DI: 1.5%
E_D,DI: 1%
E_R,DCS: 0.1%
E_D,DCS: 1.4%
E_L,TN: 0.3%
E_L,DCS: 2.1%
E_R,DF: 1.3%
E_L,DF: 2.9%
E_D,DF: 0.3%
E_D,TN: 37.3%

(c)

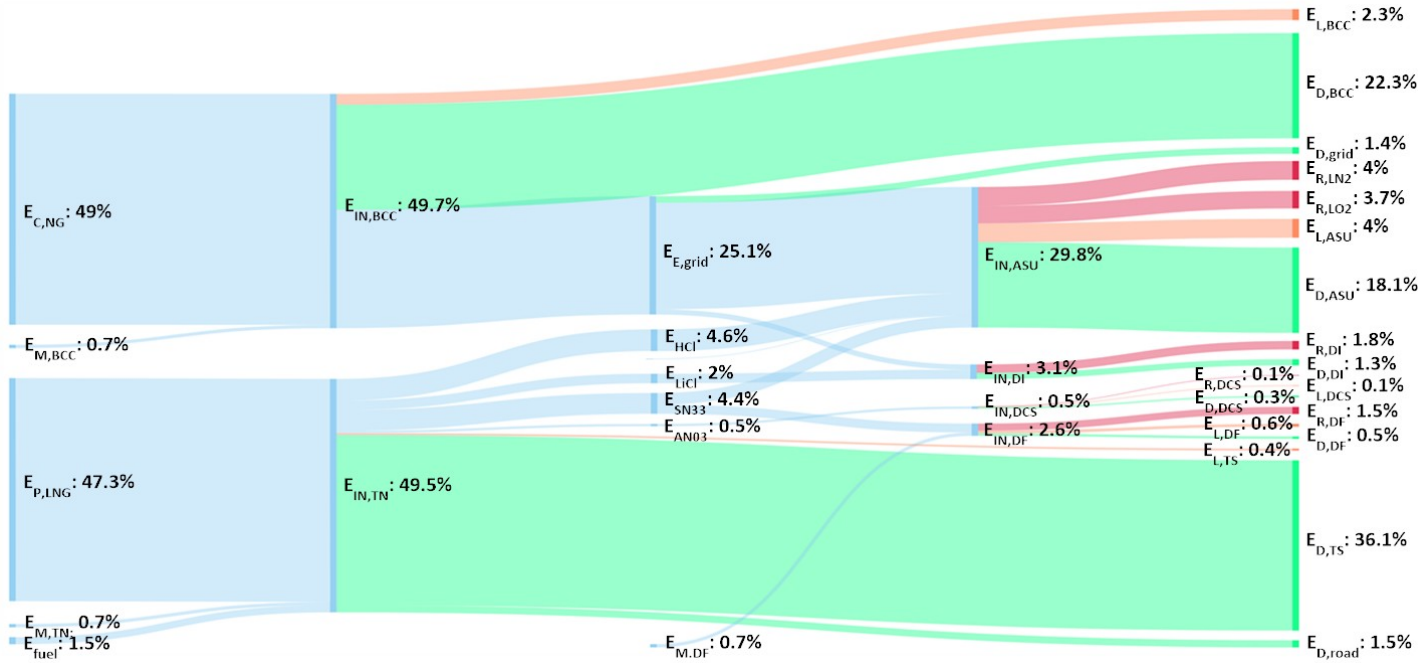

(d)

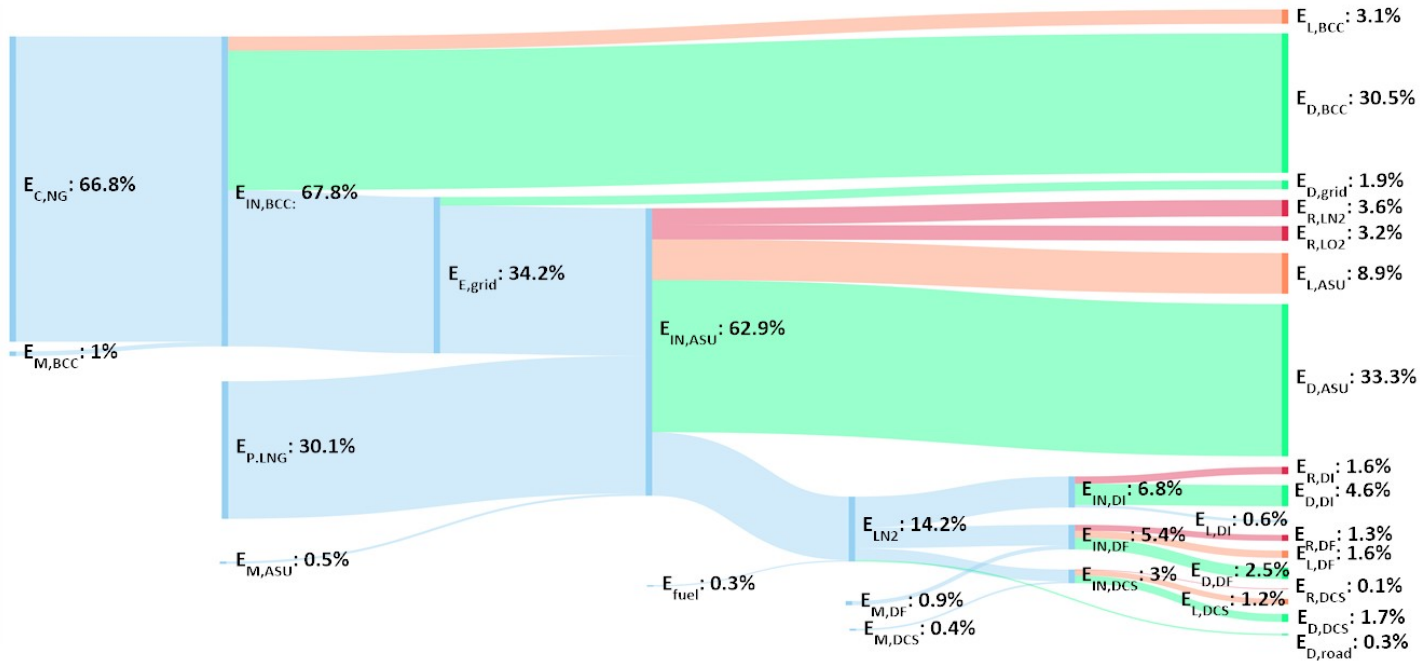

(e)

Fig. 23. Exergy flows from (a) baseline combined cycle (b) LNG assisted power cycle (c) thermal network (d) thermal storage (e) LNG assisted air separation unit when coupled to all cold applications

Fig. 23 shows the overall exergy flows and how the exergy is distributed and recovered in the cold applications. Table 20 tabulates the amount of each exergy source and the performance parameters of using each of the four energy vectors generated using different methods. As shown in Fig. 23a, for usage of electricity generated by the baseline combined cycle as main energy source for the cold applications, inevitably the main exergy input comes from the chemical exergy of the natural gas consumed by the baseline combined cycle (95% of the total exergy input or ≈ 12.8 MW). A large amount of exergy destruction occurs in the combined cycle, mainly in the combustion chamber and in the heat exchangers. About 2.7% of the total exergy is lost during electricity distribution. A large amount of electricity is supplied to the air separation unit, mainly due to the large amounts of compressor work needed to supply the sufficient cooling needed for generation

of liquid air products. This results in a significant amounts of exergy loss and exergy destruction occurring in the air separation unit (26.1% of the total exergy input). The exergy losses are due to large amounts of waste heat generated by the compressors and the unused by-products generated, while the exergy destruction is mainly caused by the MSHE, compressors and the distillation columns. For the other cold applications, due to the lower grade of cold demanded, the electricity input is much less compared to that of the air separation unit. The total amount of exergy loss and destruction in the three cold applications (i.e. dry ice production, deep freezing and district cooling) are between 3.9% and 6.6%. The overall exergy efficiency is 13%, with carbon emission of ≈ 22.3 kTPA, which is generated mainly by the baseline combined cycle.

Fig. 23b shows the exergy flows of electricity generated using the LNG assisted power cycle. The main difference with the exergy generated by the baseline combined cycle is in the power cycle, in which the dependency on natural gas chemical exergy is reduced by 18% to ≈ 10.5 MW compared to the baseline combined cycle, which is 78.4% of the total exergy input to the system. The physical exergy of LNG to be regasified by the LNG assisted power cycle contributes to another 17.9% of the total exergy input. Large amounts of exergy destruction occurs in the LNG assisted power cycle as well, mainly caused by the combustion chamber and the heat exchangers. The exergy flows of the electricity generated are almost the same as that obtained by using the electricity generated by the baseline combined cycle, and thus will not be explained again. The overall exergy efficiency has improved compared to the baseline combined cycle (13.2%) and the carbon emission is reduced by ≈ 18.3% compared to the baseline case, mainly due to reduction of natural gas consumed in the power cycle.

Fig. 23c shows the exergy flows for usage of thermal network and two selected working fluids, CO_2 and water as energy vector to assist or supply energy to the cold applications. Due to the requirement of compressor work in certain cold applications where high-grade cold is required (i.e. air separation and dry ice production), electricity is assumed to be obtained from the baseline combined cycle, where chemical exergy of natural gas consumed reduced to ≈ 8 MW, which is a 38% improvement compared to the baseline case. The exergy flows inside the baseline combined cycle are similar to that explained in Fig. 23a. The central plant for the thermal network is where heat exchange between working fluids and LNG occurs. The physical exergy of LNG to be regasified is 44.3% of the total exergy input (≈ 7.8 MW). Due to the limited phase change temperature of CO_2 (-50°C), the high-grade cold of LNG at ≈ -160°C is not utilized, causing the large amount of exergy destruction in the thermal network central plant. Similarly, for the cold applications part, the distribution of exergy is more or less similar with that using electricity as main exergy input. The overall exergy efficiency is ≈ 10%, which is less than the baseline case but it should be understood that almost half of the exergy input comes from the physical exergy of LNG, which will be wasted if not recovered. Due to large amount of reduction of the natural gas consumption in the system because of the reduced compressor work in the air separation unit and dry ice production, and the elimination of heat pump cycle in the deep freezing and returned water cooling process, the carbon emission is significantly reduced by ≈ 38.0% compared to the baseline case, and represents 13.8 kTPA.

Fig. 23d shows the exergy flows for usage of PCM as energy vector to support or assist in the cold applications. The exergy flows are similar to that using liquid CO_2 and chilled water as energy vectors, except that the cold exergy is now distributed by the PCMs. The dependency on the natural gas chemical exergy input (≈ 7.8 MW) has further decreased compared to that of liquid CO_2/chilled water as energy vectors (≈ 8.0 MW). This is mainly due to the further reduction of the compressor work in the air separation and dry ice production. This is due to the availability of lower temperature intercooling between the compression stages because of the lower operating temperature of the PCMs. Large amounts of exergy is destroyed in the thermal storage central plant where heat exchange between LNG and the PCMs occurs. However, due to the need of using trucks for distribution of the PCMs, there is a small amount of exergy input from chemical exergy of the fuel consumed by the trucks. The exergy flows and distribution in the cold applications are similar to the cold applications using other energy vector input. The overall exergy efficiency is slightly lower compared to the baseline case, due to the large amounts of LNG physical exergy input. The carbon emission is ≈ 14.0 kTPA, which is ≈ 1.5% higher than the usage of liquid CO_2/chilled water energy vector, mainly due to the use of diesel fuel for truck distribution of the PCMs.

Fig. 23e shows the exergy flows for usage of liquid nitrogen as energy vector. Large amounts of electricity is involved to drive the compressors in the air separation unit, thus the chemical exergy of the natural gas consumed by the baseline combined cycle makes the major exergy input at 66.8% of the total exergy input (≈ 12 MW), resulting in exergy loss and destruction in the baseline combined cycle at 33.6% of the total exergy input. Another major exergy input is the physical exergy of LNG input to the air separation unit, at 30.1% of the total exergy input (≈ 5.4 MW). The large amount of electricity and LNG physical exergy input to the air separation unit is due to the need for the air separation unit to produce large amounts of liquid nitrogen as energy vector for the other cold applications alongside the required amount of liquid nitrogen and liquid oxygen for the market requirement. Thus, the exergy destroyed and exergy loss in the waste streams is large, at 41.2% of the total exergy input. For the subsequent cold applications (i.e. dry ice production, deep freezing and returned water cooling process), the amount of exergy destruction is high compared to cold applications using other energy vectors, largely due to the exergy destroyed since high-grade cold contained in the liquid nitrogen energy vector is not utilized. Alongside the large amount of exergy loss and destruction in the baseline combined cycle and the air separation process, the total exergy loss and destruction in the cold applications are 12.5% due to unutilized high-grade cold in the liquid nitrogen, resulting in an overall exergy efficiency of ≈ 9.9%. Large amounts of carbon emission is mainly due to the large amount of natural gas consumption to produce electricity for the air separation unit, and it is only ≈ 6.0% less than that of the baseline combined cycle.

Table 20
Amounts of overall exergy input and overall performance for the baseline case / LNG recovery approach to satisfy demand of the cold applications

	Baseline	LNG Thermal Cycle	Thermal Network	Thermal Storage	LNG ASU
SOURCE OF EXERGY INPUT (MW)					
NG Chemical Exergy, $E_{C,NG}$	12.83	10.48	7.96	7.78	12.01
LNG Physical Exergy, $E_{P,LNG}$	0.00	2.39	7.77	7.50	5.40
Diesel Exergy, E_{fuel}	0.00	0.00	0.00	0.23	0.05
PERFORMANCE PARAMETERS					
Exergy Efficiency (%)	13.02	13.17	10.04	11.08	9.9
Carbon Emission (kTPA)	22.26	18.18	13.81	14.03	20.93

6. Conclusions

In this paper, exergy and carbon emission for different cold applications coupled to different energy vectors as main/assisting energy sources have been studied. It is demonstrated that with the introduction of these cold energy vectors which are generated or charged by using LNG cold energy, various cold applications can be modified and become more efficient and cleaner compared to their conventional setup, mainly by reducing the cold applications dependency on the electricity. For usage of energy vectors such as liquid CO_2/chilled water and PCMs as energy input to assist the air separation and dry ice production, the increased intercooling reduces the amount of compressor work required. These energy vectors can also act as the main exergy input to the lower grade cold applications by replacing heat pump cycles with simpler heat exchange processes. For usage of liquid nitrogen as the main energy input to the cold applications, its mechanical energy can be used to drive the compressors for the medium-high grade cold applications such as dry ice production; or used to drive a single heat pump cycle for a lower-grade cold applications, while providing cold at the same time, thus totally eliminating the electricity input to these cold applications.

The following main results have been obtained when the cold applications are modelled as stand-alone cases:

- For an air separation unit producing liquid nitrogen and liquid oxygen, the LNG-assisted air separation unit, which uses cold energy from LNG directly as the main energy source, is the cleanest and most exergy efficient solution.

- Dry ice production utilizing PCMs has the highest efficiency and lowest carbon emission due to significantly reduced compression work required. Compared to the conventional setup coupled to the baseline combined cycle, the overall exergy efficiency is increased by ≈ 2.7%, with a reduced carbon emission of ≈ 76%.
- Deep freezing utilizing electricity has high exergy efficiency but high carbon emission as well. The cleanest energy source for deep freezing is liquid CO_2 or PCM as energy vector which yields negligible carbon emissions.
- District cooling system has similar performance as the deep freezing process, where electricity as energy vector input yields the highest exergy efficiency, while utilizing liquid CO_2 or PCM as energy vector gives almost no carbon emission.

When the considered cold applications are grouped as a cluster, and the individual energy vectors are used to support all the cold applications at the same time, it is discovered that using energy vectors generated from a thermal network (i.e. liquid CO_2 and chilled water) and a thermal storage system (PCMs) as main/assistive energy input source to the cold applications cluster gives the cleanest overall process. The carbon emission is reduced by ≈ 38% for the liquid CO_2/chilled water combination as energy vector and reduced by ≈ 37% for the PCMs as energy vector, when compared to the baseline case. However, for these two energy vectors the exergy efficiency does not look attractive due to the large amount of exergy input from cold of LNG during the regasification process, which is considered as wasted if not utilized. The usage of liquid nitrogen as energy vector demonstrated a high flexibility when coupled to different cold applications due to its ability to generate mechanical energy and cold energy at the same time. However, due to large amounts of compressor work input in the LNG assisted air separation unit, this cold energy vector yields the highest carbon emission amongst all the energy vector produced by the LNG cold recovery approach, which is only a ≈ 6% improvement compared to the baseline energy vector.

Appendix A.1 Calculation of thermal and friction loss in a pipeline

Pipeline energy losses can be divided into two types: thermal and friction loss. Thermal loss can be deduced by using the formula below:

$$W_{loss,thermal} = \frac{\Delta T}{R_{ov}} \tag{10}$$

where ΔT represents the temperature difference between the working fluid and the environment and R_{ov} represents the overall thermal resistance which can be deduced using the following formula:

$$R_{ov} = R_{conv,in} + R_{cond,pipe} + R_{cond,ins} + R_{conv,out} \tag{11}$$

where
$R_{conv,in}$ is the convection resistance between working fluid and pipe
$R_{cond,pipe}$ is the conduction resistance of pipeline material
$R_{cond,ins}$ is the conduction resistance of pipeline insulation
$R_{conv,out}$ is the convection resistance between pipe and the ambient environment

Each resistance can be deduced using the following formula:

$$R_{conv} = {}^{1}/_{HA} \tag{12}$$

$$R_{cond} = \frac{\ln {}^{D_{outer}}/_{D_{inner}}}{2\pi kL} \tag{13}$$

where H represents the convective heat transfer coefficient, A represents the surface area for heat transfer, D represents the diameter of the pipe, k represents the thermal conductivity of pipeline material or insulation and L represents the length of the pipe.

For insulation material with very small thermal conductivity, it is expected that $R_{cond,ins}$ dominates compared to other resistance terms and thus, we can simplify Equation (11) into

$$R_{ov} \approx R_{cond,ins} \quad (14)$$

The friction loss is calculated by using the following formula:

$$W_{loss,friction} = \frac{fL\rho v^2}{2D} \quad (15)$$

where f is the friction factor that is obtained with information on a fluid flow's Reynold's number and pipe roughness value, L is the length of the pipe, ρ represents the working fluid density, v represents the velocity of working fluid and D represents the inner diameter of the pipe.

References

[1] S. Mokhatab, J. Y. Mak, J. V. Valappil, and D. A. Wood, *Handbook of liquefied natural gas*. Gulf Professional Publishing, 2013.

[2] W. Kun, G. Anzhong, L. Xuesheng, and S. Yumei, "Utilization Technology and Economy Analysis of LNG's Cryogenic Energy," *Natural Gas Industry,* vol. 24, pp. 122-125, 2004.

[3] M. R. Gómez, R. F. Garcia, J. R. Gómez, and J. C. Carril, "Review of thermal cycles exploiting the exergy of liquefied natural gas in the regasification process," *Renewable and Sustainable Energy Reviews,* vol. 38, pp. 781-795, 2014.

[4] Eia.gov. (2016). *International Energy Outlook 2016*. Available: https://www.eia.gov/outlooks/ieo/pdf/0484(2016).pdf [accessed May 2017].

[5] K. Jiang, "Economic Analysis of LNG Cold Energy Utilization," in *Energy Solutions to Combat Global Warming*: Springer, 2017, pp. 119-132.

[6] T. Yamamoto, Y. Fujiwara, and S. Kitagaki, "Challenges of Advanced Utilization of LNG Cold in Osaka Gas Senboku LNG Terminals," in *Design for Innovative Value Towards a Sustainable Society: Proceedings of EcoDesign 2011: 7th International Symposium on Environmentally Conscious Design and Inverse Manufacturing*, M. Matsumoto, Y. Umeda, K. Masui, and S. Fukushige, Eds. Dordrecht: Springer Netherlands, 2012, pp. 148-153.

[7] H. Kim and S. Hong, "Review on economical efficiency of LNG cold energy use in South Korea," in *23rd World Gas Conference, Amsterdam*, 2006, pp. 1285-1294.

[8] T. Sung and K. C. Kim, "LNG Cold Energy Utilization Technology," in *Energy Solutions to Combat Global Warming*: Springer, 2017, pp. 47-66.

[9] H. Dhameliya and P. Agrawal, "LNG Cryogenic Energy Utilization," *Energy Procedia,* vol. 90, pp. 660-665, 2016.

[10] L. Zhao, H. Dong, J. Tang, and J. Cai, "Cold energy utilization of liquefied natural gas for capturing carbon dioxide in the flue gas from the magnesite processing industry," *Energy,* vol. 105, pp. 45-56, 2016.

[11] H. Sun, H. Zhu, F. Liu, and H. Ding, "Simulation and optimization of a novel Rankine power cycle for recovering cold energy from liquefied natural gas using a mixed working fluid," *Energy,* vol. 70, pp. 317-324, 2014/06/01/ 2014.

[12] G. Angelino and C. M. Invernizzi, "The role of real gas Brayton cycles for the use of liquid natural gas physical exergy," *Applied Thermal Engineering,* vol. 31, no. 5, pp. 827-833, 2011.

[13] M. R. Gómez, R. F. Garcia, J. R. Gómez, and J. C. Carril, "Thermodynamic analysis of a Brayton cycle and Rankine cycle arranged in series exploiting the cold exergy of LNG (liquefied natural gas)," *Energy,* vol. 66, pp. 927-937, 2014.
[14] M. R. Gómez, J. R. Gómez, L. M. López-González, and L. M. López-Ochoa, "Thermodynamic analysis of a novel power plant with LNG (liquefied natural gas) cold exergy exploitation and CO 2 capture," *Energy,* vol. 105, pp. 32-44, 2016.
[15] Y. Liu and K. Guo, "A novel cryogenic power cycle for LNG cold energy recovery," *Energy,* vol. 36, no. 5, pp. 2828-2833, 2011.
[16] T. Morosuk and G. Tsatsaronis, "Comparative evaluation of LNG – based cogeneration systems using advanced exergetic analysis," *Energy,* vol. 36, no. 6, pp. 3771-3778, 2011/06/01/ 2011.
[17] R. F. García, J. C. Carril, J. R. Gomez, and M. R. Gomez, "Power plant based on three series Rankine cycles combined with a direct expander using LNG cold as heat sink," *Energy Conversion and Management,* vol. 101, pp. 285-294, 2015.
[18] R. F. García, J. C. Carril, J. R. Gomez, and M. R. Gomez, "Combined cascaded Rankine and direct expander based power units using LNG (liquefied natural gas) cold as heat sink in LNG regasification," *Energy,* vol. 105, pp. 16-24, 2016.
[19] M. R. Gómez, R. F. Garcia, J. C. Carril, and J. R. Gómez, "High efficiency power plant with liquefied natural gas cold energy utilization," *Journal of the Energy Institute,* vol. 87, no. 1, pp. 59-68, 2014.
[20] U. Lee, K. Kim, and C. Han, "Design and optimization of multi-component organic rankine cycle using liquefied natural gas cryogenic exergy," *Energy,* vol. 77, pp. 520-532, 2014.
[21] U. Lee and C. Han, "Simulation and optimization of multi-component organic Rankine cycle integrated with post-combustion capture process," *Computers & Chemical Engineering,* vol. 83, pp. 21-34, 2015.
[22] P. Li, J. Li, G. Pei, A. Munir, and J. Ji, "A cascade organic Rankine cycle power generation system using hybrid solar energy and liquefied natural gas," *Solar Energy,* vol. 127, pp. 136-146, 2016.
[23] N. Arcuri, R. Bruno, and P. Bevilacqua, "LNG as cold heat source in OTEC systems," *Ocean Engineering,* vol. 104, pp. 349-358, 2015.
[24] H. Wang, X. Shi, and D. Che, "Thermodynamic optimization of the operating parameters for a combined power cycle utilizing low-temperature waste heat and LNG cold energy," *Applied Thermal Engineering,* vol. 59, no. 1, pp. 490-497, 2013.
[25] W.-J. Rao, L.-J. Zhao, C. Liu, and M.-G. Zhang, "A combined cycle utilizing LNG and low-temperature solar energy," *Applied Thermal Engineering,* vol. 60, no. 1, pp. 51-60, 2013.
[26] M. Mehrpooya, M. M. M. Sharifzadeh, and M. A. Rosen, "Energy and exergy analyses of a novel power cycle using the cold of LNG (liquefied natural gas) and low-temperature solar energy," *Energy,* vol. 95, pp. 324-345, 2016.
[27] X. Shi and D. Che, "A combined power cycle utilizing low-temperature waste heat and LNG cold energy," *Energy conversion and management,* vol. 50, no. 3, pp. 567-575, 2009.
[28] S. Deng, H. Jin, R. Cai, and R. Lin, "Novel cogeneration power system with liquefied natural gas (LNG) cryogenic exergy utilization," *Energy,* vol. 29, no. 4, pp. 497-512, 2004.
[29] G. Oliveti, N. Arcuri, R. Bruno, and M. De Simone, "A rational thermodynamic use of liquefied natural gas in a waste incinerator plant," *Applied thermal engineering,* vol. 35, pp. 134-144, 2012.
[30] G. Angelino and C. M. Invernizzi, "Carbon dioxide power cycles using liquid natural gas as heat sink," *Applied Thermal Engineering,* vol. 29, no. 14, pp. 2935-2941, 2009/10/01/ 2009.
[31] N. Zhang, N. Lior, M. Liu, and W. Han, "COOLCEP (cool clean efficient power): a novel CO 2-capturing oxy-fuel power system with LNG (liquefied natural gas) coldness energy utilization," *Energy,* vol. 35, no. 2, pp. 1200-1210, 2010.
[32] J. Wang, Z. Yan, M. Wang, and Y. Dai, "Thermodynamic analysis and optimization of an ammonia-water power system with LNG (liquefied natural gas) as its heat sink," *Energy,* vol. 50, pp. 513-522, 2013.
[33] I.-H. Choi, S. Lee, Y. Seo, and D. Chang, "Analysis and optimization of cascade Rankine cycle for liquefied natural gas cold energy recovery," *Energy,* vol. 61, pp. 179-195, 2013.

[34] H. Y. Lee and K. H. Kim, "Energy and exergy analyses of a combined power cycle using the organic rankine cycle and the cold energy of liquefied natural gas," *Entropy,* vol. 17, no. 9, pp. 6412-6432, 2015.
[35] Y. Song, J. Wang, Y. Dai, and E. Zhou, "Thermodynamic analysis of a transcritical CO 2 power cycle driven by solar energy with liquified natural gas as its heat sink," *Applied energy,* vol. 92, pp. 194-203, 2012.
[36] X. Shi, B. Agnew, D. Che, and J. Gao, "Performance enhancement of conventional combined cycle power plant by inlet air cooling, inter-cooling and LNG cold energy utilization," *Applied Thermal Engineering,* vol. 30, no. 14, pp. 2003-2010, 2010.
[37] T. Otsuka, "Evolution of an LNG terminal: Senboku terminal of Osaka GAS."
[38] J. Lian *et al.*, "Research on High Efficient Utilization of LNG Cold Energy," 2015.
[39] H. Si, N. Mei, and X. Wang, "Optimized Utilization of Liquefied Natural Gas (LNG) Cold Energy," in *2010 14th International Heat Transfer Conference*, 2010, pp. 157-166: American Society of Mechanical Engineers.
[40] A. Messineo and G. Panno, "LNG cold energy use in agro-food industry: a case study in Sicily," *Journal of Natural Gas Science and Engineering,* vol. 3, no. 1, pp. 356-363, 2011.
[41] C. Dispenza, G. Dispenza, V. La Rocca, and G. Panno, "Exergy recovery in regasification facilities–Cold utilization: A modular unit," *Applied Thermal Engineering,* vol. 29, no. 17, pp. 3595-3608, 2009.
[42] S. Henchoz, P. Chatelan, F. Maréchal, and D. Favrat, "Key energy and technological aspects of three innovative concepts of district energy networks," *Energy,* vol. 117, pp. 465-477, 2016.
[43] K. D. Timmerhaus and T. M. Flynn, "Separation and Purification Systems," in *Cryogenic Process Engineering*Boston, MA: Springer US, 1989, pp. 287-376.
[44] R. C. Arora, *Refrigeration and air conditioning*. PHI Learning Pvt. Ltd., 2010.
[45] R. Kehlhofer, F. Hannemann, B. Rukes, and F. Stirnimann, *Combined-cycle gas & steam turbine power plants*. Pennwell Books, 2009.
[46] S. Henchoz, C. Weber, F. Maréchal, and D. Favrat, "Performance and profitability perspectives of a CO 2 based district energy network in Geneva's City Centre," *Energy,* vol. 85, pp. 221-235, 2015.
[47] I. Dincer and M. Rosen, *Thermal energy storage: systems and applications*. John Wiley & Sons, 2002.
[48] E. Oró, A. De Gracia, A. Castell, M. Farid, and L. Cabeza, "Review on phase change materials (PCMs) for cold thermal energy storage applications," *Applied Energy,* vol. 99, pp. 513-533, 2012.
[49] ciat.uk.com. *Thermal Energy Storage*. Available: http://www.ciat.uk.com/wp-content/uploads/2017/02/cristopia-brochure.pdf [accessed Sep 2017].
[50] D. Strahan, "Liquid Air on the Highway: The environmental and business case for liquid air commercial vehicles in the UK," 2014.
[51] M. Mehrpooya, M. M. M. Sharifzadeh, and M. A. Rosen, "Optimum design and exergy analysis of a novel cryogenic air separation process with LNG (liquefied natural gas) cold energy utilization," *Energy,* vol. 90, pp. 2047-2069, 2015.
[52] H. Zhou *et al.*, "Process configurations and simulations for a novel single-column cryogenic air separation process," *Industrial & Engineering Chemistry Research,* vol. 51, no. 47, pp. 15431-15439, 2012.
[53] W. Xu, J. Duan, and W. Mao, "Process study and exergy analysis of a novel air separation process cooled by LNG cold energy," *Journal of Thermal Science,* vol. 23, no. 1, pp. 77-84, 2014.
[54] A. Ebrahimi and M. Ziabasharhagh, "Optimal design and integration of a cryogenic Air Separation Unit (ASU) with Liquefied Natural Gas (LNG) as heat sink, thermodynamic and economic analyses," *Energy,* vol. 126, pp. 868-885, 2017.
[55] Eia.gov. (2017). *State Electricity Profiles - Energy Information Administration*. Available: https://www.eia.gov/electricity/state/ [accessed June 2017].
[56] Hyperphysics.phy-astr.gsu.edu. *Thermal Conductivity*. Available: http://hyperphysics.phy-astr.gsu.edu/hbase/Tables/thrcn.html [accessed Feb 2017].

[57] www.epa.gov. (2015). *Emission Factors for Greenhouse Gas Inventories*. Available: https://www.epa.gov/sites/production/files/2015-11/documents/emission-factors_nov_2015.pdf [accessed May 2017].

[58] Linde-engineering.com. (2017). *The Linde Standard Tanks*. Available: http://www.linde-engineering.com/internet.global.lindeengineering.global/en/images/P_3_3_e_12_150dpi19_5774.pdf [accessed Feb 2017].